Table of Content

1. Materials and methods

All reactions and manipulations were carried out under an atmosphere of dry argon using standard Schlenk techniques or in a glovebox under an inert atmosphere unless stated otherwise. All reagents were purchased from commercial sources and used without further purification. Dry, oxygen-free solvents were employed. Solution ^{1}H, ^{13}C, ^{31}P and ^{29}Si NMR spectra were recorded on a Bruker Avance 300, 400 and 600 spectrometers at 298 K unless otherwise stated. Chemical shifts (δ) are expressed with a positive sign, in parts per million. ^{1}H and ^{13}C chemical shifts are referenced internally to residual protio (^{1}H) or deutero (^{13}C) solvent, while ^{31}P and ^{29}Si chemical shifts are relative to 85% H_3PO_4 and tetramethylsilane respectively. The following abbreviations and their combination are used: br, broad; s, singlet; d, doublet; t, triplet; m, multiplet. The ^{1}H and ^{13}C resonance signals were attributed by means of COSY, HSQC, HMBC experiments.

Mass spectra were recorded on a Waters UPLC Xevo G2 QTOF apparatus. High resolution ESI mass spectra were recorded using a 7 T hybrid FTICR Solarix FT-ICR mass spectrometer or using a TIMS-ToF mass spectrometer (Bruker Daltonik GmbH, Bremen, Germany). The samples were introduced into the ESI source of the mass spectrometer using an infusion pump at a flow rate of 300 µL/h. Stock solutions (10 mg/mL, DMSO) were freshly diluted in CH_3CN before injection at a 2 µg/mL concentration for **H** and 20 µg/mL concentration for (**G** or **1** or **2**) + **H**. Negative-ion mode was used for ESI experiments. The following ionization and transmission parameters were used: capillary voltage 4.2 kV, endplate offset -500V. Nitrogen was used as the desolvation gas (3 L/mn). The source and desolvation temperatures were kept at 250 °C. The mass resolving power (full width at half maximum height) was set at $3x10^5$ FWHM at m/z 400 for the FT-ICR and $7x10^4$ for the TIMS-ToF. Each mass spectrum was the average of 100 scans (0.002s accumulation time and 2s transient length) for the FT-ICR and 2 minutes for the TIMS-ToF.

^{1}H-DOSY experiments were carried out on a Bruker AVANCE 400 MHz spectrometer equipped with a 5 mm Z-gradient TCI cryogenic probe. The pulse program used was dstebpgp3s The Z pulsed field gradients were generated with a 10 A GRASP II/P gradient amplifier. Thus, the z-maximum gradient strength (g) was 53.5 G/cm. Experiments were performed by varying g and keeping all other timing parameters constant. The Δ (time between the two gradients) and the δ (gradient pulse length) durations were 800-1200 µs and 60-140 ms respectively and g (gradient strength) was varied from 2.675 (strength of 5%) to 50.825 (strength of 95%) G/cm. The cyclotricatechylene (**C**)[1], the $L_2(AuCl)_n$[2] precursors and the $(dmpm)_2(AuCl)_2$ (**2**)[3] were synthesized based on reported protocols.

2. Preparation of the cage (H):

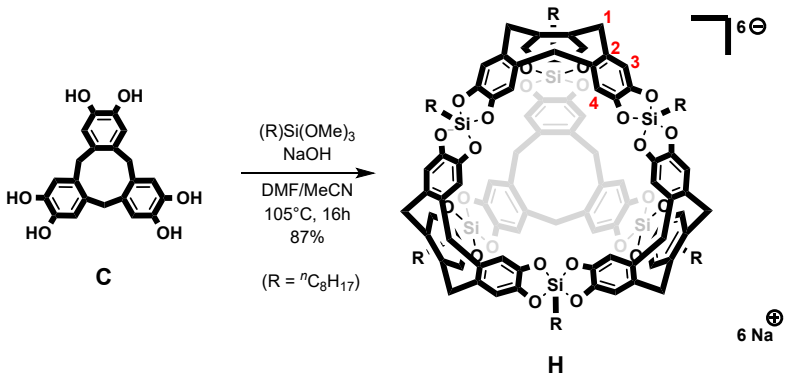

$C_4(Si^nC_8H_{17})_6Na_6DMF_{12}$

H was synthesized by a modified protocol based on a known method.[4] Cyclotricatechylene (**C**) (2 g, 5.46 mmol) trimethoxy(octyl)silane (2.33 mL, 9 mmol, 1.65 equiv.) and NaOH (338 mg, 8.46 mmol, 1.55 equiv.) was stirred in a mixture of dry DMF (56 mL) and dry MeCN (20 mL) in a sealed tube at 105 °C during 16 hours. The solvent was removed under reduced pressure and the resulting residue was washed with pentane (4 x 10 mL) and dried under vacuum at 40°C during 24 hours, to give the title cage as a beige solid (3.9 g, 87%). **^{1}H NMR** (400 MHz, CD_3OD) δ 7.61 (s, 12H, *H*CON$(CH_3)_2$), 6.66 (s, 24H, Ar*H*), 4.60 (d, *J* = 13.3 Hz, 12H, CH_2), 3.27 (d, *J* = 13.2 Hz, 12H, CH_2), 2.68 (s, 36H, HCON(C$H_3)_2$), 2.65 (s, 36H, HCON(C$H_3)_2$), 1.36-1.02 (m, 72H, 6 x CH_2-octyl), 0.89 (t, *J* = 7.1 Hz, 18H, CH_3-octyl), 0.55 (t, *J* = 8.0 Hz, 12H, Si-CH_2). **^{13}C NMR** (101 MHz, CD_3OD) δ 164.6 (s, H*C*ON$(CH_3)_2$), 148.8 (s, *C*3), 131.2 (s, *C*2), 112.4 (s, *C*3), 37.2 (s, *C*1), 36.5 (s, HCON(*C*$H_3)_2$), 34.6 (s, *C*H_2-octyl), 32.6 (s, *C*H_2-octyl), 31.4 (s, HCON(*C*$H_3)_2$), 30.5 (2 x s, 2 x *C*H_2-octyl), 25.3 (s, *C*H_2-octyl), 23.8 (s, *C*H_2-octyl), 17.7 (s, Si-*C*H_2), 14.5 (s, *C*H_3-octyl). **^{29}Si NMR** (119 MHz, CD_3OD) δ 75.3 (s). **^{1}H NMR** (300 MHz, $(CD_3)_2CO$) δ 7.86 (s, 12H, *H*CON$(CH_3)_2$), 6.50 (s, 24H, Ar*H*), 4.55 (d, *J* = 13.4 Hz, 12H, CH_2), 3.19 (d, *J* = 13.4 Hz, 12H, CH_2), 2.83 (s, 36H, HCON(C$H_3)_2$), 2.71 (s, 36H, HCON(C$H_3)_2$), 1.33-1.1 (m, 72H, 6 x CH_2-octyl), 0.87 (t, *J* = 6.9 Hz, 18H, CH_3-octyl), 0.53-0.46 (m, 12H, Si-CH_2). ESI-FTICR (see S13).

3. Preparation of the gold complexes:

The gold complexes **G**, **1**, **3** and **4** were synthesized by a slightly modified protocol based on a known method.[2b] To a solution of the corresponding L_2AuCl (0.04M) in dry CH_2Cl_2, $AgPF_6$ (1 equiv.) was added and the reaction was stirred at room temperature during 2 hours in the dark. The precipitated AgCl was removed by filtration, the solvent was evaporated and the residue was washed with two times with pentane and dried to give the title compounds.

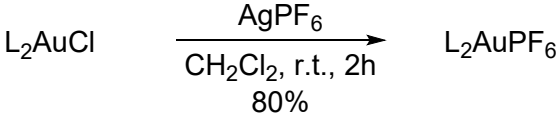

	L
G	PMe_3
1	PEt_3
3	P^tBu_3
4	PPh_3

$(PMe_3)_2AuPF_6$ (**G**):

Isolated as a white solid (80%). **^{1}H NMR** (300 MHz, CD_3OD) δ 1.61 (t, J_{PH} = 4.3 Hz). **^{31}P{H} NMR** (122 MHz, CD_3OD) δ 9.3 (s), -144.6 (hept, J_{FP} = 707 Hz, PF_6). **HRMS** (ESI+) calcd. for $[M]^+ = C_6H_{18}P_2Au$: 349.0549, found 349.0551. (ESI-) calcd. for $[PF_6]^- = PF_6$: 144.9642, found 144.9641. Analytical data are in agreement with those of the reported $(PMe_3)_2AuBF_4$ analogue.[2b]

$(PEt_3)_2AuPF_6$ (**1**):

Isolated as a white solid (50%). **^{1}H NMR** (300 MHz, CD_3OD) δ 2.06 (m, 12H, C*H*$_2$), 1.27 (m, 18H, C*H*$_3$). **^{31}P{H} NMR** (122 MHz, CD_3OD) δ 47.8 (s), -144.6 (hept, J_{FP} = 707 Hz, PF_6). **HRMS** (ESI+) calcd. for $[M]^+ = C_{12}H_{30}P_2Au$: 433.1488, found 433.1497. (ESI-) calcd. for $[PF_6]^- = PF_6$: 144.9642, found 144.9639. Analytical data are in agreement with those of the reported $(PEt_3)_2AuBF_4$ analogue.[2b]

$(P^tBu_3)_2AuPF_6$ (**3**):

Isolated as a white solid (82%). **^{1}H NMR** (300 MHz, CD_3OD) δ 1.61 (t, J_{PH} = 7.0 Hz). **^{31}P{H} NMR** (122 MHz, CD_3OD) δ 96.9 (s), -144.6 (hept, J_{FP} = 707 Hz, PF_6). **^{1}H NMR** (300 MHz, $(CD_3)_2CO$) δ 1.65 (t, J_{PH} = 7.1 Hz). **^{31}P{H} NMR** (122 MHz, $(CD_3)_2CO$) δ 95.6 (s), -144.3 (hept, J_{FP} = 708 Hz, PF_6). **HRMS** (ESI+) calcd. for $[M]^+ = C_{24}H_{54}P_2Au$: 601.3366, found 601.3367. (ESI-) calcd. for $[PF_6]^- = PF_6$: 144.9642, found 144.9645. Analytical data are in agreement with those of the reported $(P^tBu_3)_2AuBF_4$ analogue.[2b]

$(PPh_3)_2AuPF_6$ (**4**):

Isolated as a white solid (71%). **^{1}H NMR** (300 MHz, CD_3OD) δ 7.71-7.56 (m, Ar*H*). **^{31}P{H} NMR** (122 MHz, CD_3OD) δ 44.8 (s), -144.6 (hept, J_{FP} = 707 Hz, PF_6). **^{1}H NMR** (300 MHz, $(CD_3)_2CO$) δ 7.78-7.63 (m, Ar*H*). **^{31}P{H} NMR** (122 MHz, $(CD_3)_2CO$) δ 44.4 (s), -144.3 (hept, J_{FP} = 708 Hz, PF_6). **HRMS** (ESI+) calcd. for $[M]^+ = C_{36}H_{30}P_2Au$: 721.1488, found 721.1503. (ESI-) calcd. for $[PF_6]^- = PF_6$: 144.9642, found 144.9654. Analytical data are in agreement with those previously reported.[5]

$(dmpm)_2(AuCl)_2$ (**2**):

This complex was synthesized by a known protocol and isolated as a white solid (45%).[3] **^{1}H NMR** (300 MHz, CD_3OD) δ 3.05 (quin, J_{PH} = 5.3 Hz, 4H, C*H*$_2$), 1.84 (m, 24H, C*H*$_3$). **^{31}P{H} NMR** (122 MHz, CD_3OD) δ 14.3 (s). Analytical data is in agreement with that of the reported $dmpm_2(AuCl)_2$. **HRMS** (ESI+) calcd. for $[M\text{-}H]^+ = C_{10}H_{27}P_4Au_2$: 665.0394, found 665.0394; calcd. for $[M]^{2+} = C_{10}H_{28}P_4Au_2$: 333.0240, found 333.0236.[3]

4. NMR spectra

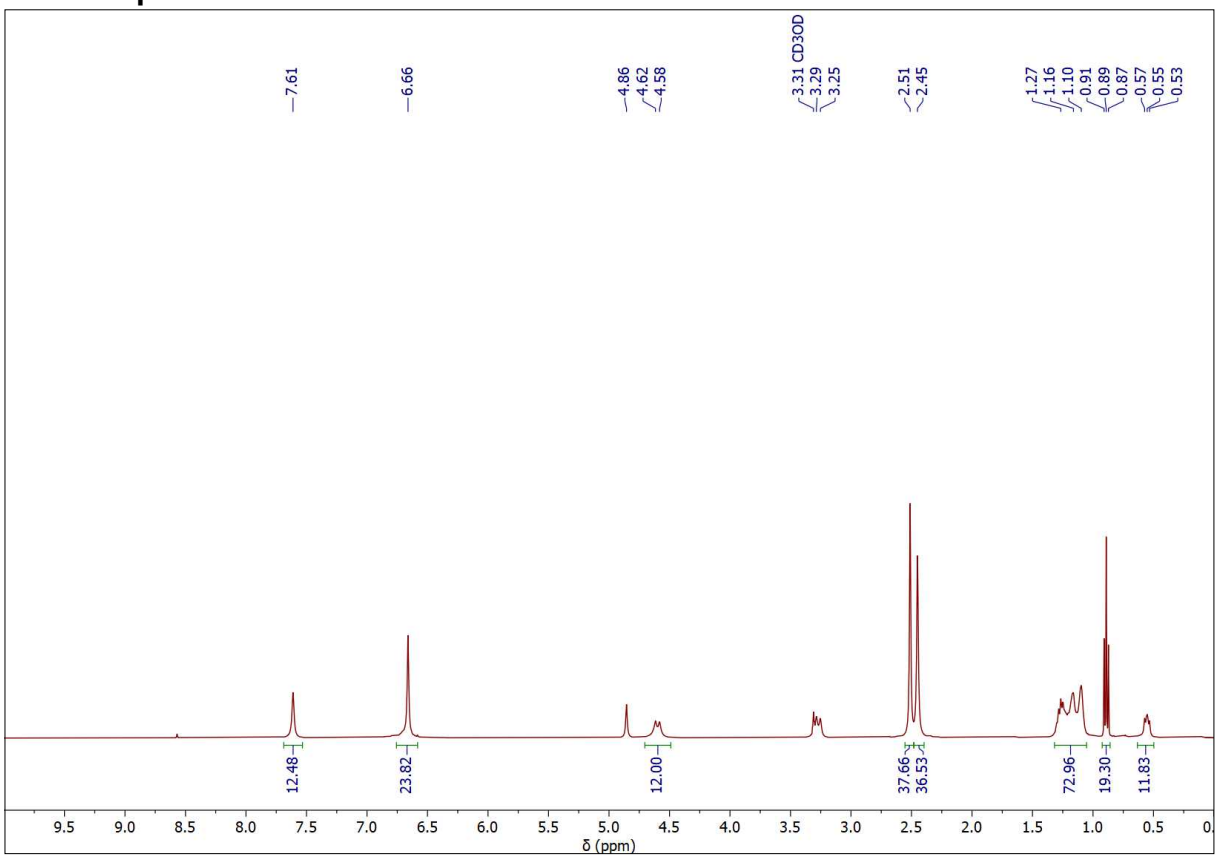

Figure S1. ^{1}H NMR spectrum of $C_4(SiC_8H_{17})_6Na_6DMF_{12}$ (**H**) in CD_3OD.

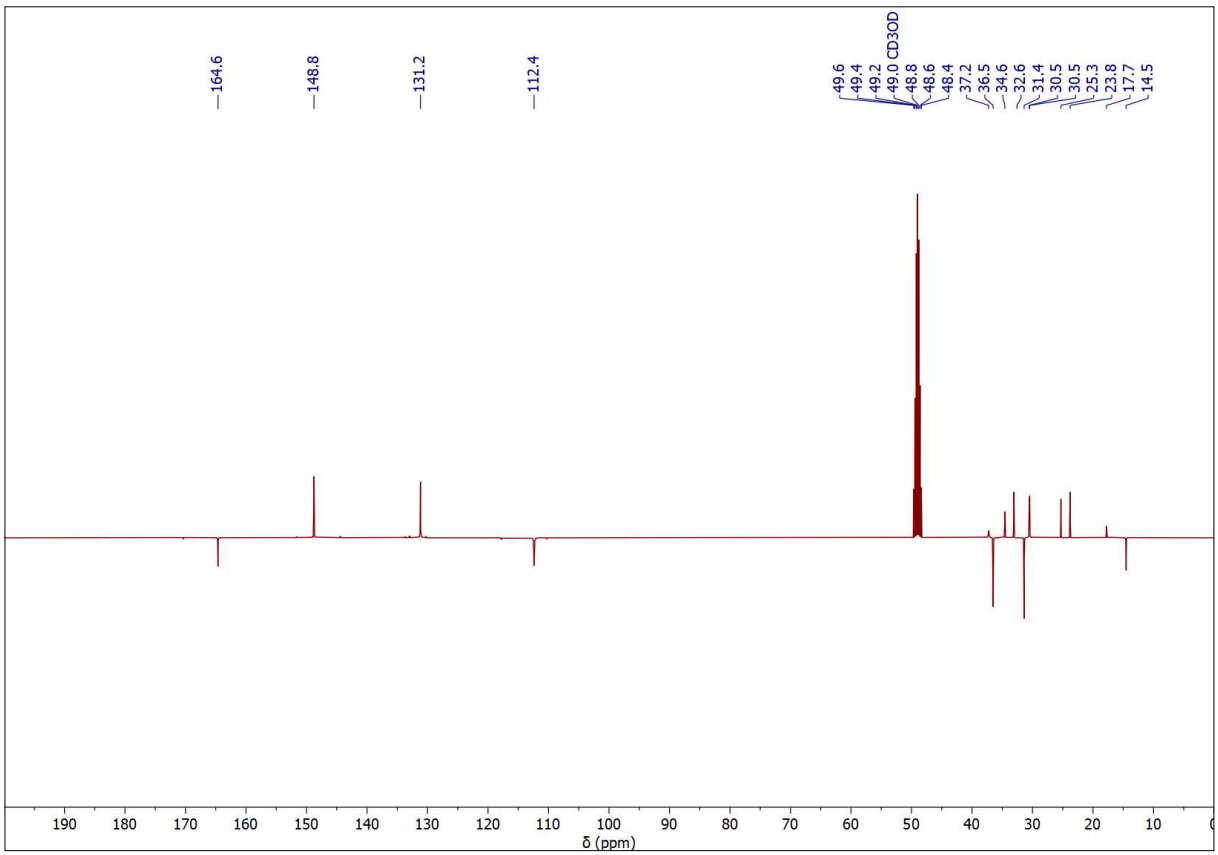

Figure S2. ^{13}C NMR spectrum of $C_4(SiC_8H_{17})_6Na_6DMF_{12}$ (**H**) in CD_3OD.

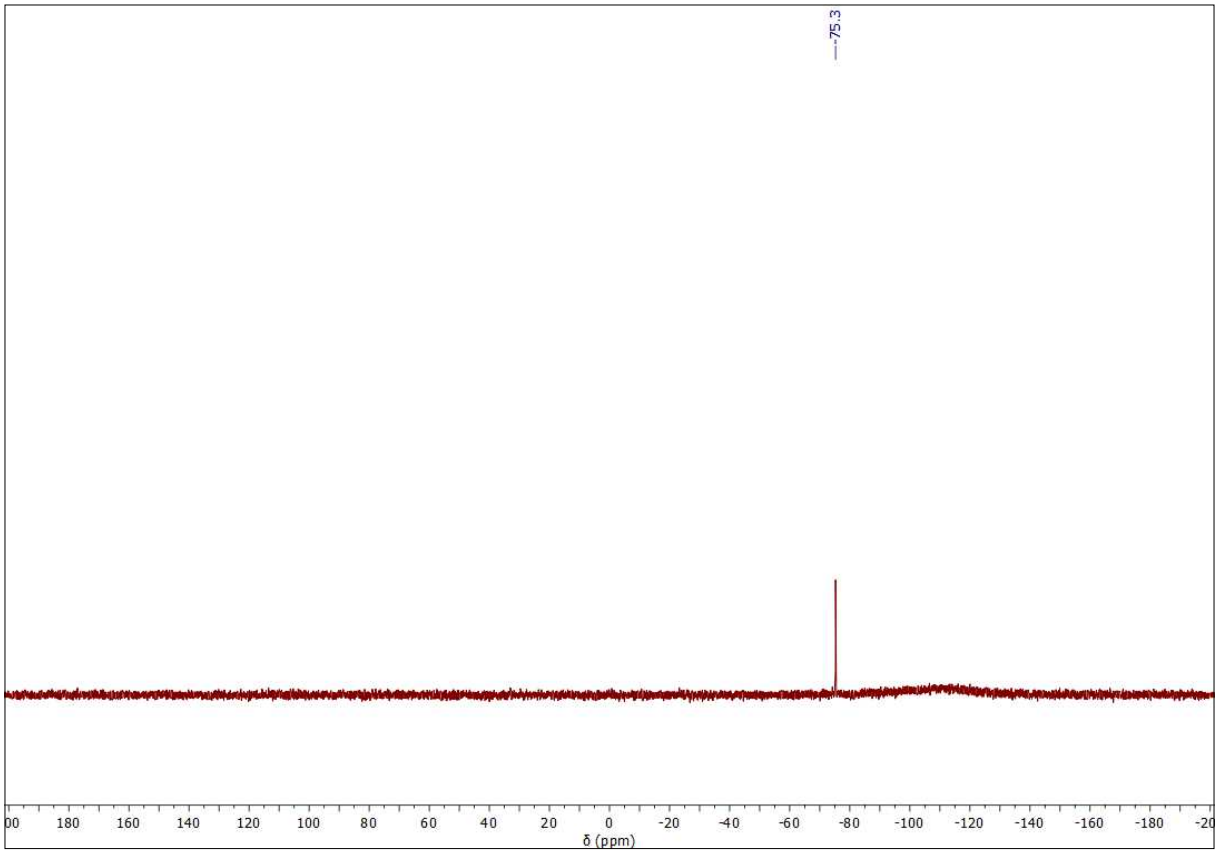

Figure S3. ^{29}Si NMR spectrum of $C_4(SiC_8H_{17})_6Na_6DMF_{12}$ (**H**) in CD_3OD.

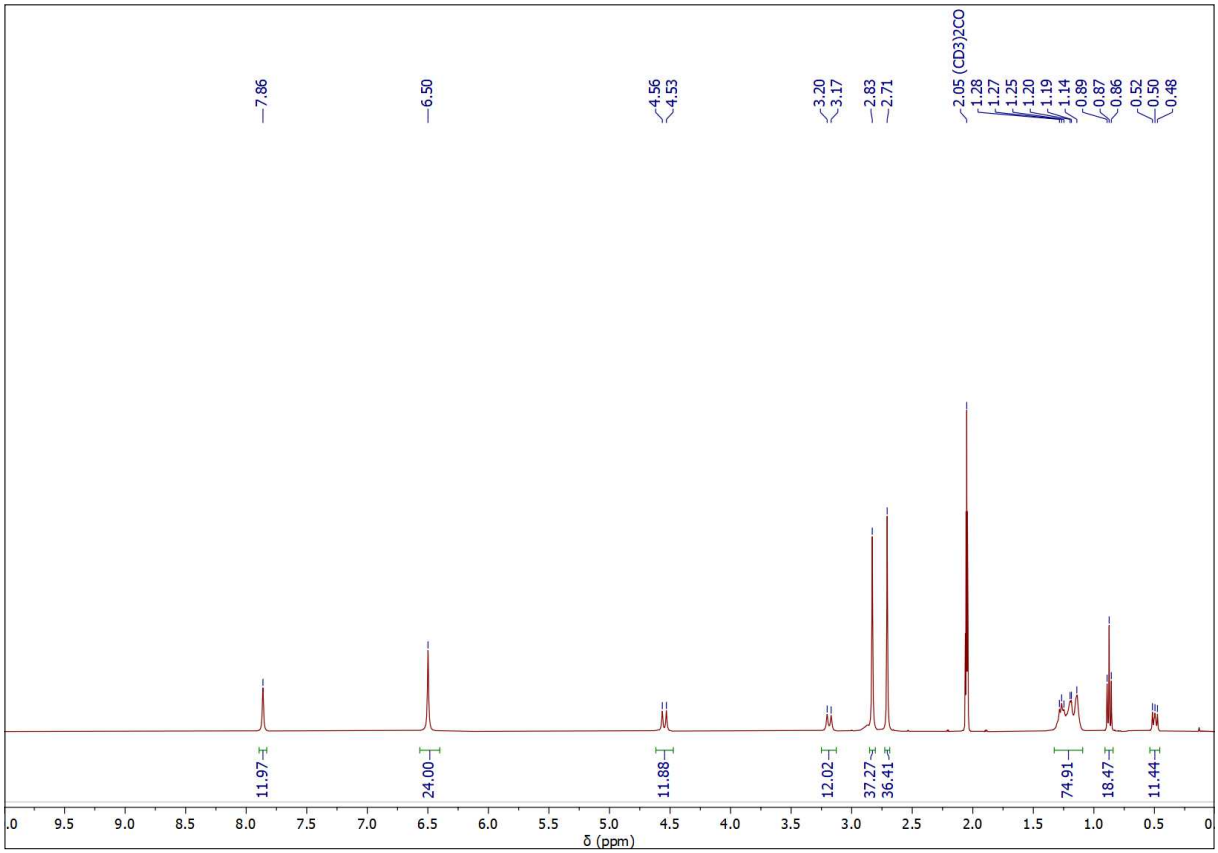

Figure S4. ^{1}H NMR spectrum of $C_4(SiC_8H_{17})_6Na_6DMF_{12}$ (**H**) in $(CD_3)_2CO$.

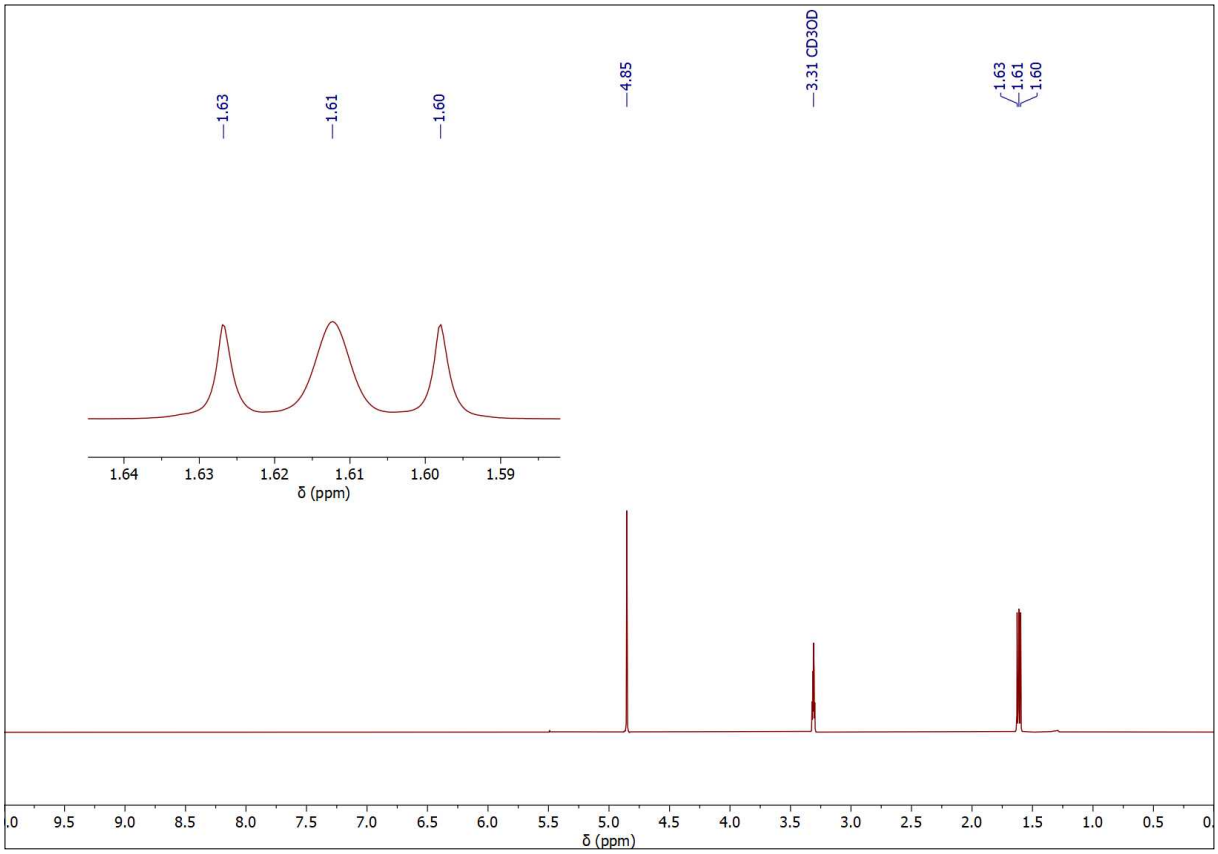

Figure S5. ^{1}H NMR spectrum of $(PMe_3)_2AuPF_6$ (**G**) in CD_3OD.

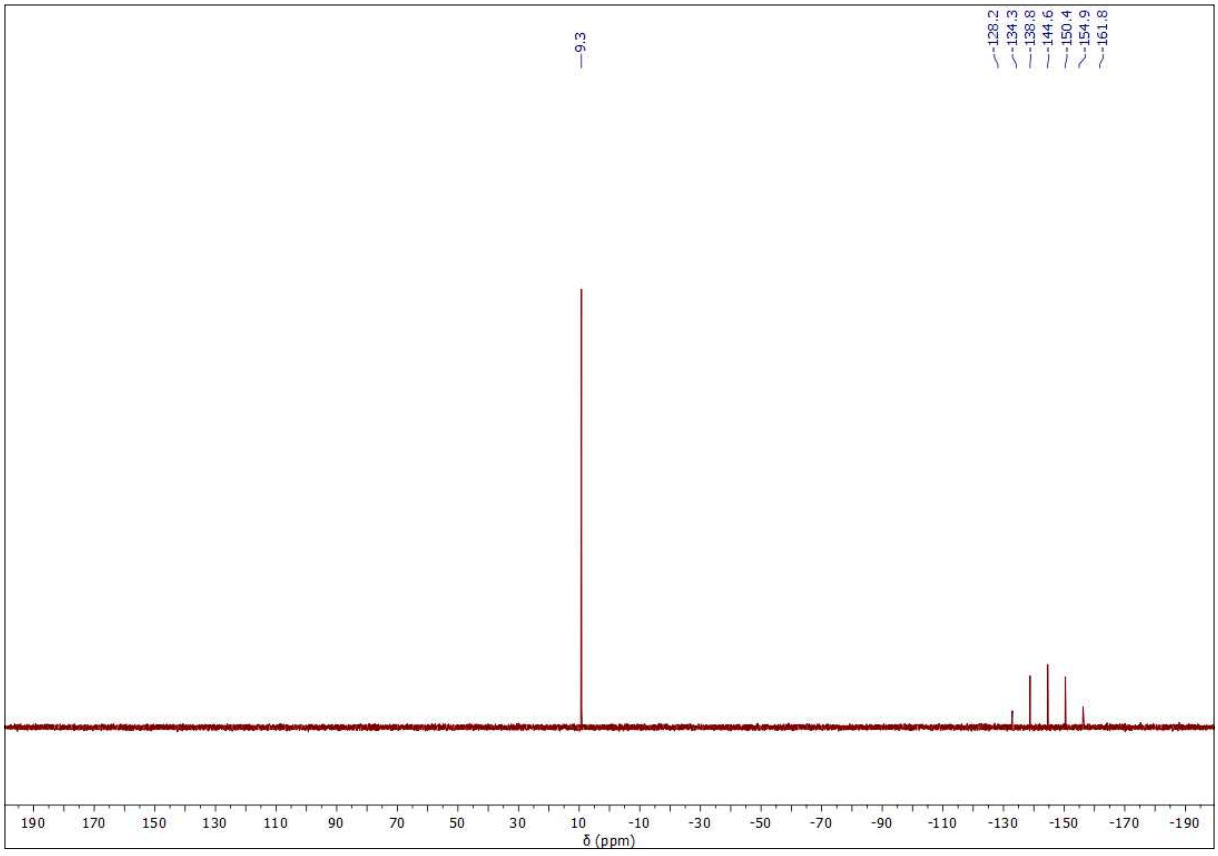

Figure S6. $^{31}P\{H\}$ NMR spectrum of $(PMe_3)_2AuPF_6$ (**G**) in CD_3OD.

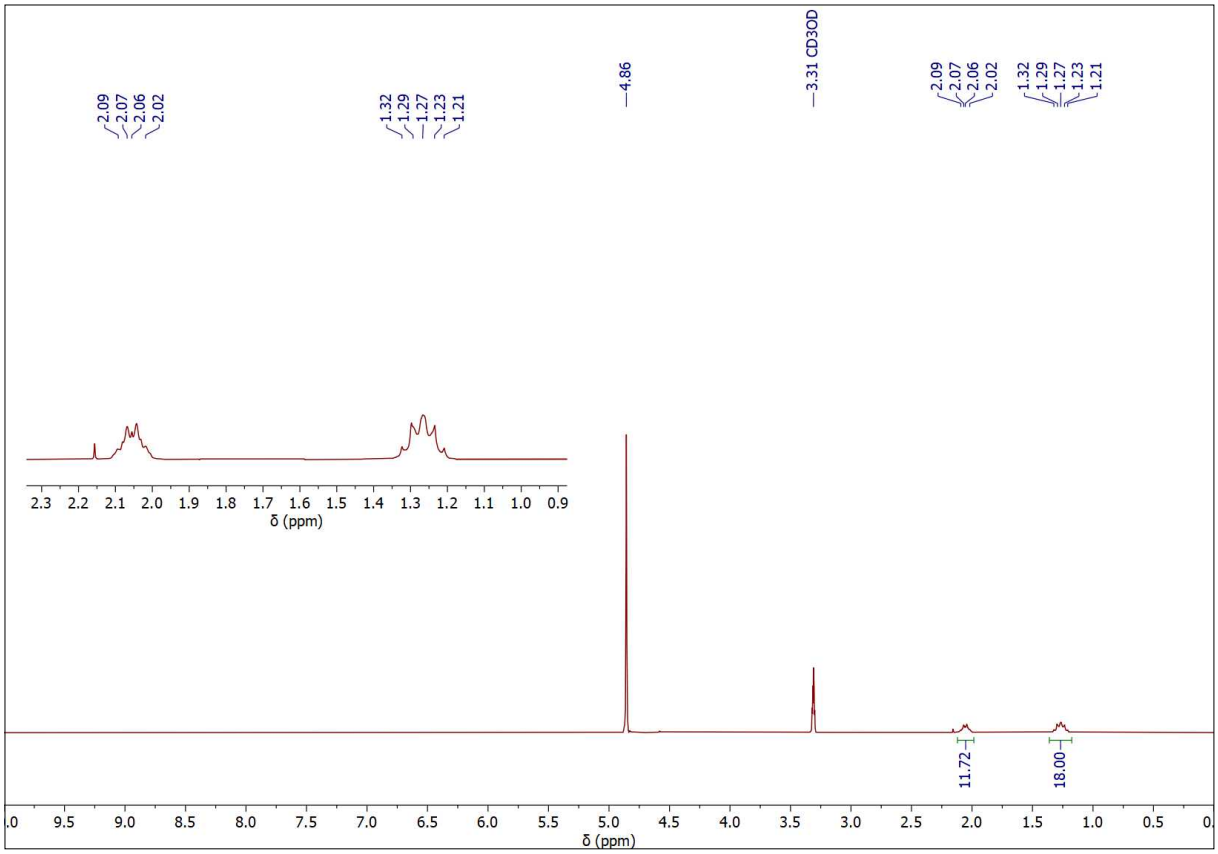

Figure S7. ^{1}H NMR spectrum of $(PEt_3)_2AuPF_6$ (**1**) in CD_3OD.

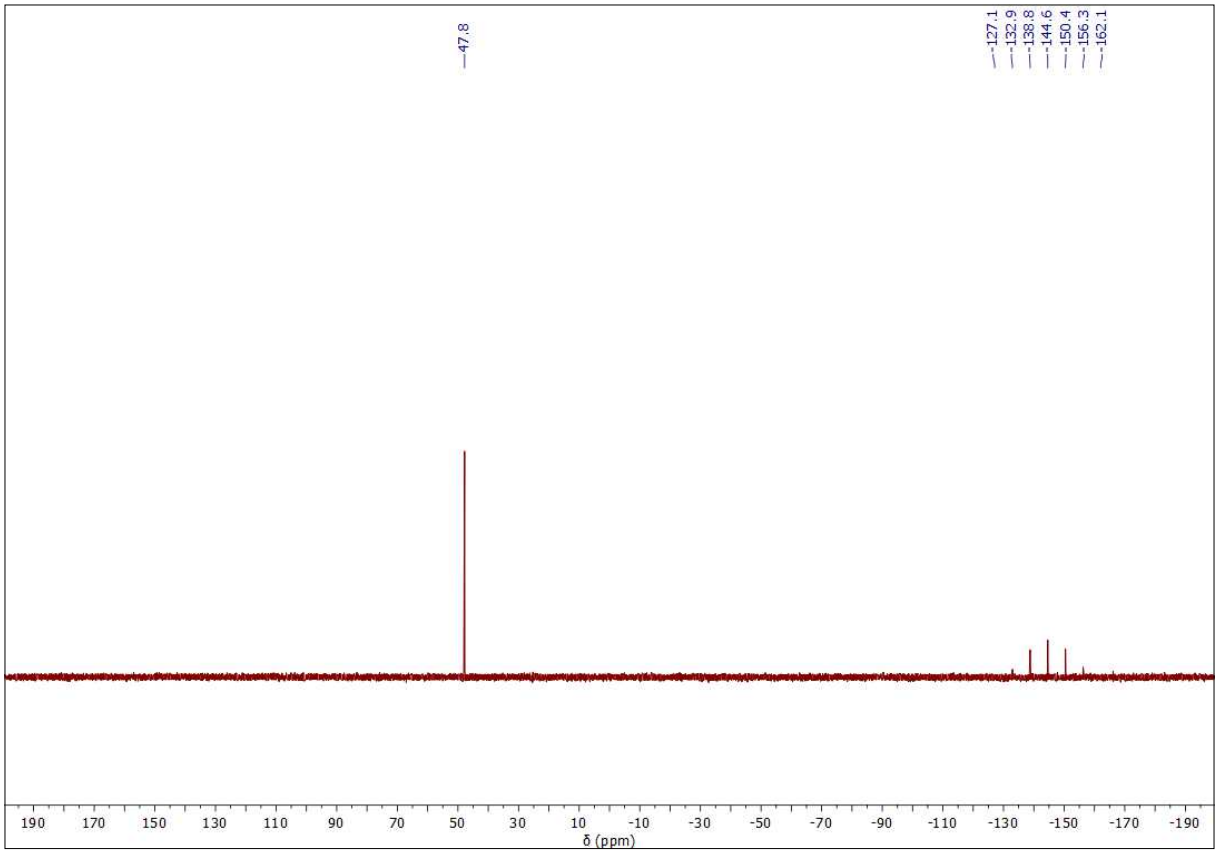

Figure S8. $^{31}P\{H\}$ NMR spectrum of $(PEt_3)_2AuPF_6$ (**1**) in CD_3OD.

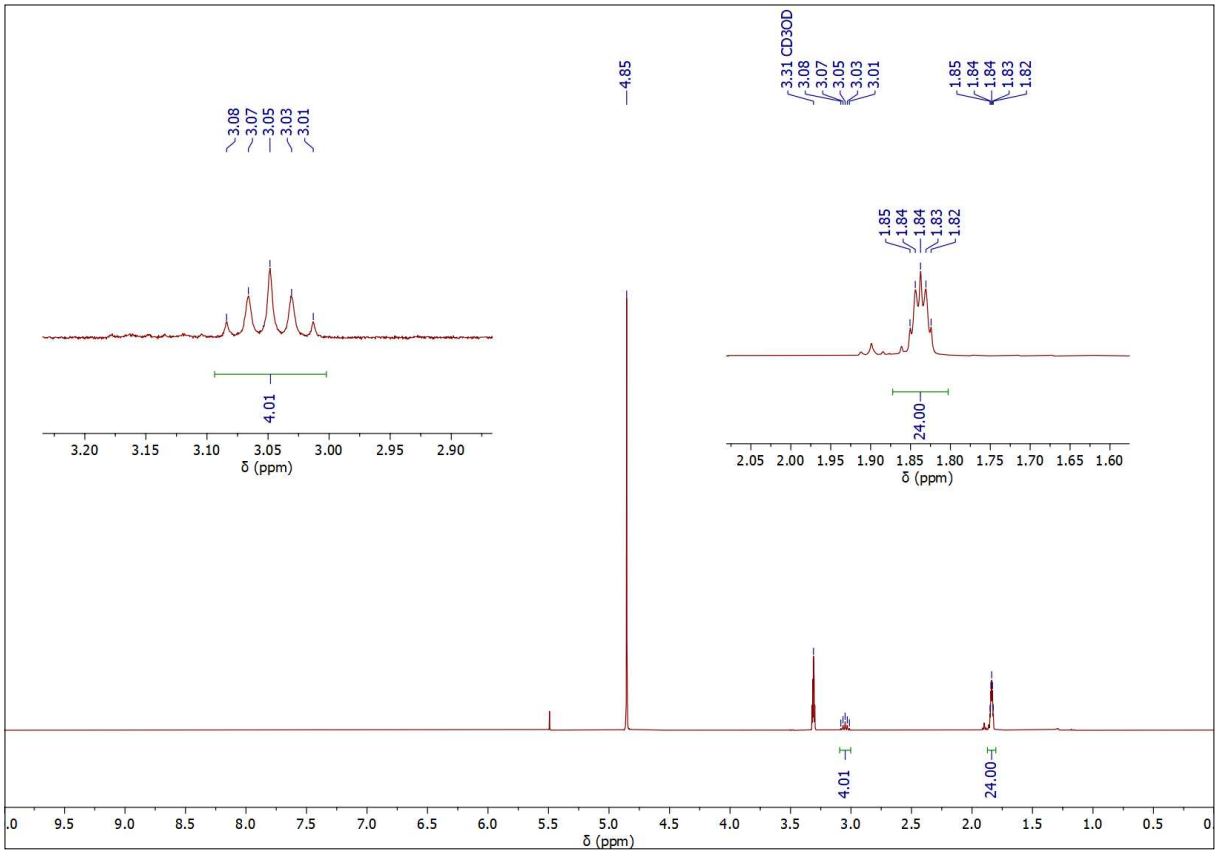

Figure S9. ^{1}H NMR spectrum of $dmpm_2(AuCl)_2$ (**2**) in CD_3OD.

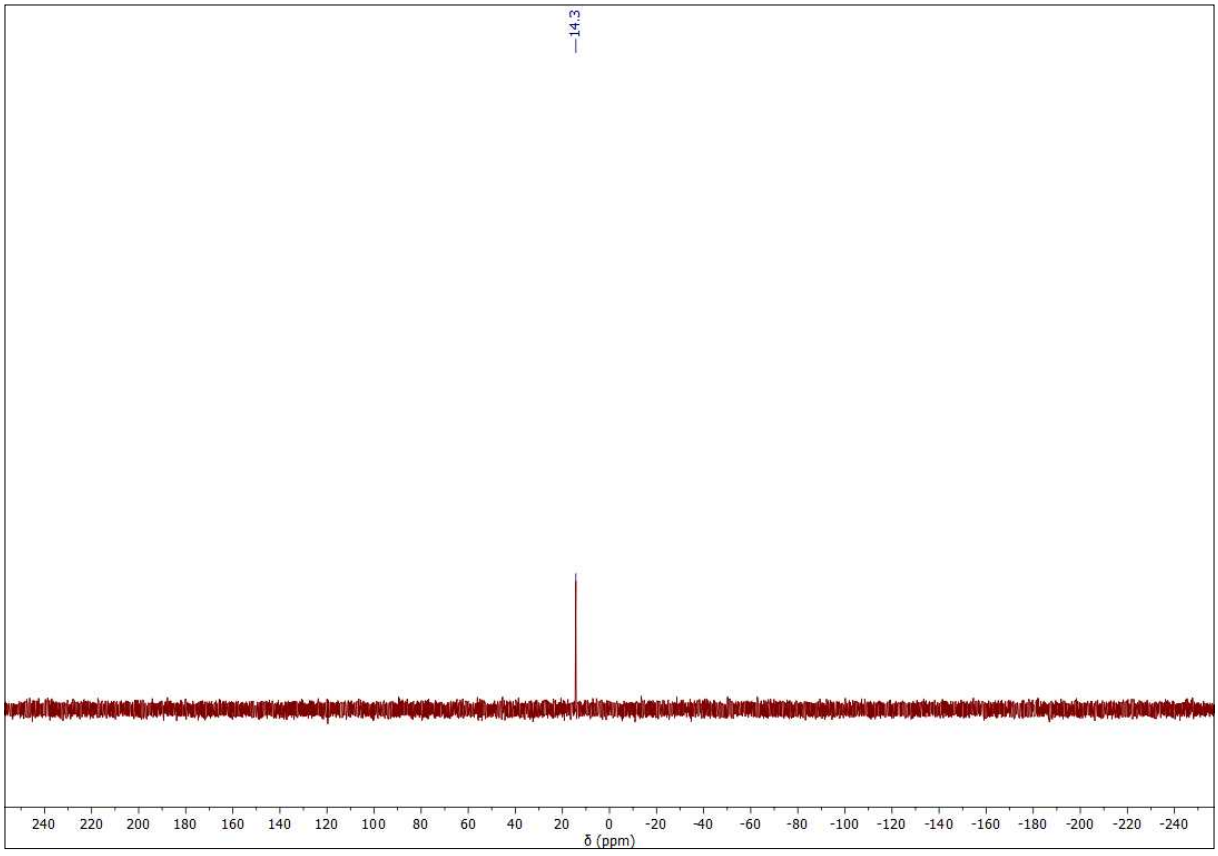

Figure S10. $^{31}P\{H\}$ NMR spectrum of $dmpm_2(AuCl)_2$ (**2**) in CD_3OD.

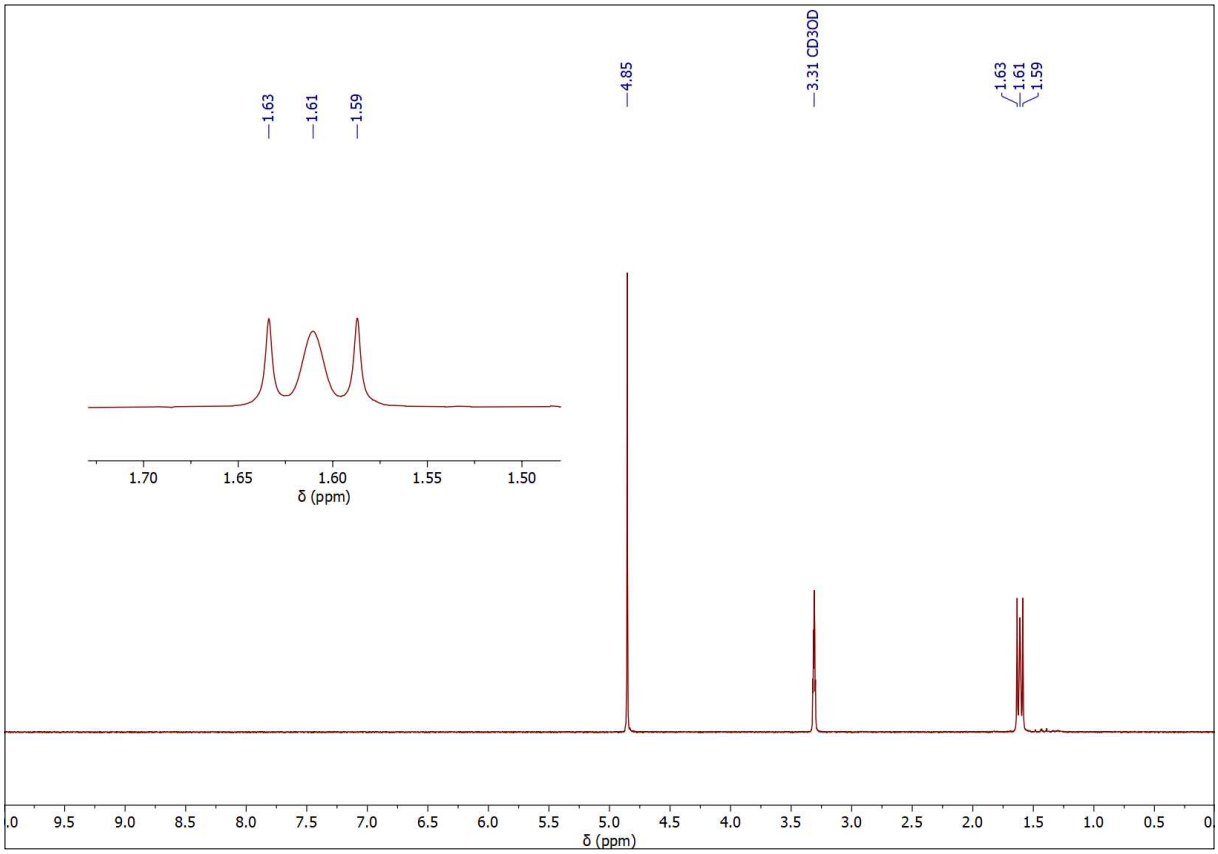

Figure S11. ^{1}H NMR spectrum of $(P^{t}Bu_3)_2AuPF_6$ (**3**) in CD_3OD.

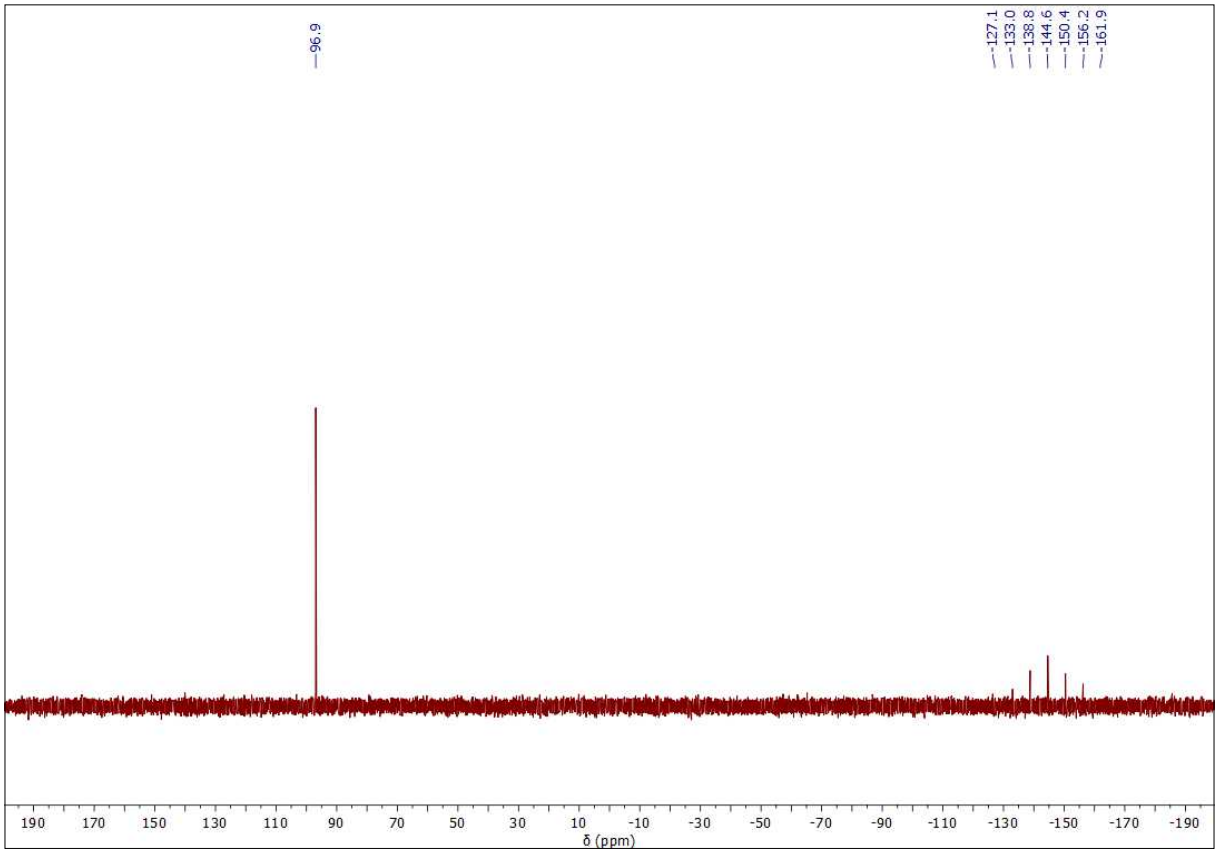

Figure S12. $^{31}P\{H\}$ NMR spectrum of $(P^{t}Bu_3)_2AuPF_6$ (**3**) in CD_3OD.

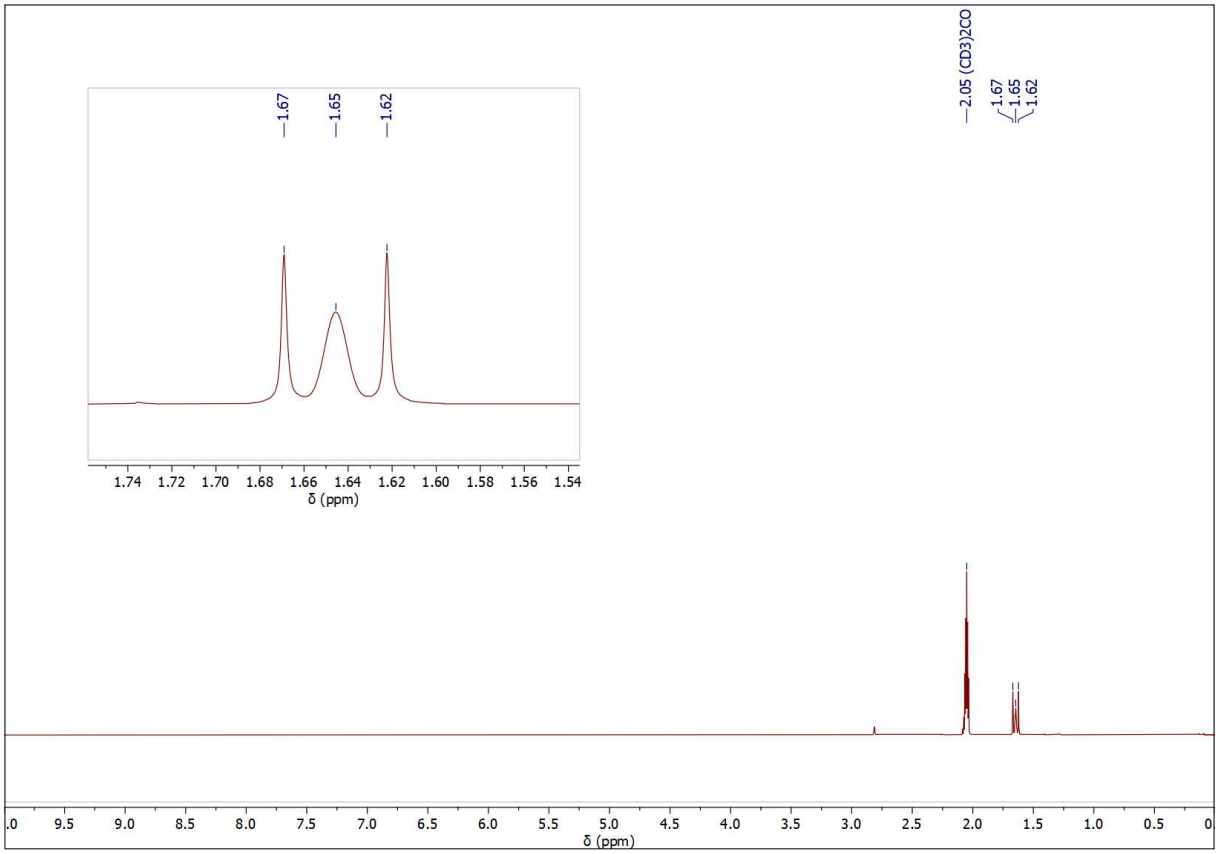

Figure S13. ^{1}H NMR spectrum of $(P^{t}Bu_3)_2AuPF_6$ (**3**) in $(CD_3)_2CO$.

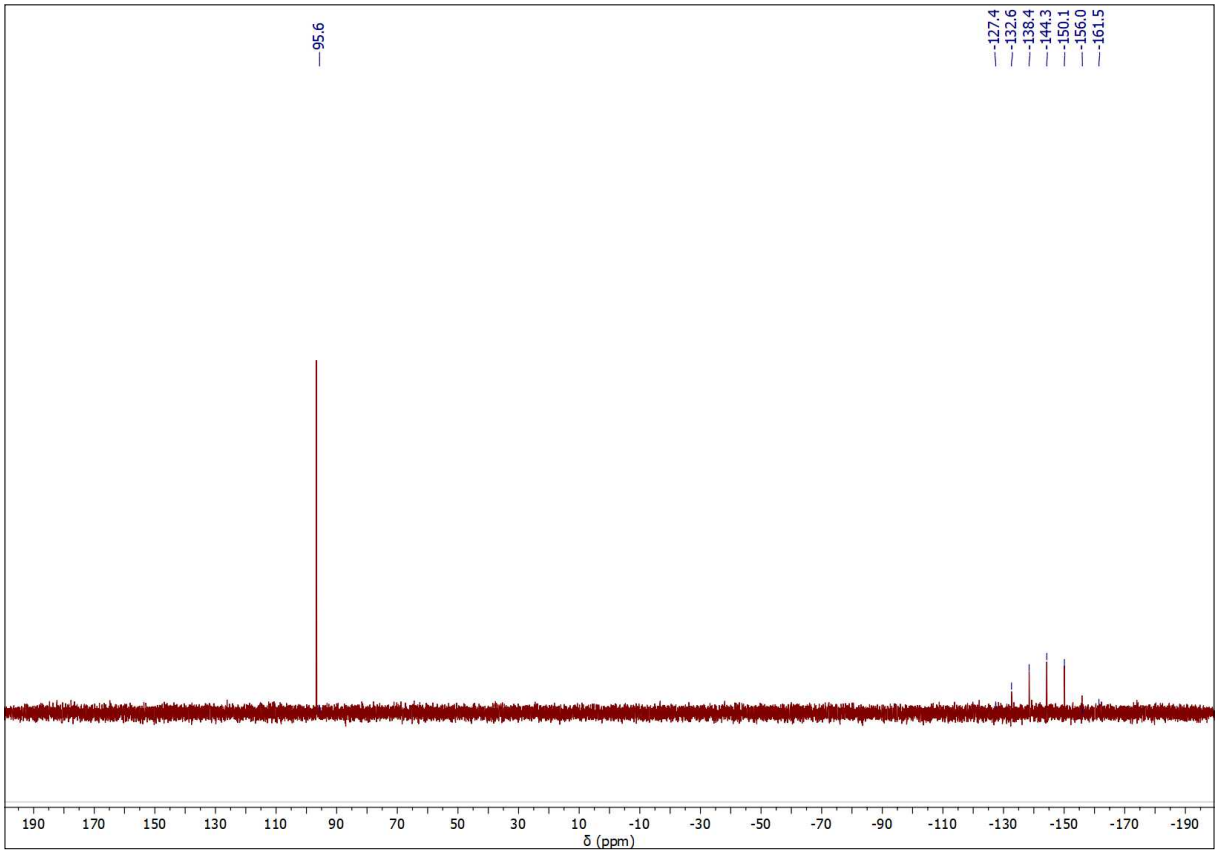

Figure S14. ^{31}P{H} NMR spectrum of $(P^{t}Bu_3)_2AuPF_6$ (**3**) in $(CD_3)_2CO$.

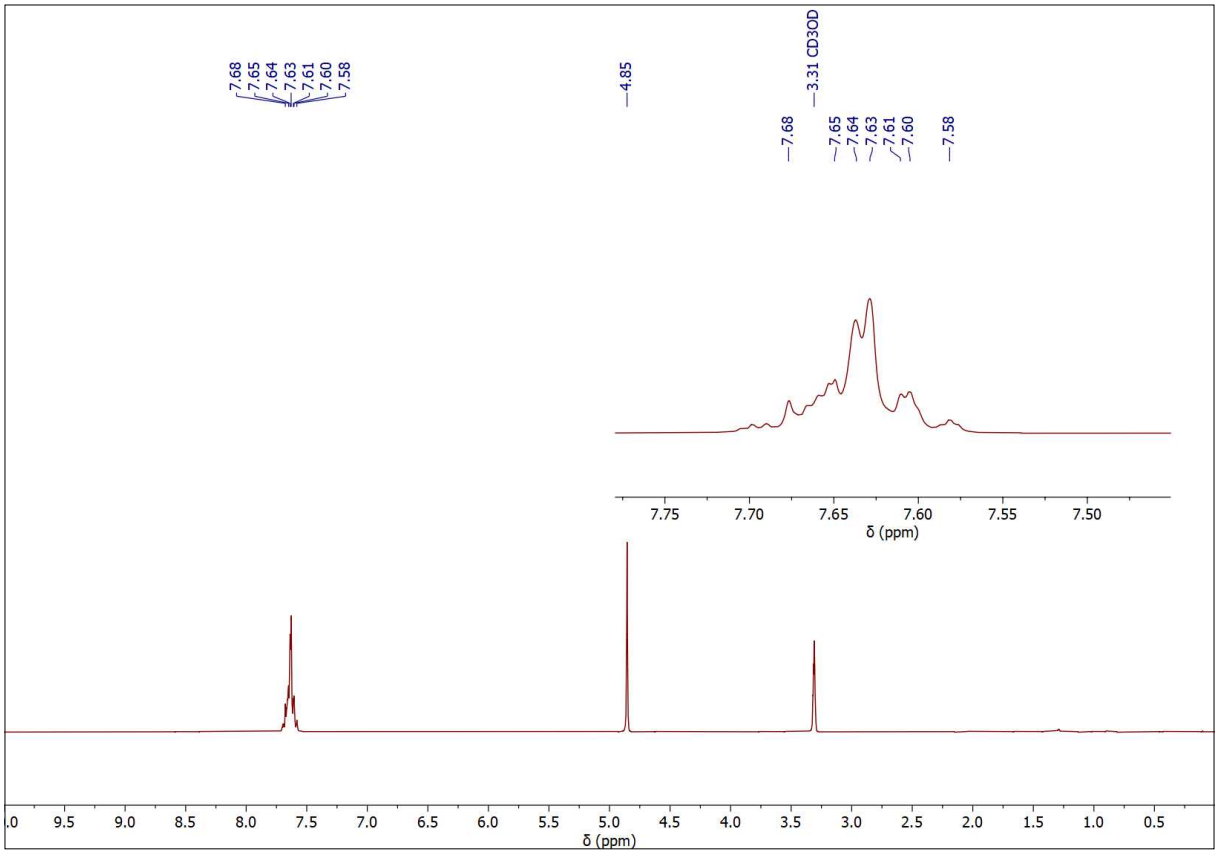

Figure S15. ^{1}H NMR spectrum of $(PPh_3)_2AuPF_6$ (**4**) in CD_3OD.

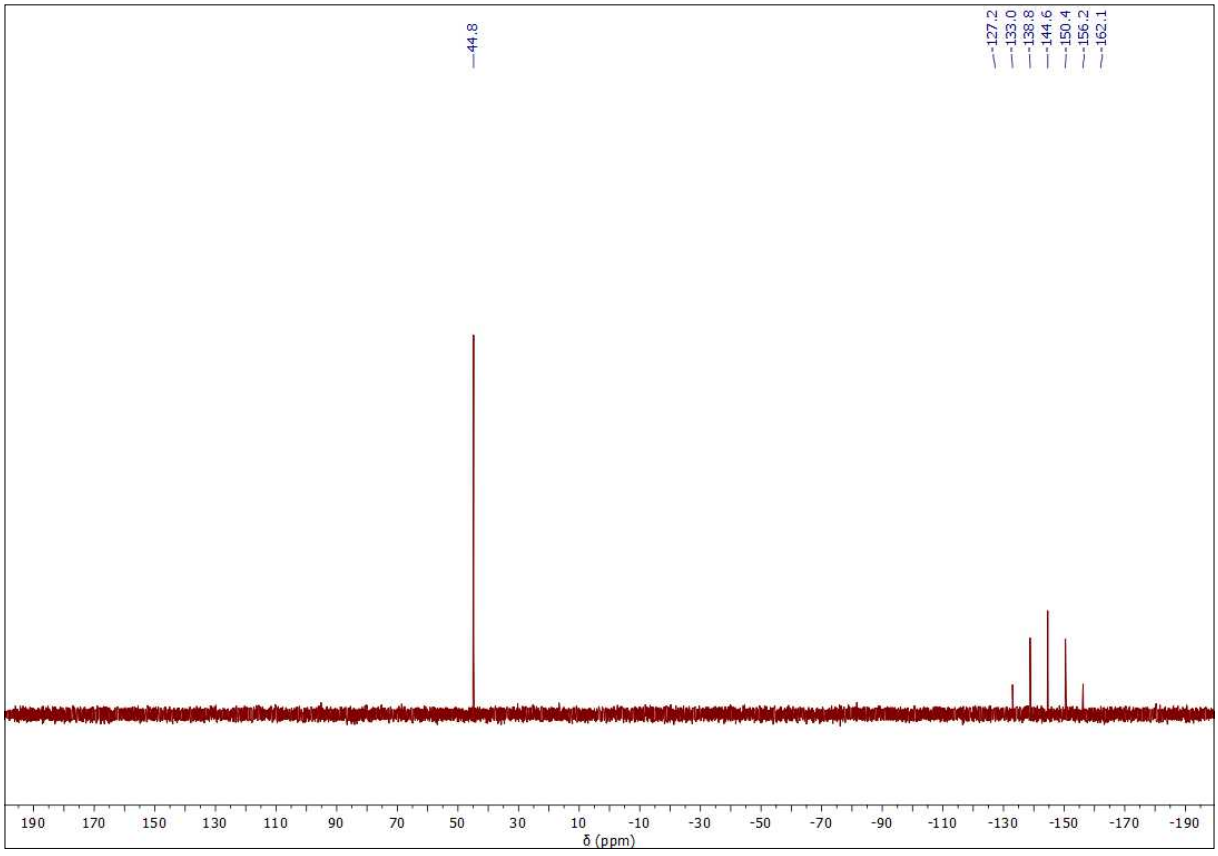

Figure S16. $^{31}P\{H\}$ NMR spectrum of $(PPh_3)_2AuPF_6$ (**4**) in CD_3OD.

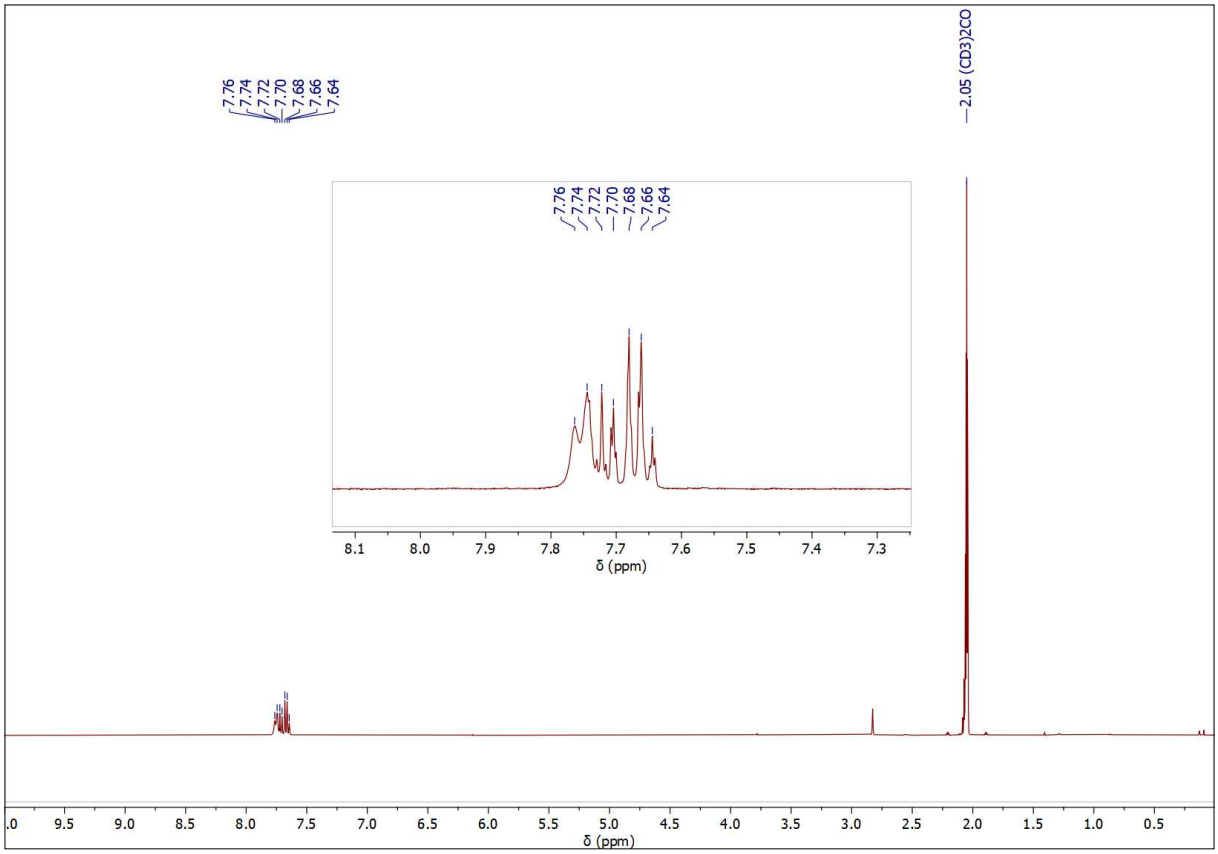

Figure S17. ^{1}H NMR spectrum of $(PPh_3)_2AuPF_6$ (**4**) in $(CD_3)_2CO$.

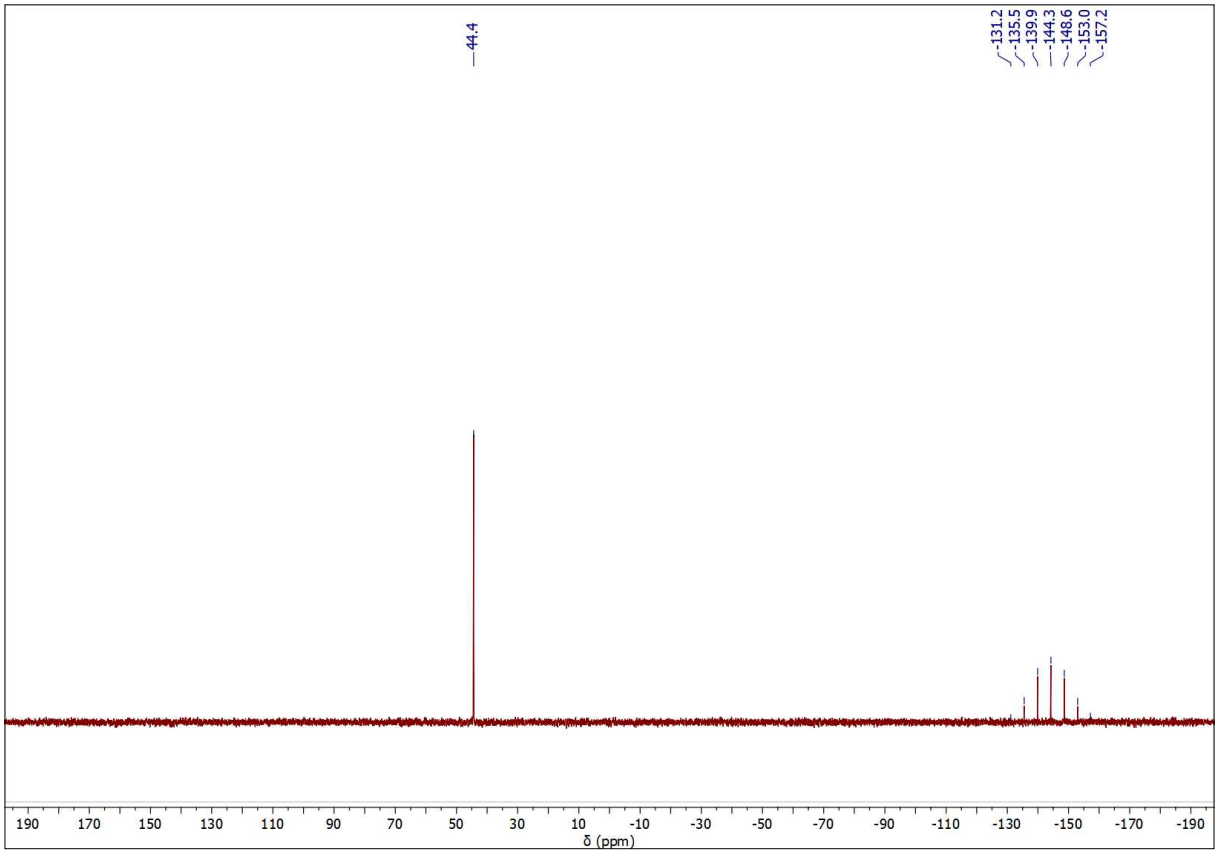

Figure S18. $^{31}P\{H\}$ NMR spectrum of $(PPh_3)_2AuPF_6$ (**4**) in $(CD_3)_2CO$.

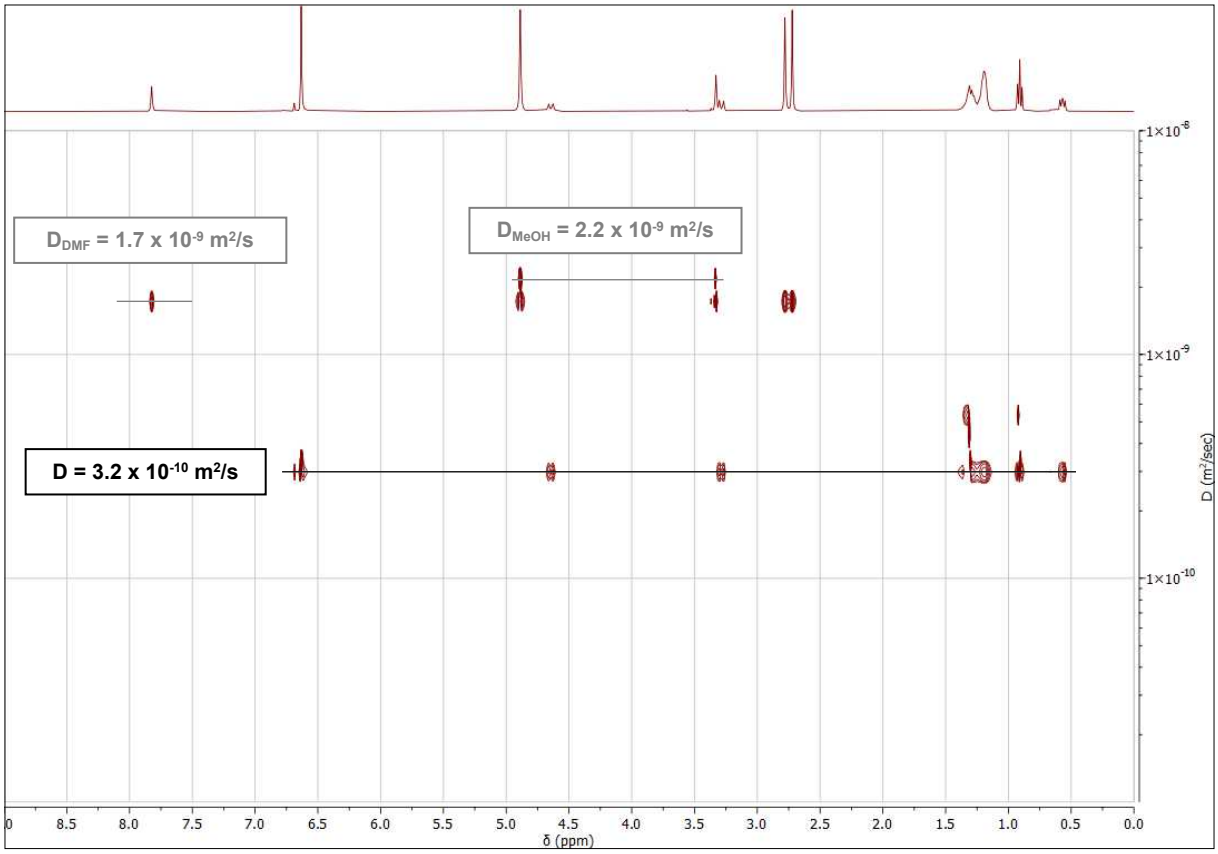

Figure S19. ^{1}H DOSY NMR spectrum of $C_4(SiC_8H_{17})_6Na_6DMF_{12}$ (**H**) in CD_3OD. (D = diffusion coefficient, Δ=120 ms, δ=1000 μs).

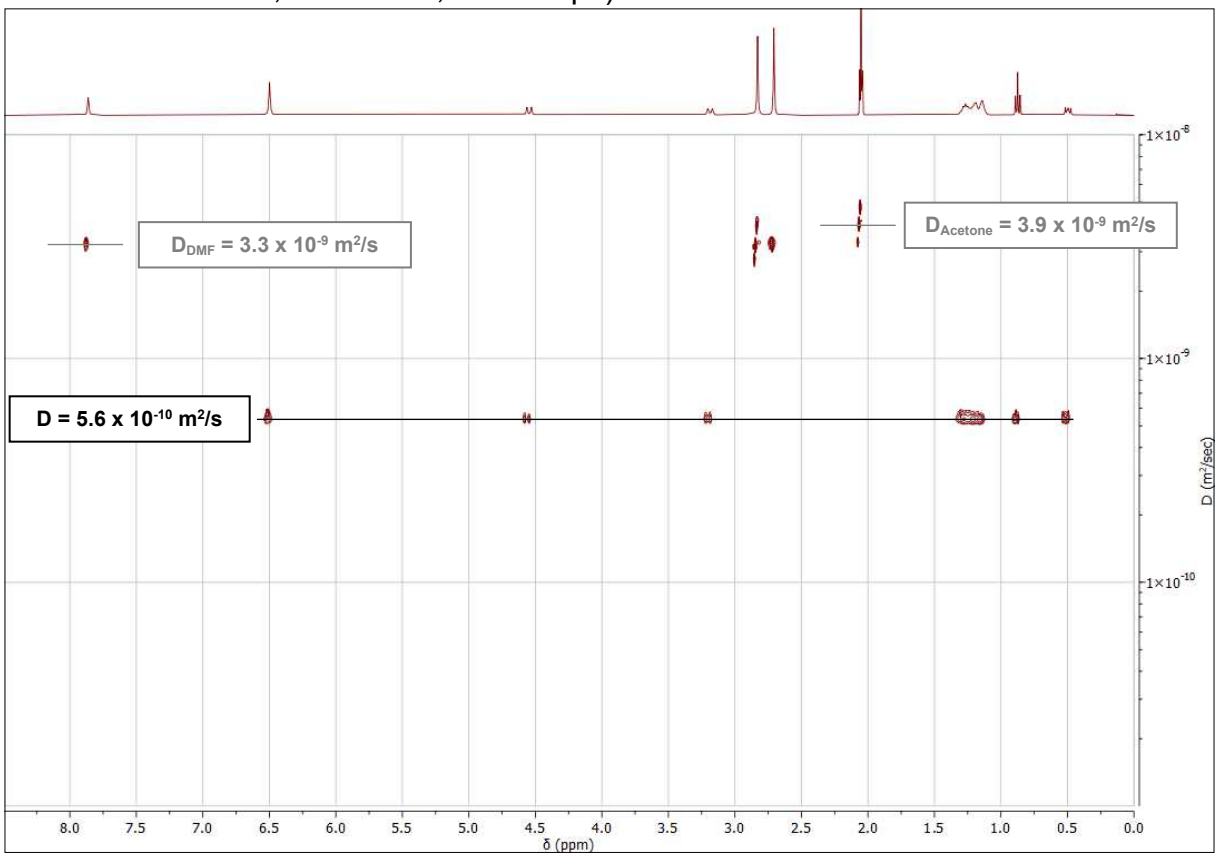

Figure S20. ^{1}H DOSY NMR spectrum of $C_4(SiC_8H_{17})_6Na_6DMF_{12}$ (**H**) in $(CD_3)_2CO$. (Δ=110 ms, δ=1000 μs).

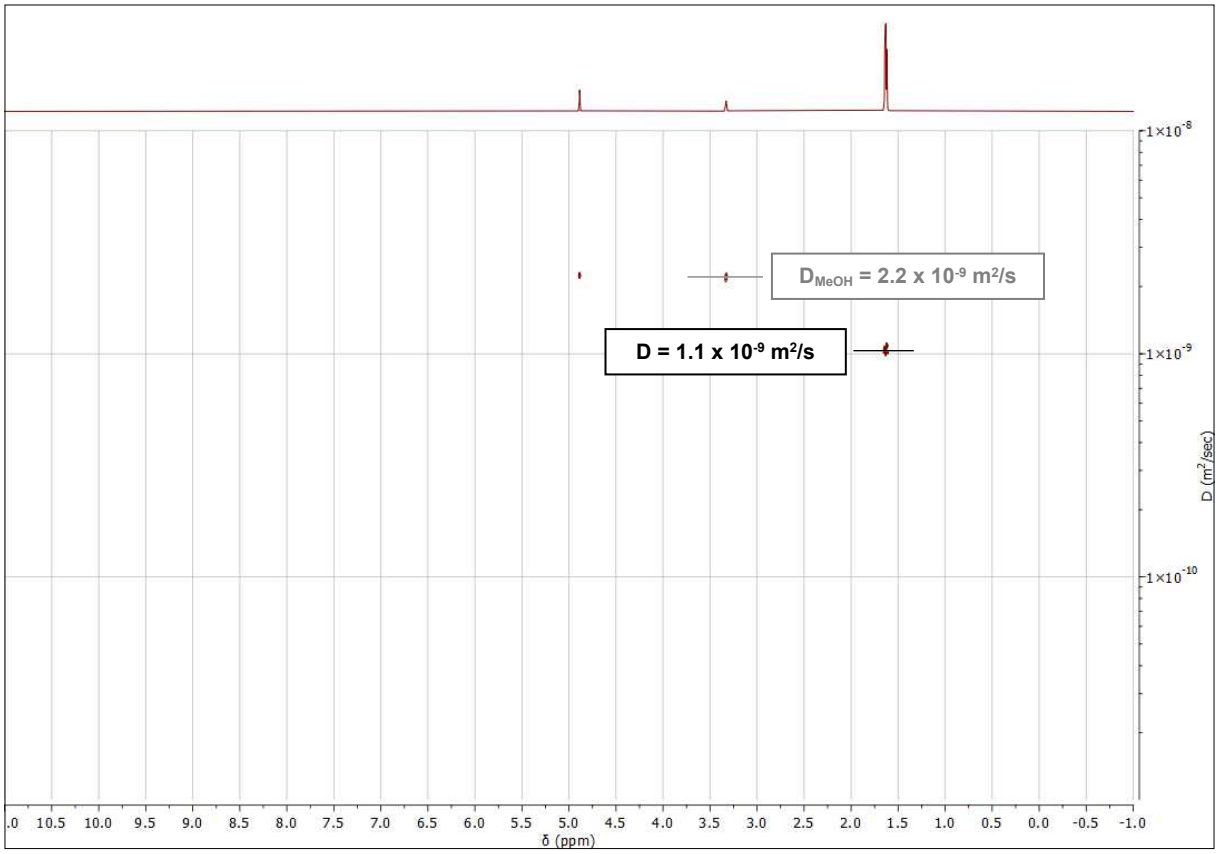

Figure S21. ^{1}H DOSY NMR spectrum of $(PMe_3)_2AuPF_6$ in (**G**) CD_3OD. (Δ=100 ms, δ=800 μs).

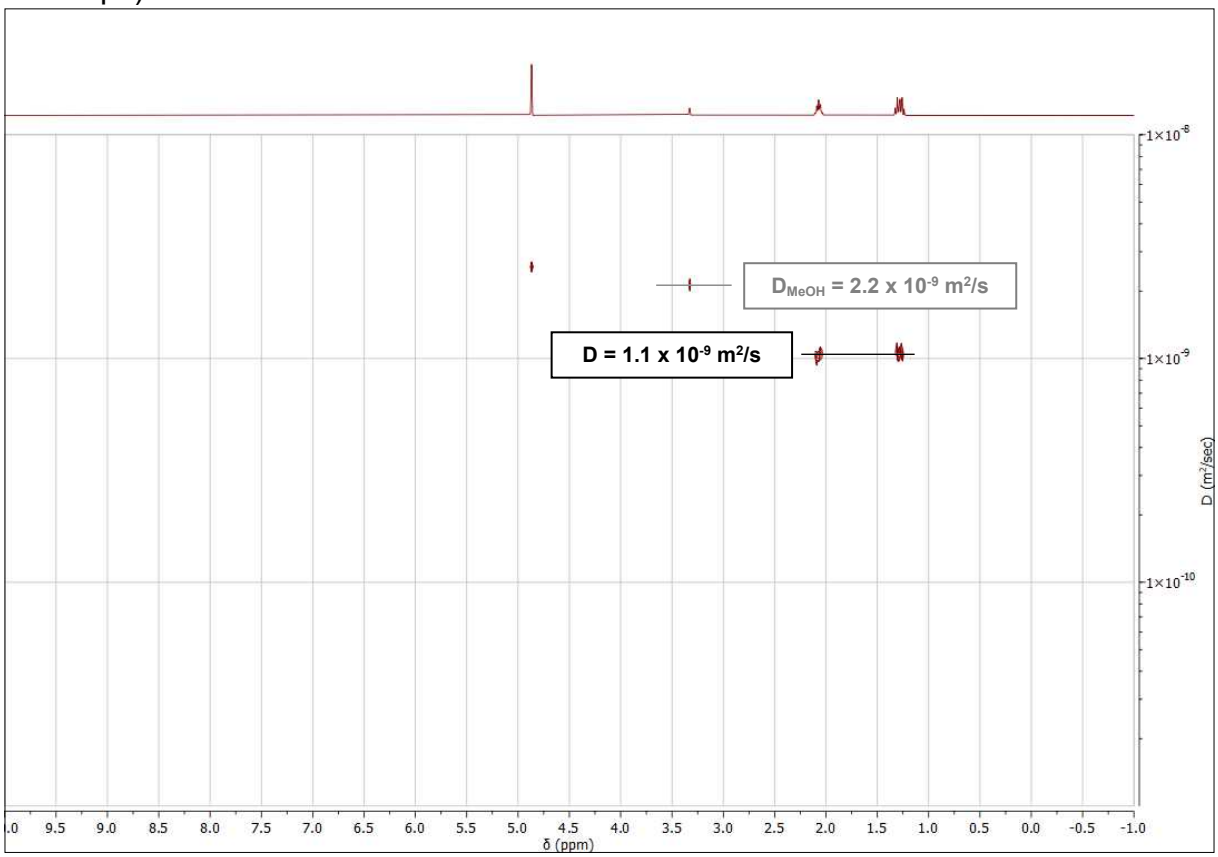

Figure S22. ^{1}H DOSY NMR spectrum of $(PEt_3)_2AuPF_6$ in (**1**) CD_3OD. (Δ=100 ms, δ=800 μs).

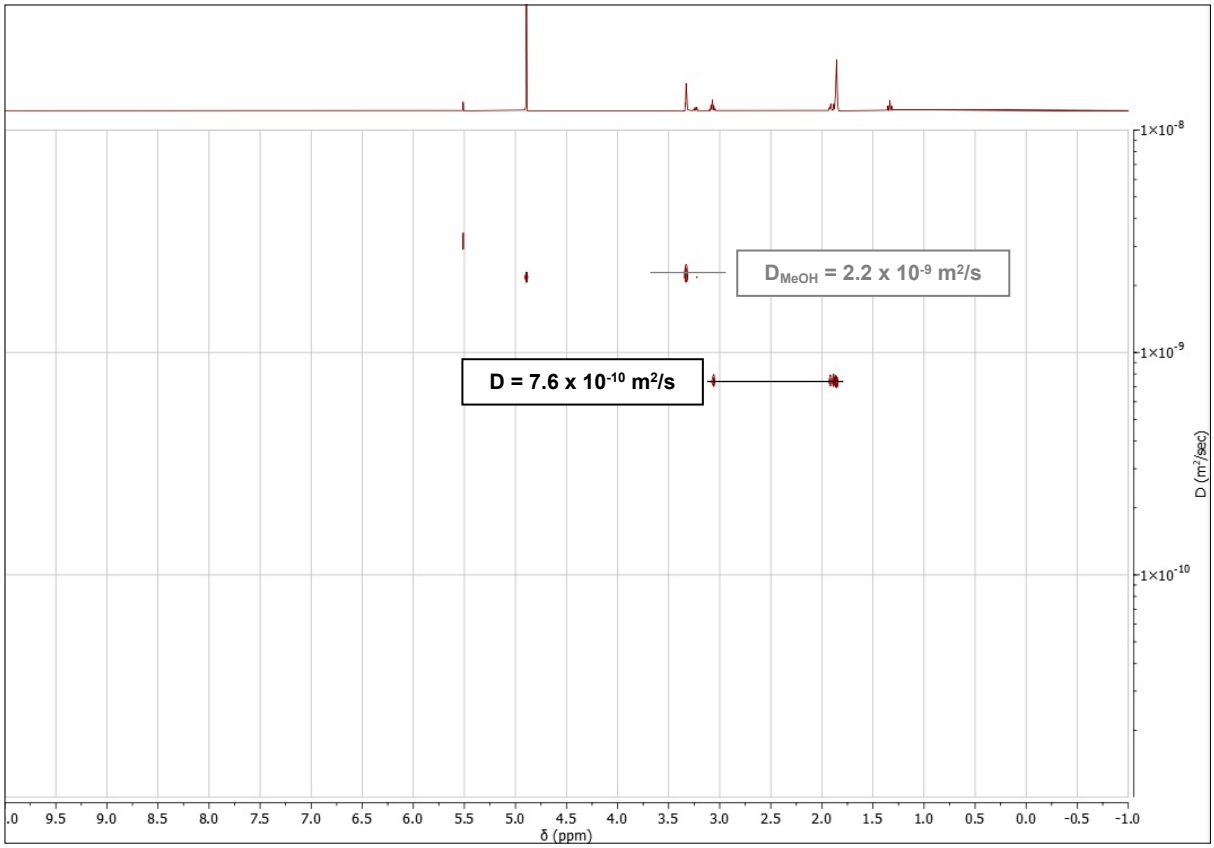

Figure S23. ^{1}H DOSY NMR spectrum of $dmpm_2(AuCl)_2$ (**2**) CD_3OD. (Δ=100 ms, δ=800 μs).

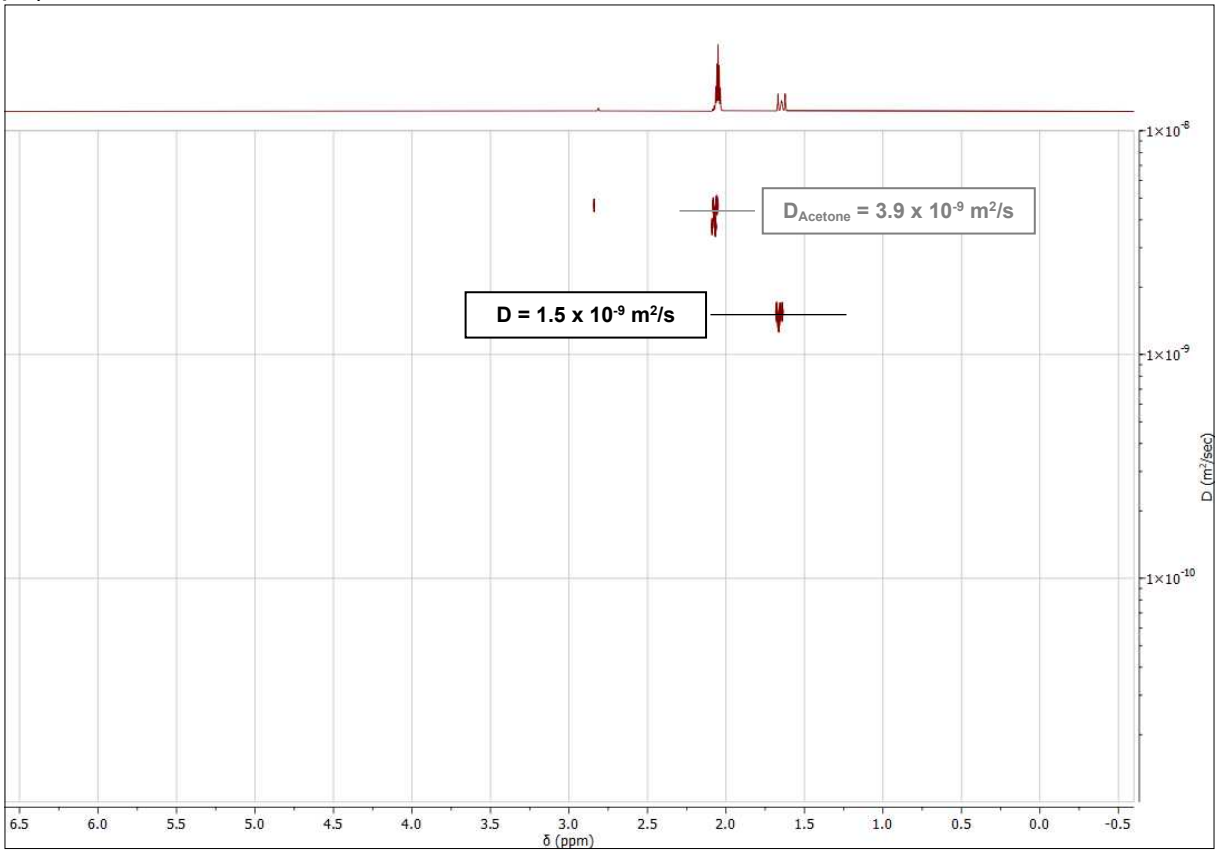

Figure S24. ^{1}H DOSY NMR spectrum of $(P^tBu_3)_2AuPF_6$ (**3**) in $(CD_3)_2CO$. (Δ=60 ms, δ=800 μs).

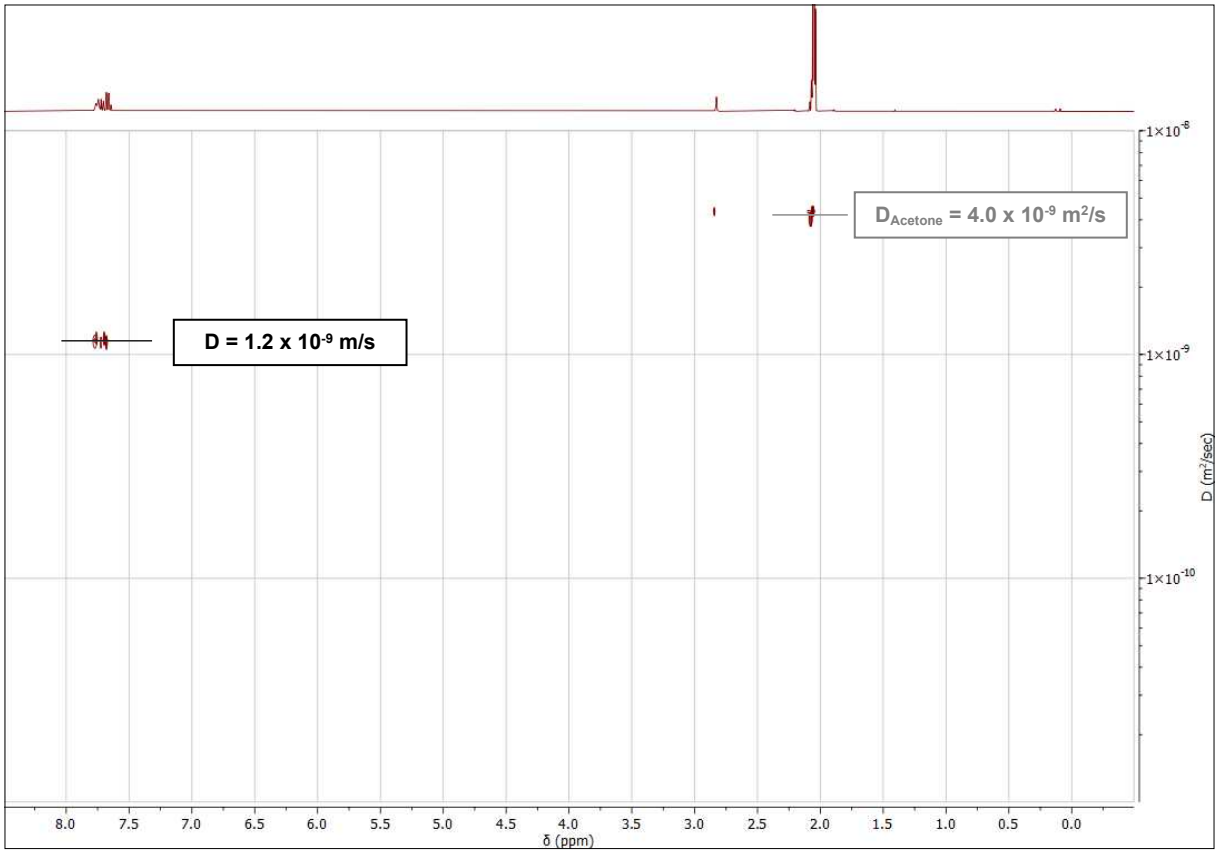

Figure S25. ^{1}H DOSY NMR spectrum of $(PPh_3)_2AuPF_6$ (**4**) in $(CD_3)_2CO$. (Δ=80 ms, δ=800 μs).

5. Solubility tests:

The analogous **H-Ph** was synthesized under identical conditions as **H** but by using the corresponding silane ($PhSiOMe_3$).

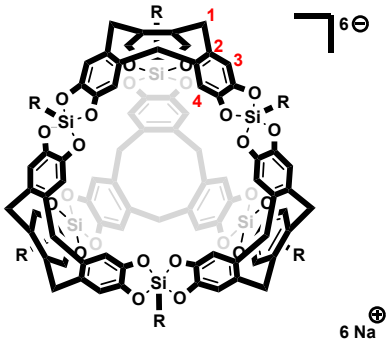

H (R = $^{n}C_8H_{17}$)

H-Ph (R = Ph)

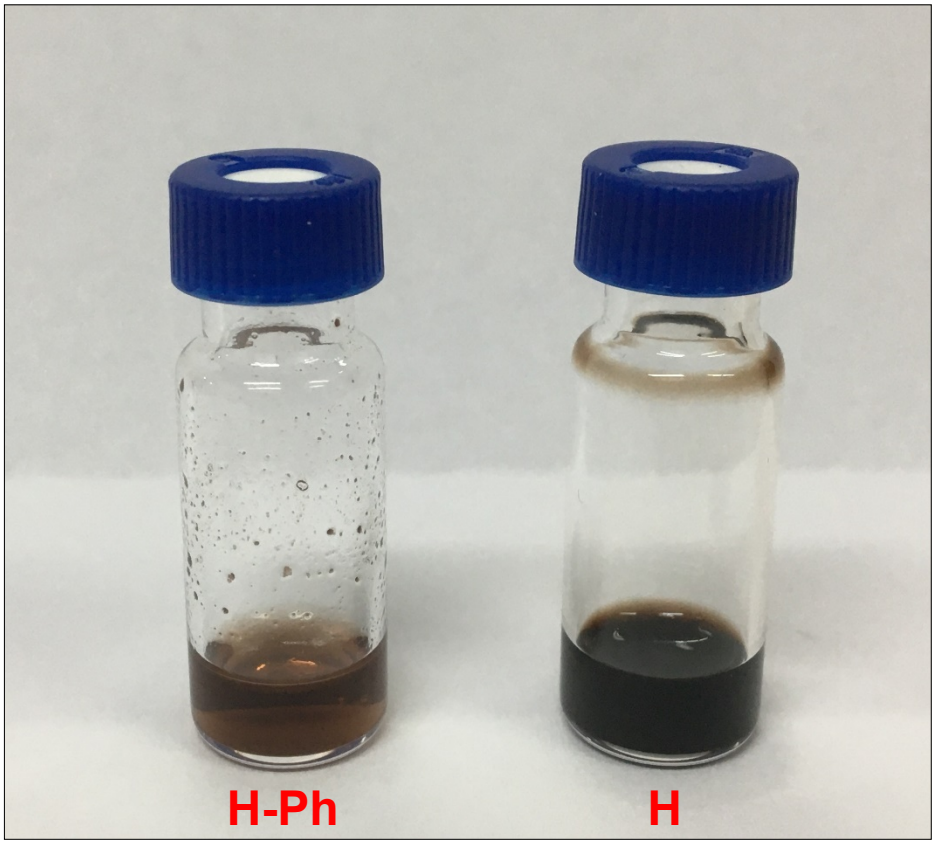

Figure S26. Vials containing 8 mg of **H-Ph** (left) and 75 mg of **H** (right) in 0.25 mL MeOH. Even at a significantly lower concentration (and after sonication), there is some insoluble material in the solution of **H-Ph**. In contrast, **H** can be solubilized at a much higher concentration, even without sonication.

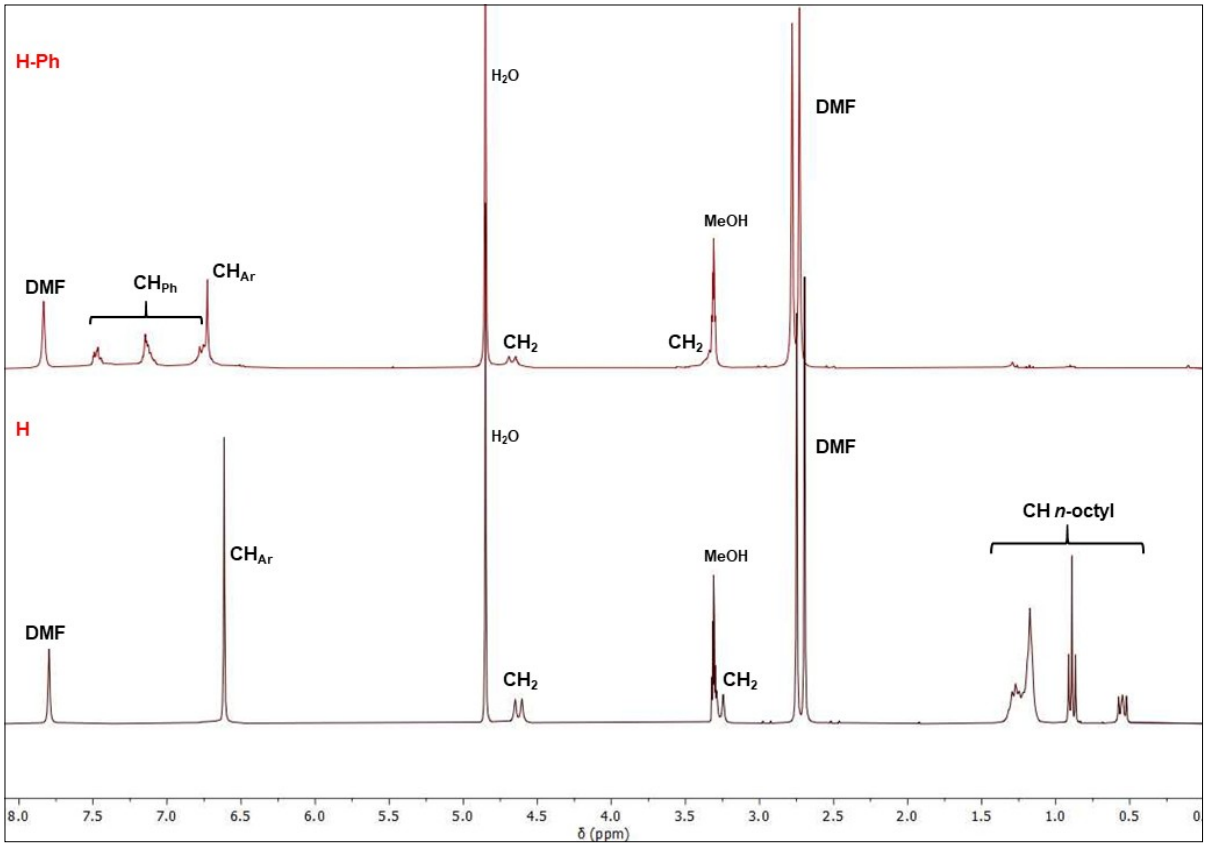

Figure S27. ^{1}H-NMR spectra of **H-Ph** and **H** at equimolar concentrations in CD_3OD. Note that the peaks of **H-Ph** are less intense and generally broader than those of **H**.

6. Encapsulation studies:

Encapsulation experiments were carried out in the depicted deuterated solvents. In each experiment, 0.005 mmol of **H** was dissolved in 0.5 mL of the deuterated solvent and the corresponding amount of guest was added. The **H**-guest stoichiometry was verified each time by integration of the corresponding ^{1}H NMR signals. In some cases (e.g. **H** + **1**) signals of the guest overlapped with that of the cage.
When mixing **3** or **4** with **H** an instantaneous precipitation occurred in CD_3OD, which prevented NMR characterization. Therefore, these encapsulation experiments were carried out in $(CD_3)_2CO$.

6.1 Encapsulation studies with $(dmpm)_2(AuCl)_2$ (2):

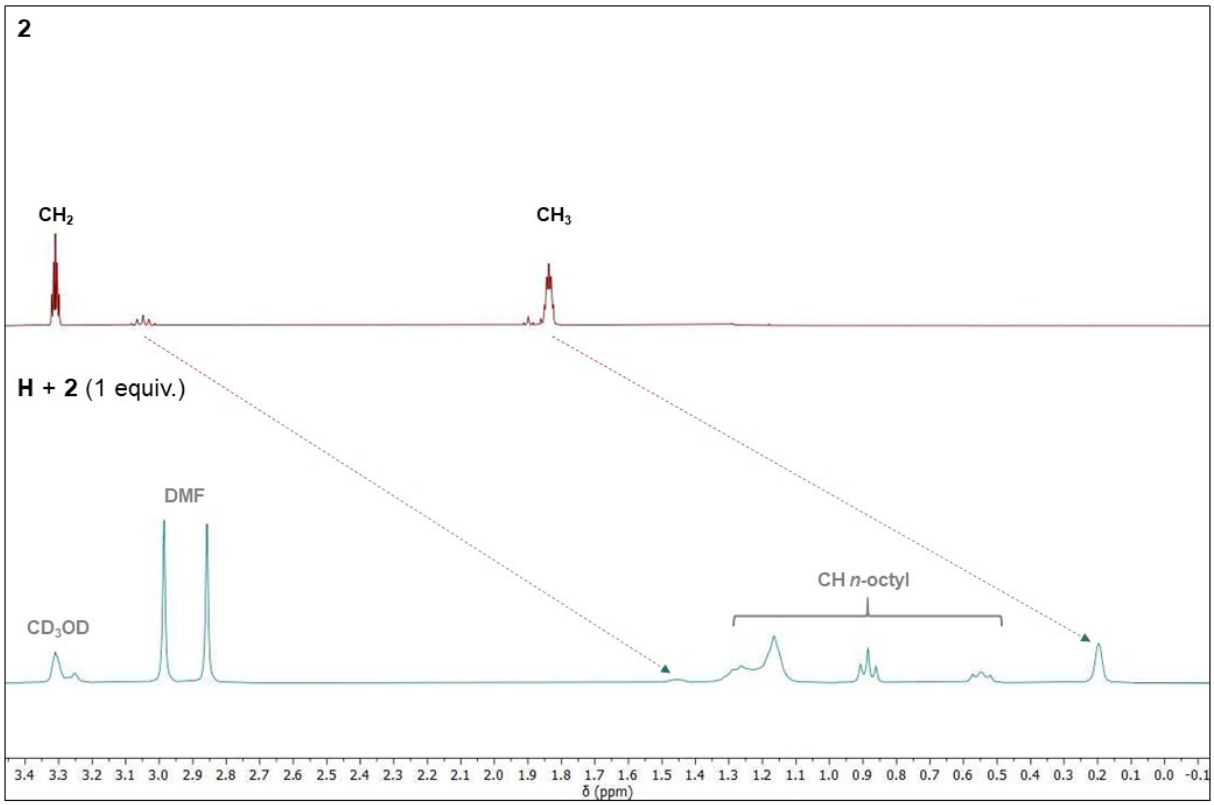

Figure S28. ^{1}H NMR spectra of **2** and **H** in the presence of 1 equivalent of **2** in CD_3OD.

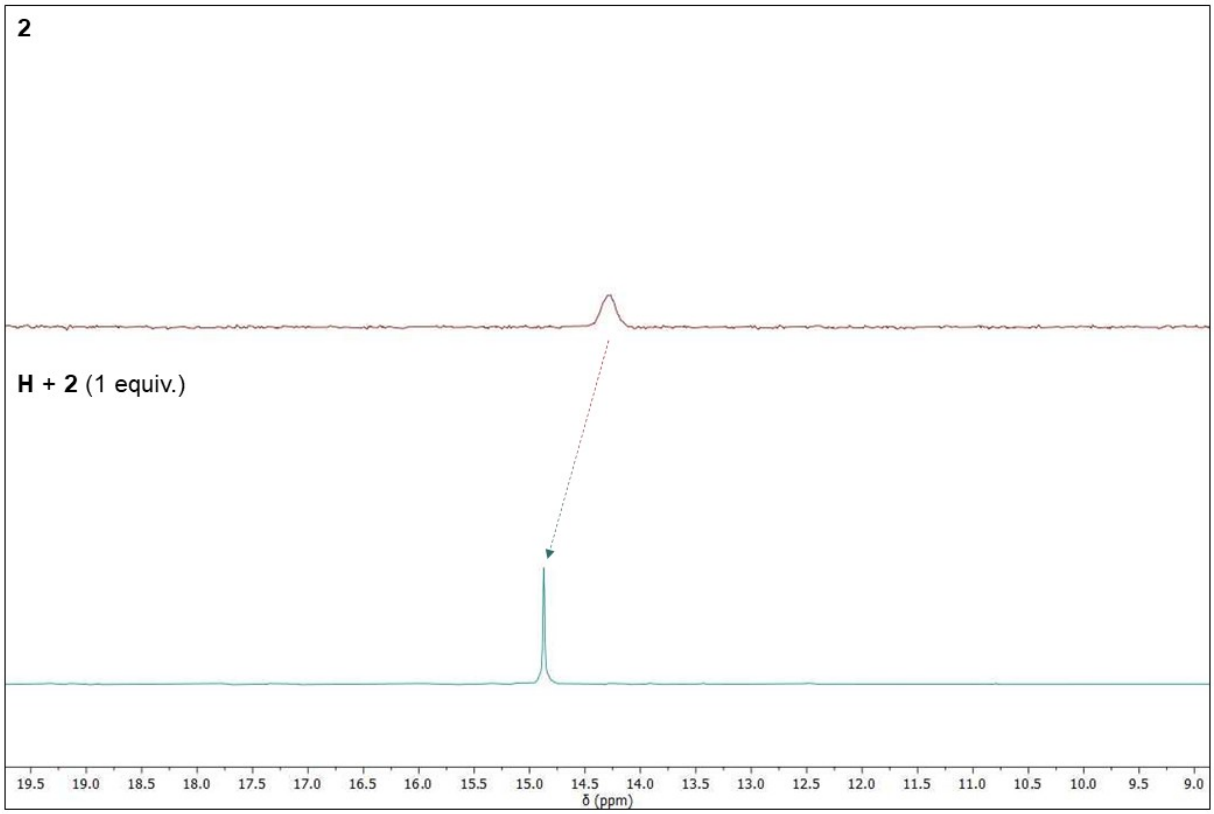

Figure S29. $^{31}P\{H\}$ NMR spectra of **2** and **H** in the presence of 1 equivalent of **2** in CD_3OD.

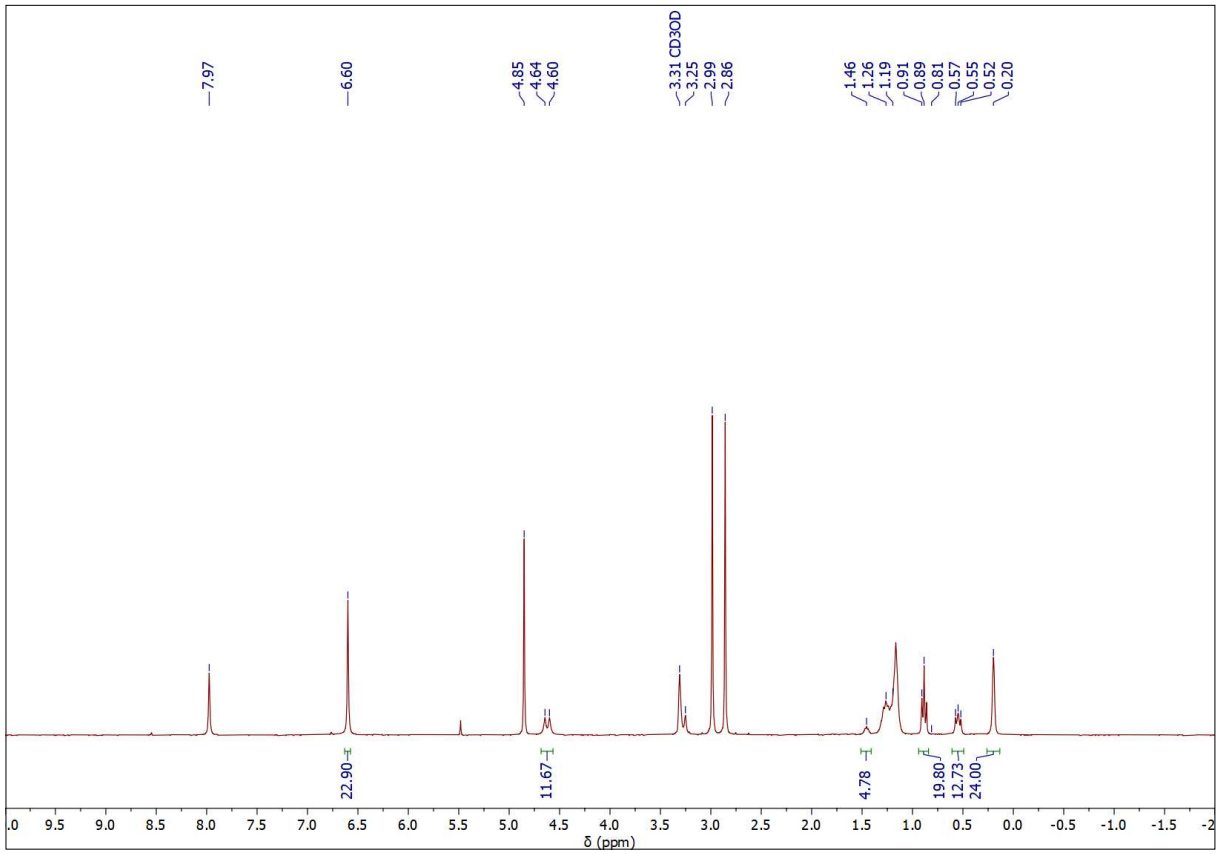

Figure S30. ^{1}H NMR spectra of **H** in the presence of 1 equivalent of **2** in CD_3OD (with integrals to confirm stoichiometry).

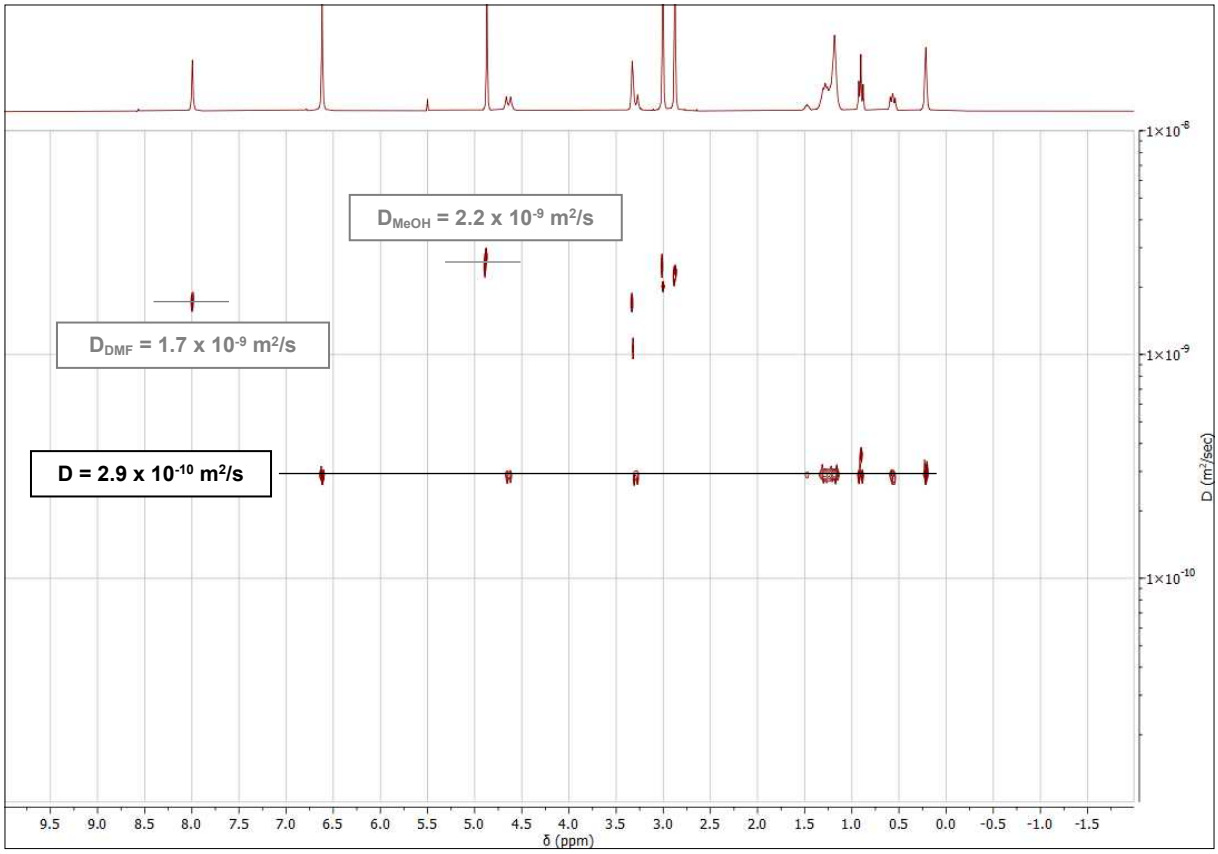

Figure S31. ^{1}H DOSY NMR spectrum of a 1/1 mixture of **2** and **H** in CD_3OD. (Δ=140 ms, δ=1200 μs).

6.2 Encapsulation studies with $(PMe_3)_2AuPF_6$ (G):

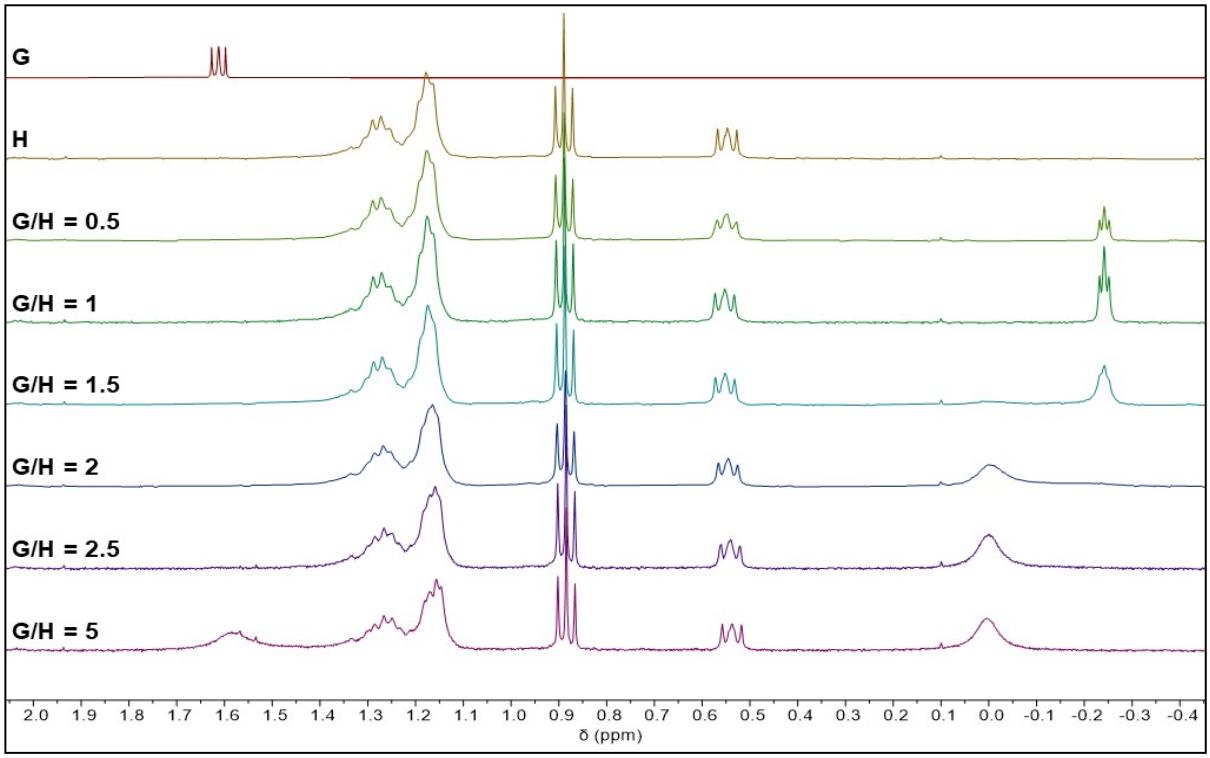

Figure S32. ^{1}H NMR spectra of **G**, **H**, and **H** in the presence of different quantities of **G** in CD_3OD.

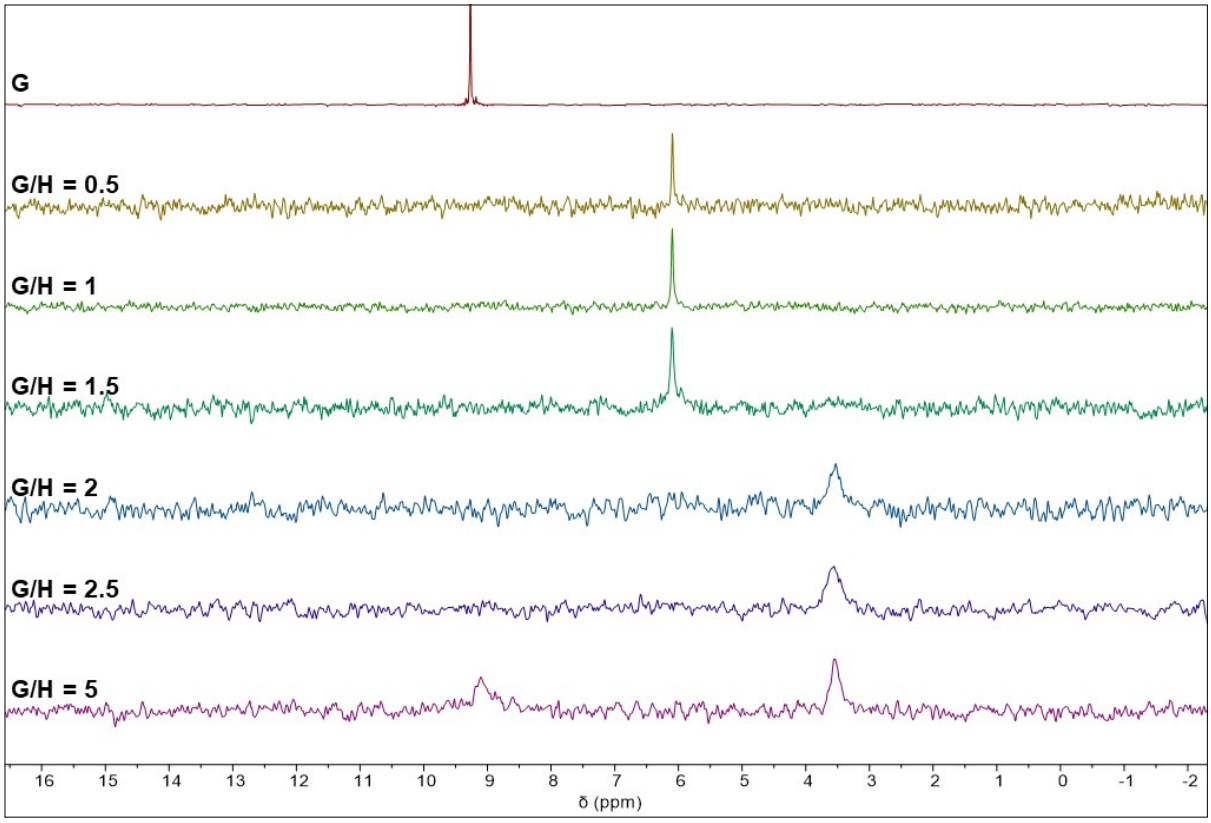

Figure S33. $^{31}P\{H\}$ NMR spectra of **G**, **H**, and **H** in the presence of different quantities of **G** in CD_3OD.

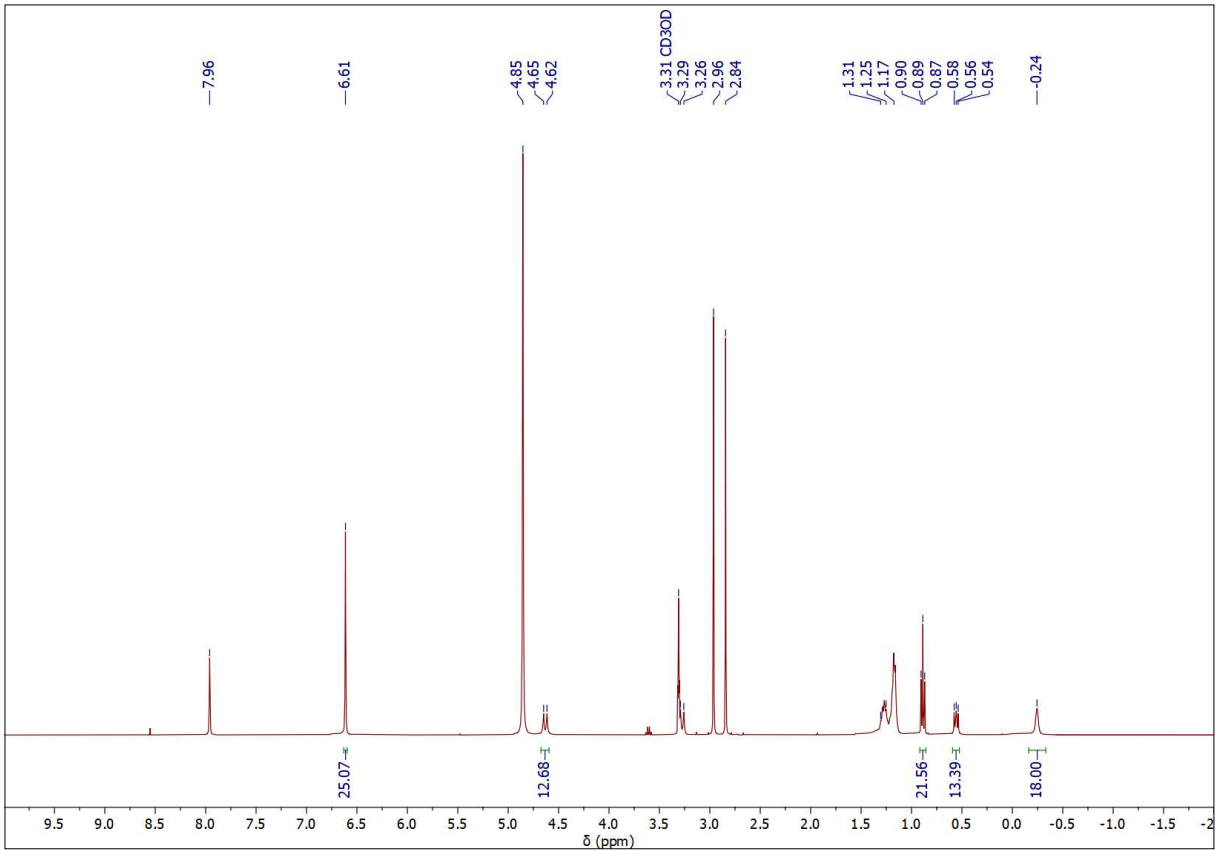

Figure S34. ^{1}H NMR spectra of **H** in the presence of 1 equivalent of **G** in CD_3OD (with integrals to confirm stoichiometry).

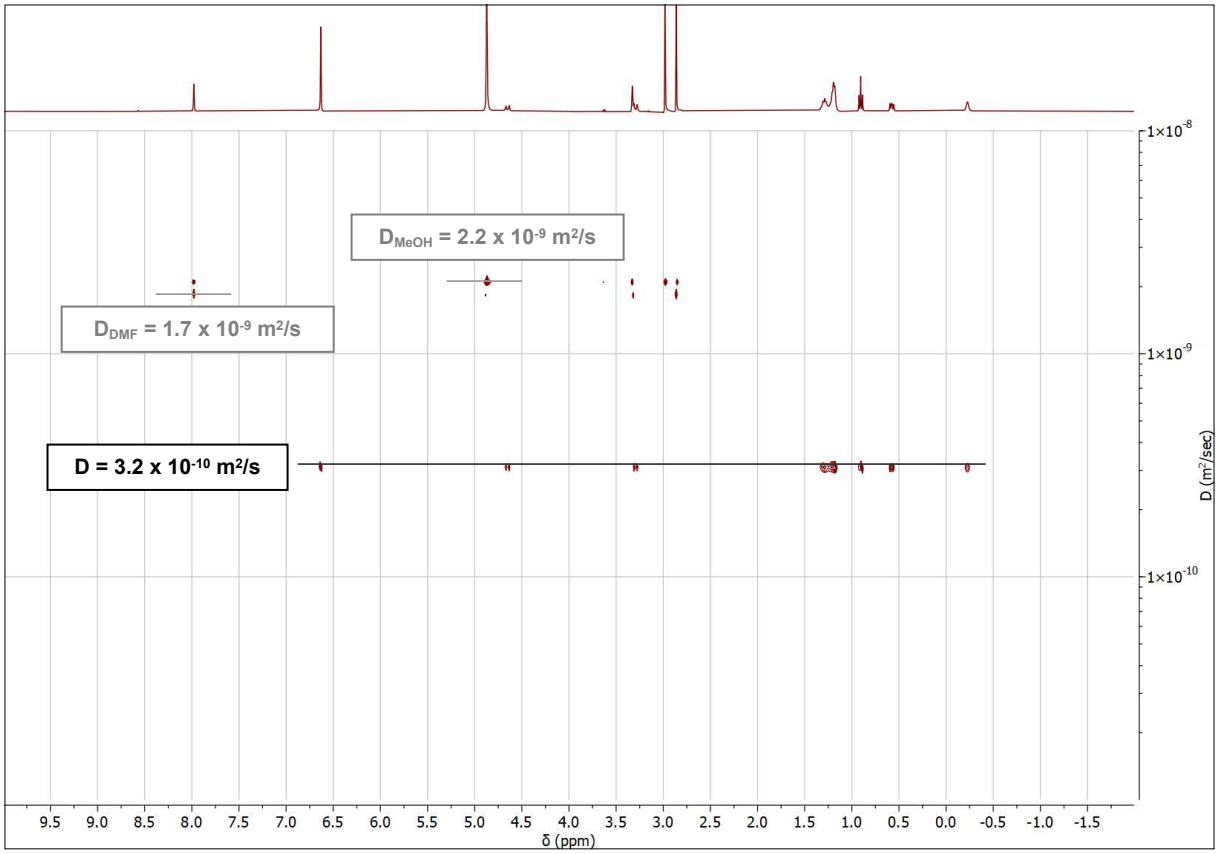

Figure S35. ^{1}H DOSY NMR spectrum of a 1/1 mixture of **G** and **H** in CD_3OD. (Δ=120 ms, δ=1000 μs).

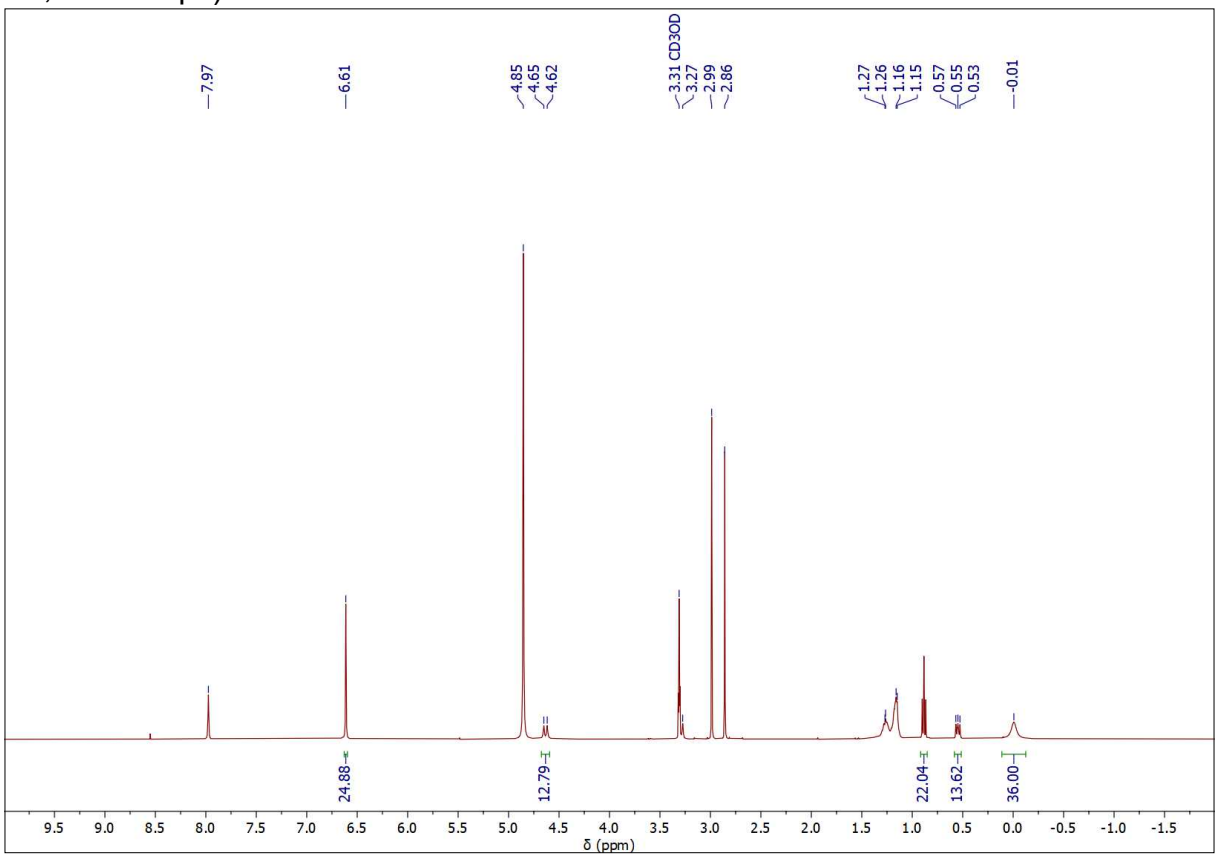

Figure S36. ^{1}H NMR spectra of **H** in the presence of 2 equivalents of **G** in CD_3OD (with integrals to confirm stoichiometry).

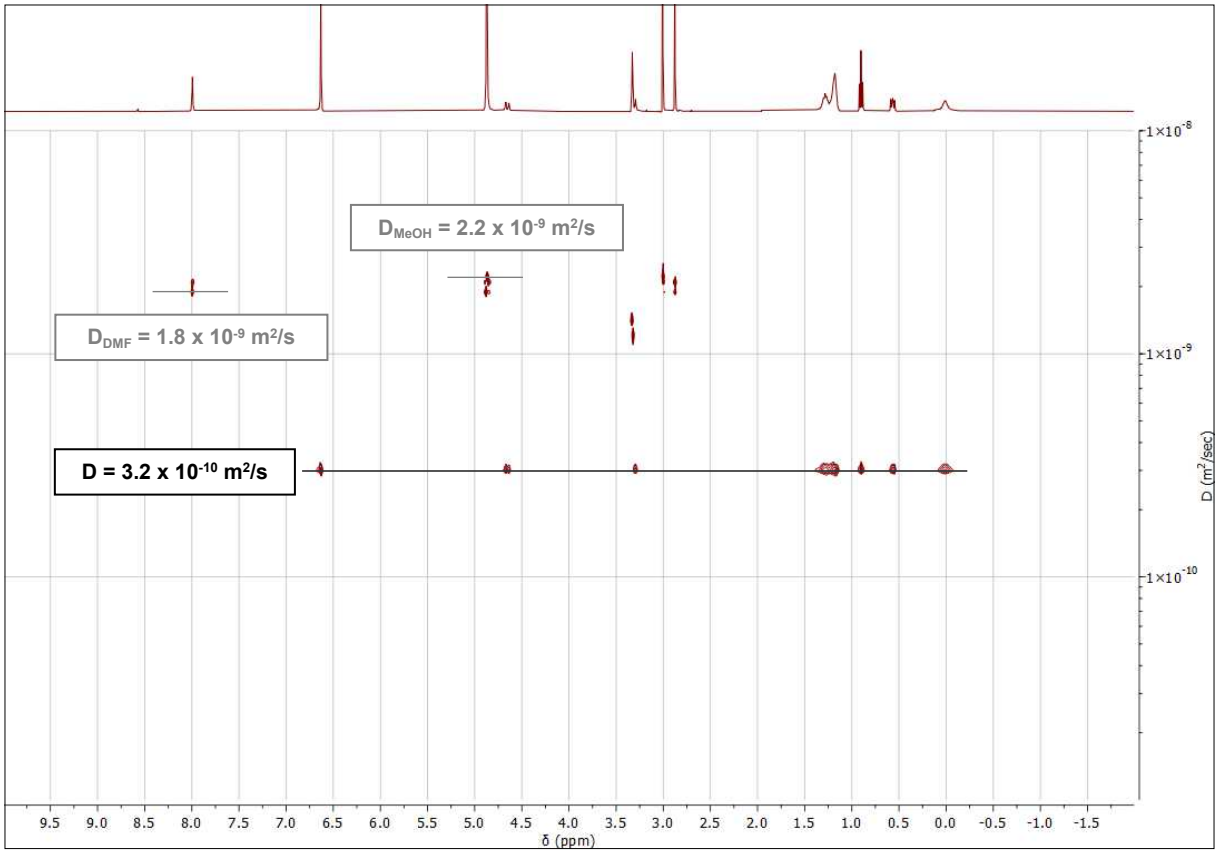

Figure S37. ^{1}H DOSY NMR spectrum of a 2/1 mixture of **G** and **H** in CD_3OD. (Δ=120 ms, δ=1000 μs).

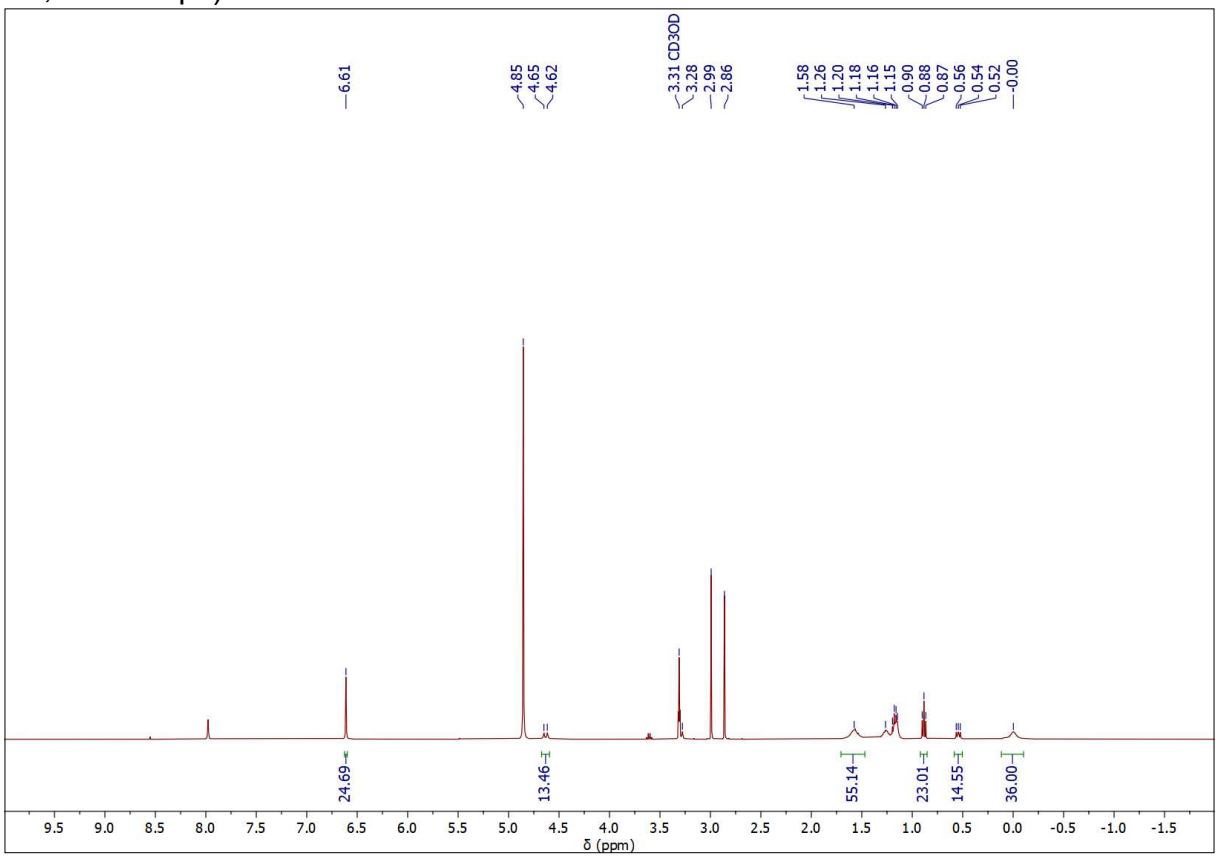

Figure S38. ^{1}H NMR spectra of **H** in the presence of 5 equivalents of **G** in CD_3OD (with integrals to confirm stoichiometry).

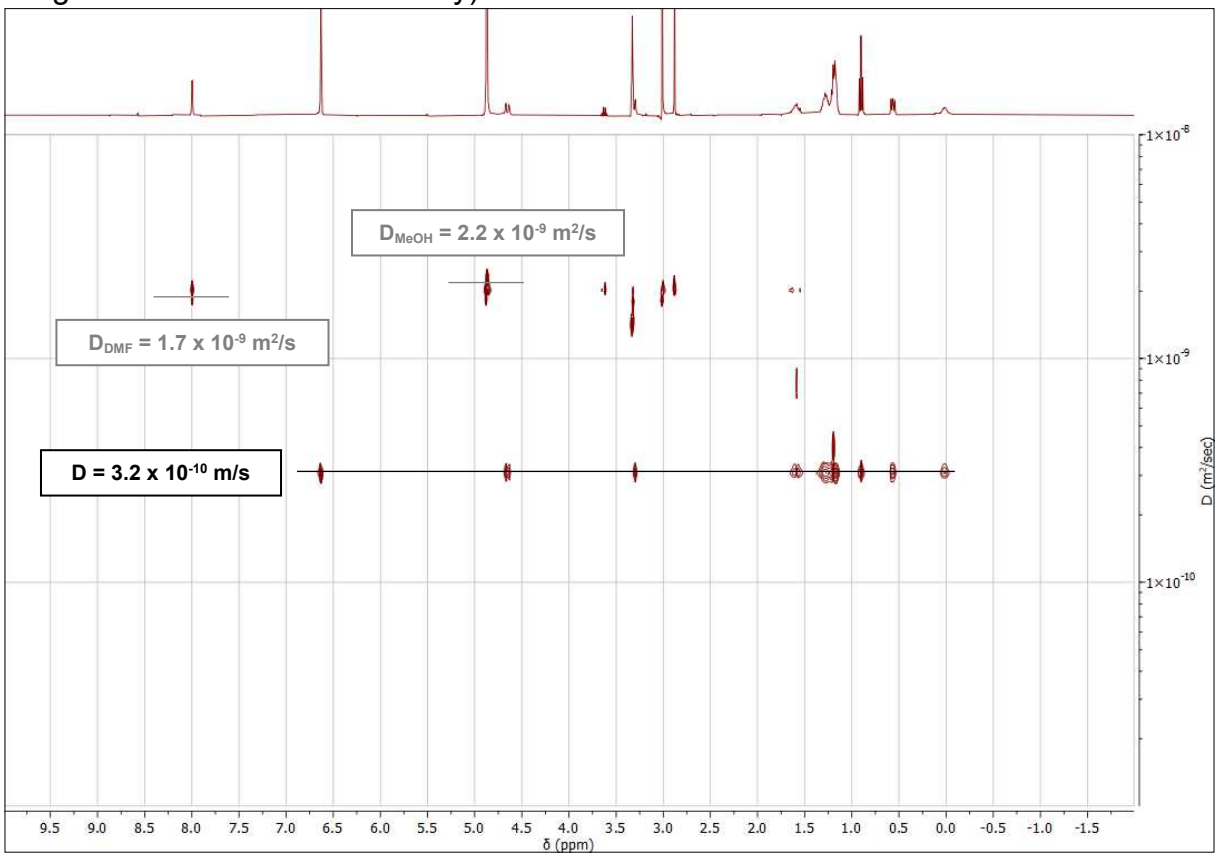

Figure S39. ^{1}H DOSY NMR spectrum of a 5/1 mixture of **G** and **H** in CD_3OD. (Δ=120 ms, δ=1000 μs).

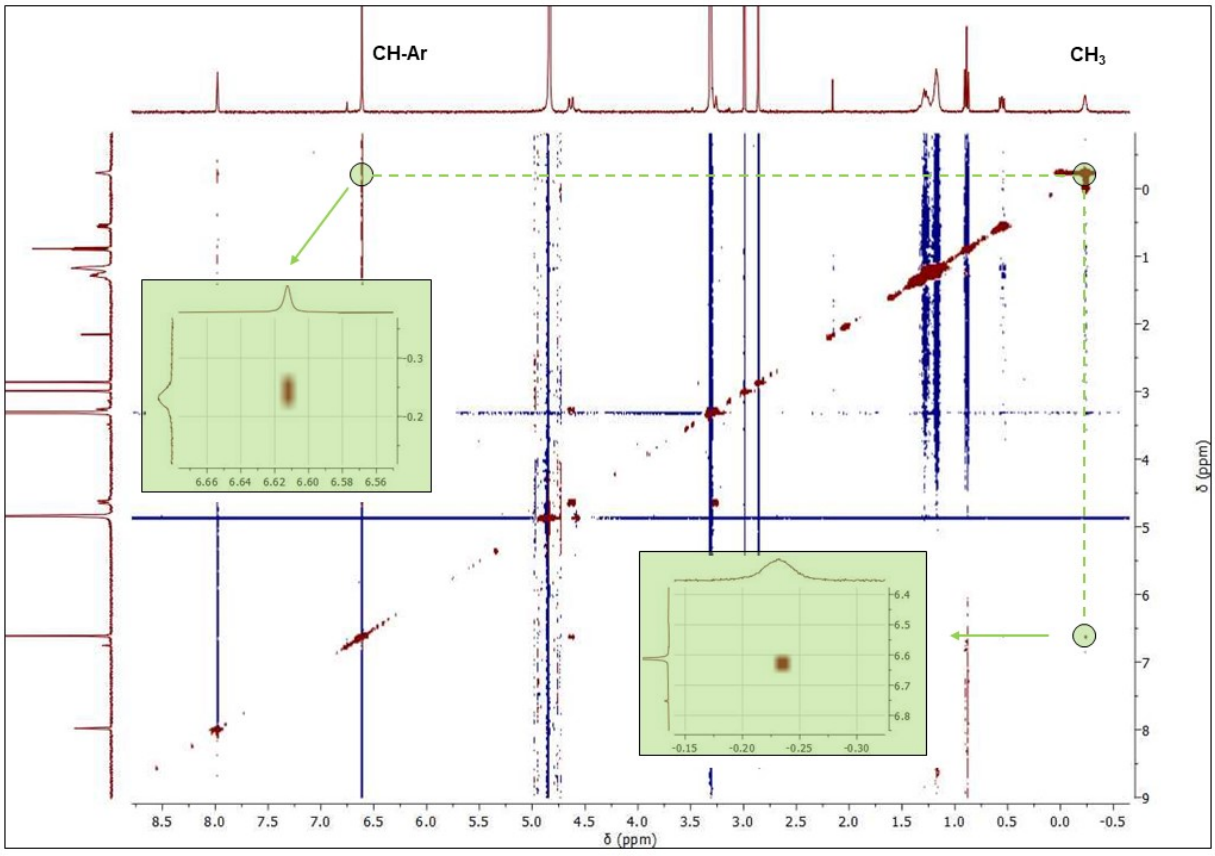

Figure S40. ^{1}H NOESY NMR spectrum of a 1/1 mixture of **G** and **H** in CD_3OD. (mixing time 800 ms).

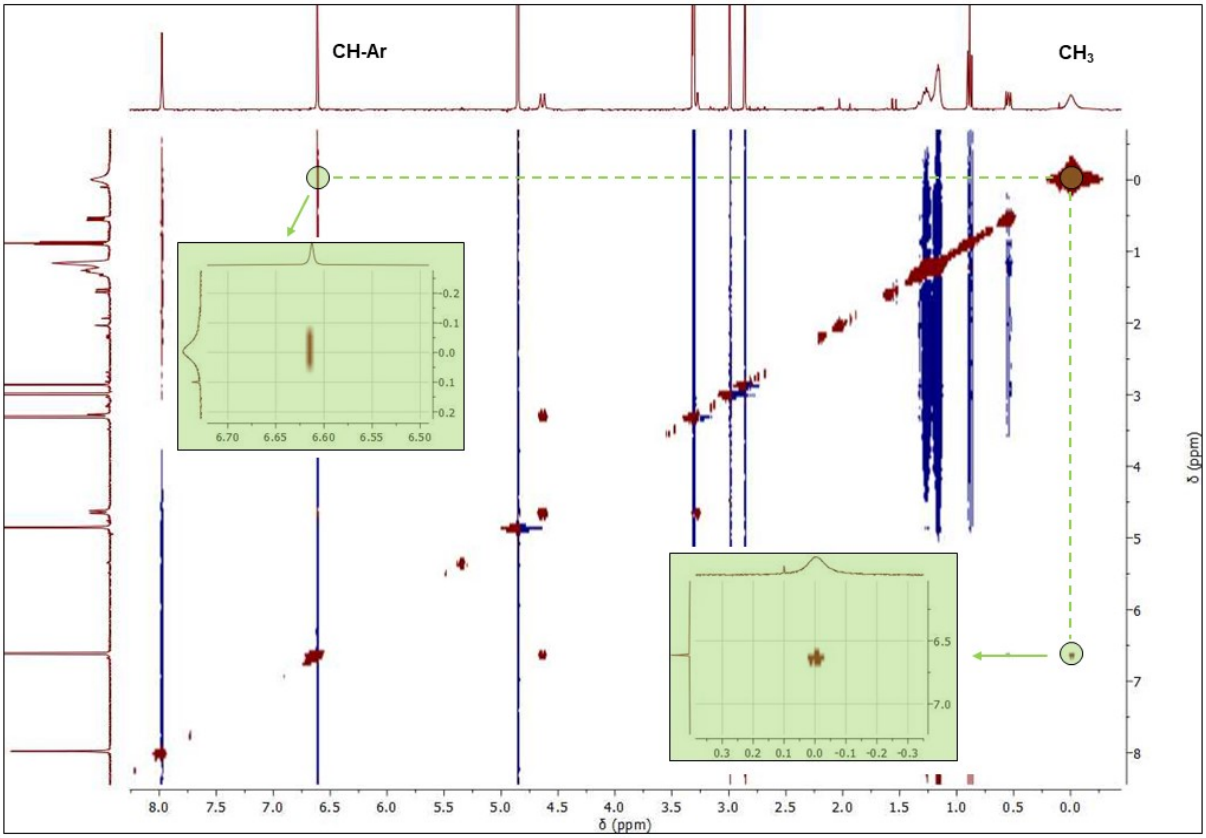

Figure S41. ^{1}H NOESY NMR spectrum of a 2/1 mixture of **G** and **H** in CD_3OD. (mixing time 800 ms).

6.3 Encapsulation studies with $(PEt_3)_2AuPF_6$ (1):

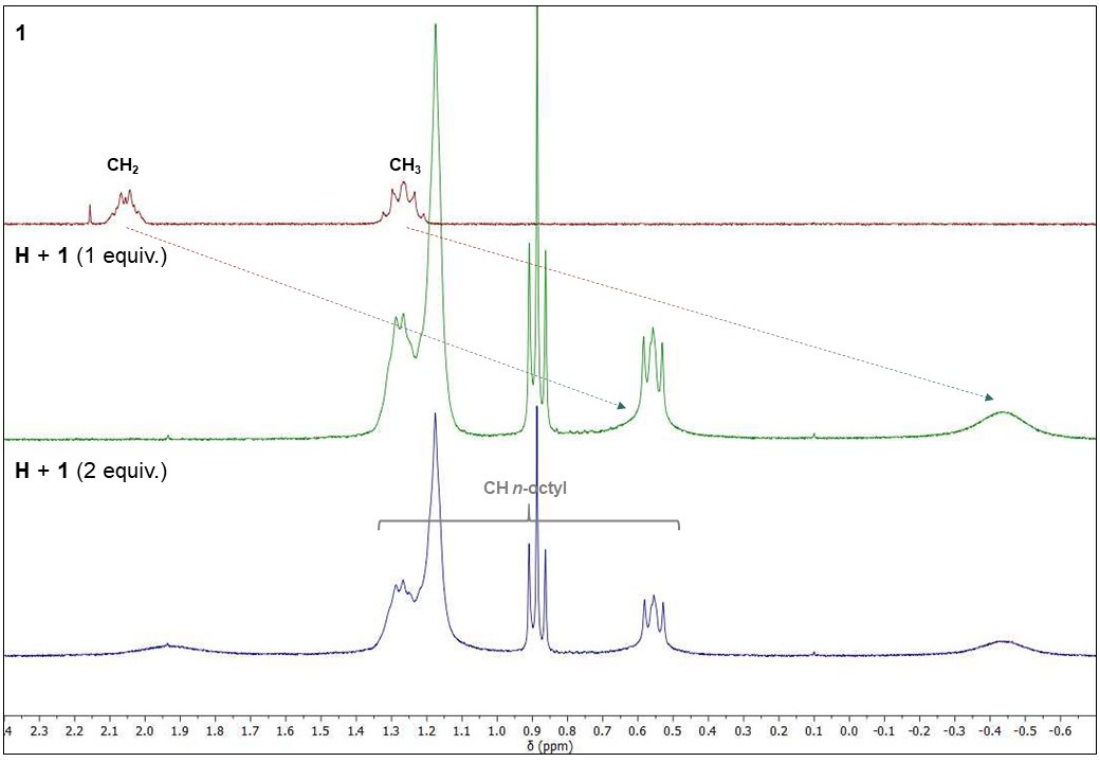

Figure S42. ^{1}H NMR spectra of **1** and **H** in the presence of different quantities of **1** in CD_3OD.

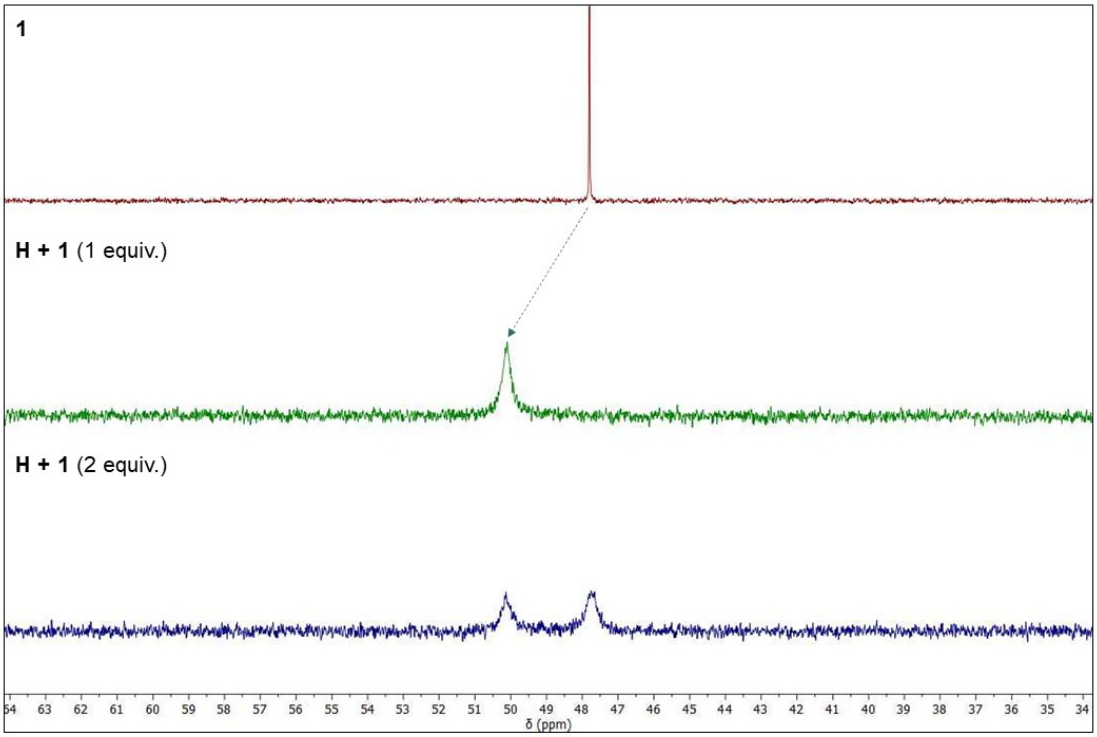

Figure S43. $^{31}P\{H\}$ NMR spectra of **1** and **H** in the presence of different quantities of **1** in CD_3OD.

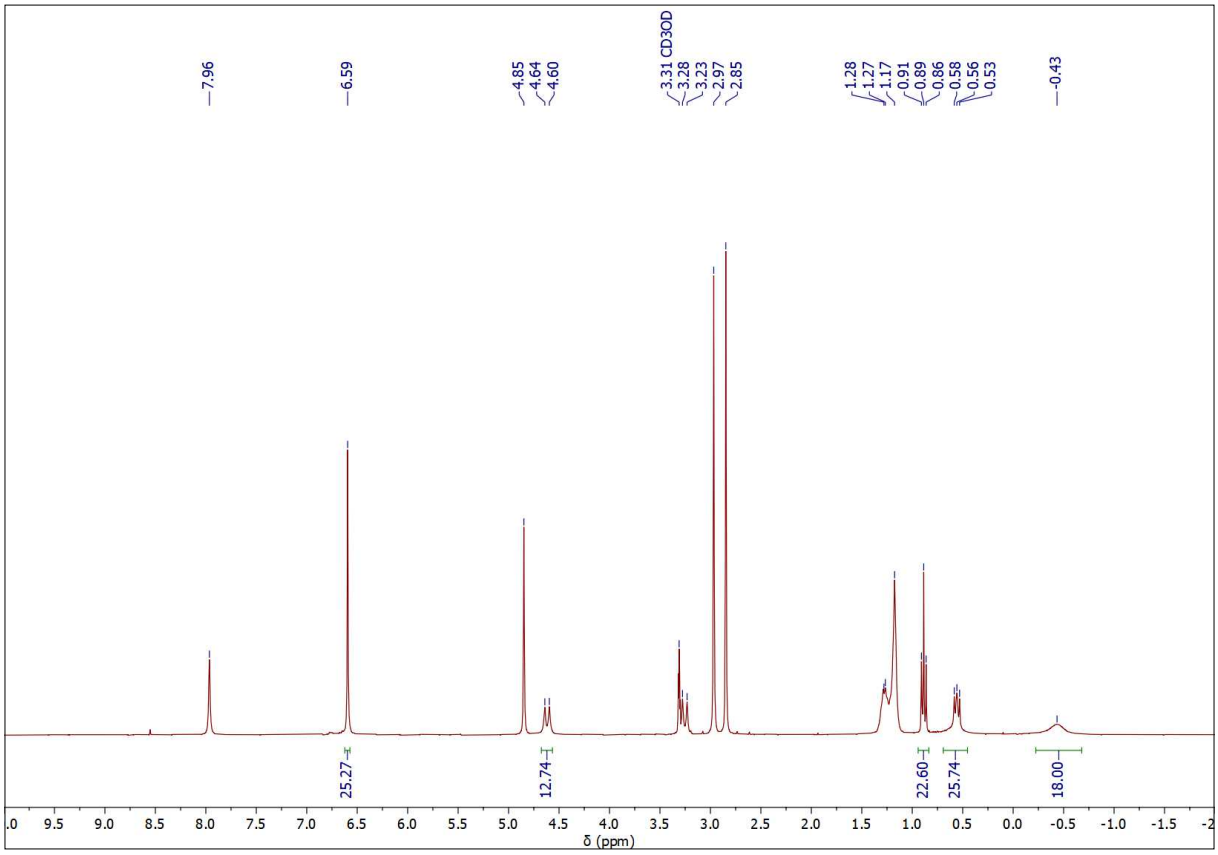

Figure S44. ^{1}H NMR spectra of **H** in the presence of 1 equivalent of **1** in CD_3OD (with integrals to confirm stoichiometry).

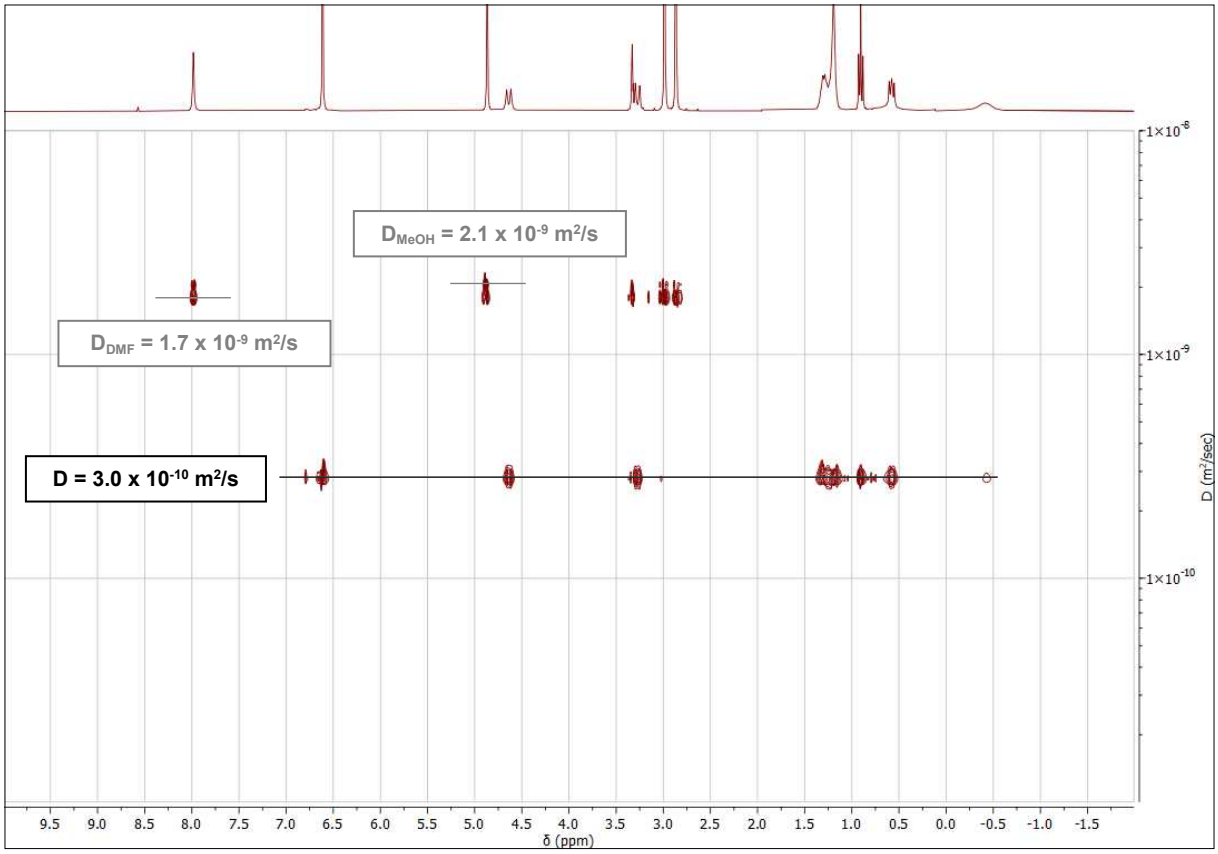

Figure S45. ^{1}H DOSY NMR spectrum of a 1/1 mixture of **1** and **H** in CD_3OD. (Δ=100 ms, δ=1200 μs).

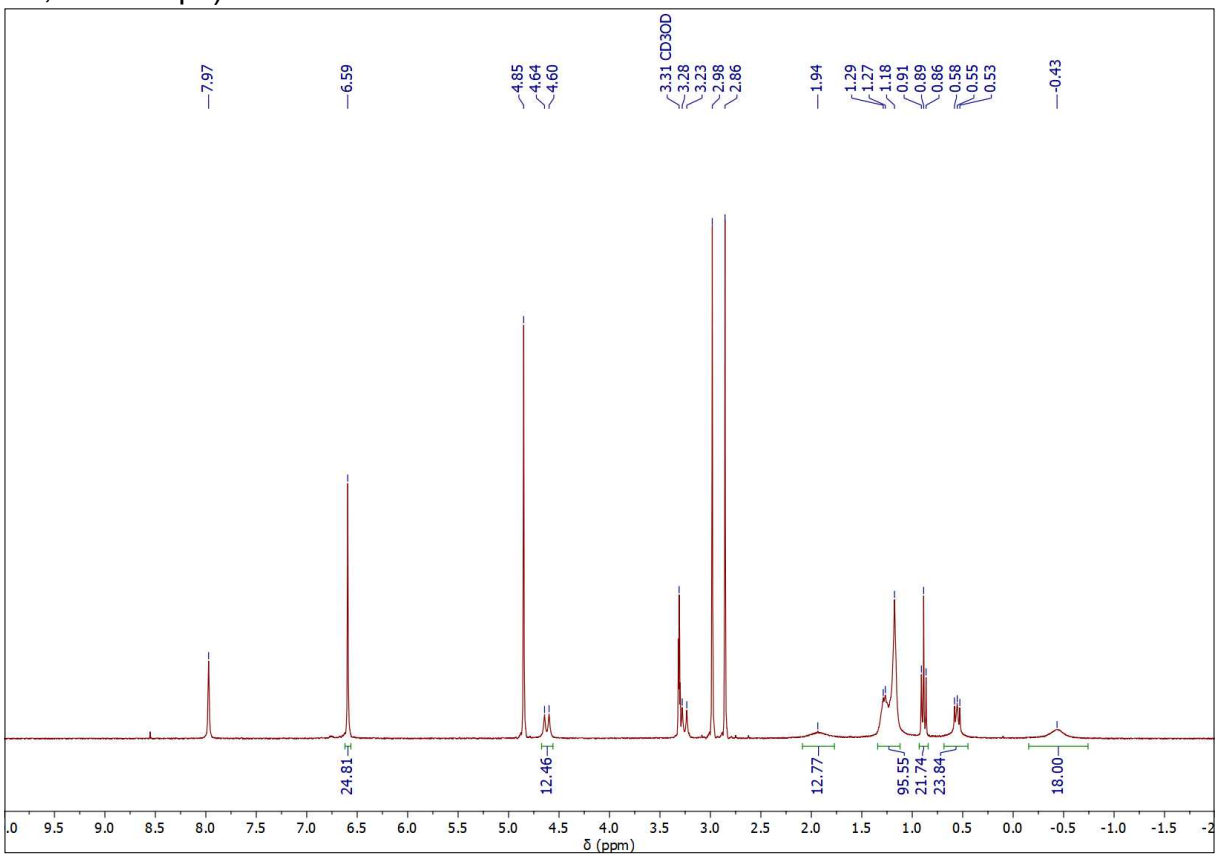

Figure S46. ^{1}H NMR spectra of **H** in the presence of 2 equivalents of **1** in CD_3OD (with integrals to confirm stoichiometry).

6.4 Encapsulation studies with $(P^tBu_3)_2AuPF_6$ (3):

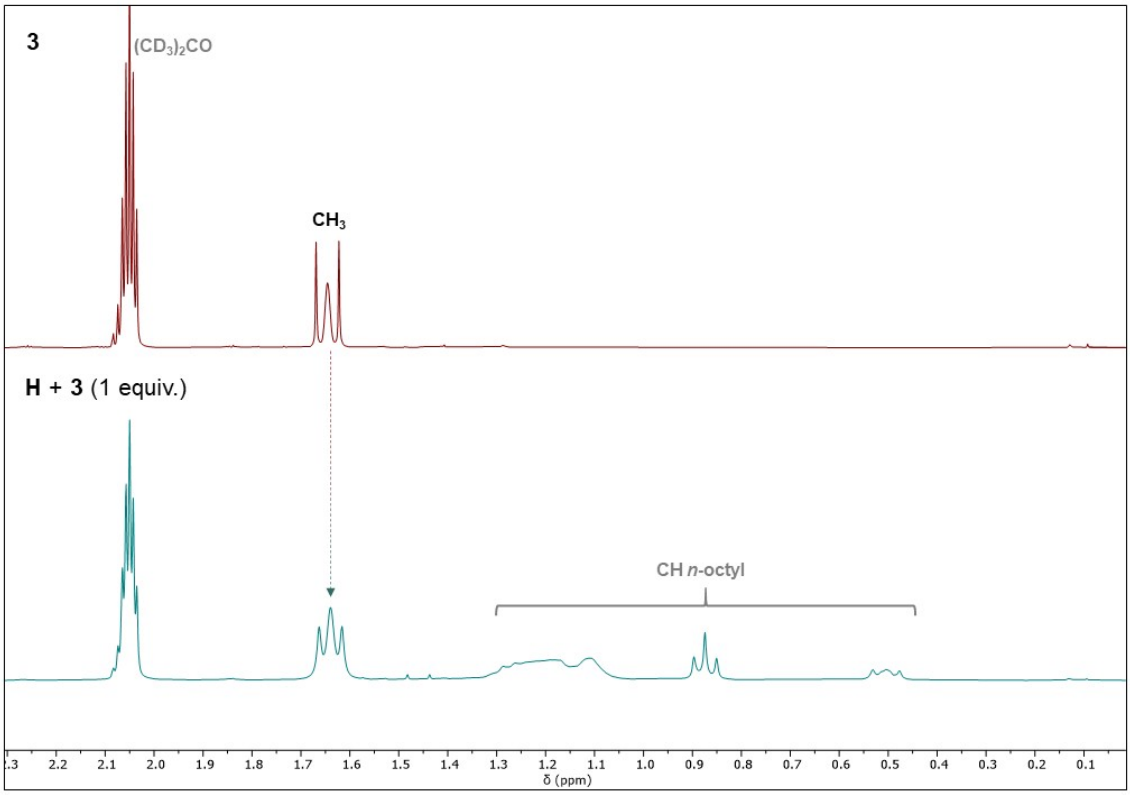

Figure S47. ^{1}H NMR spectra of **3** and **H** in the presence of 1 equivalent of **3** in $(CD_3)_2CO$.

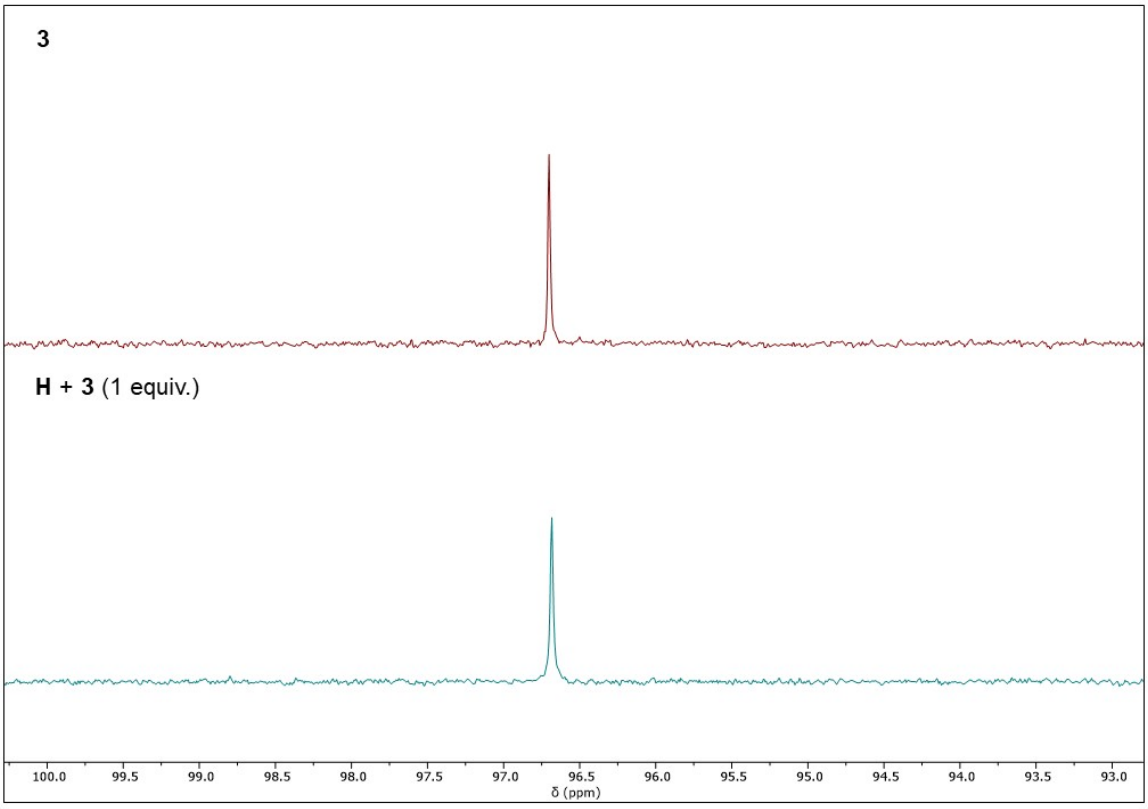

Figure S48. ^{31}P{H} NMR spectra of **3** and **H** in the presence of 1 equivalent of **3** in $(CD_3)_2CO$.

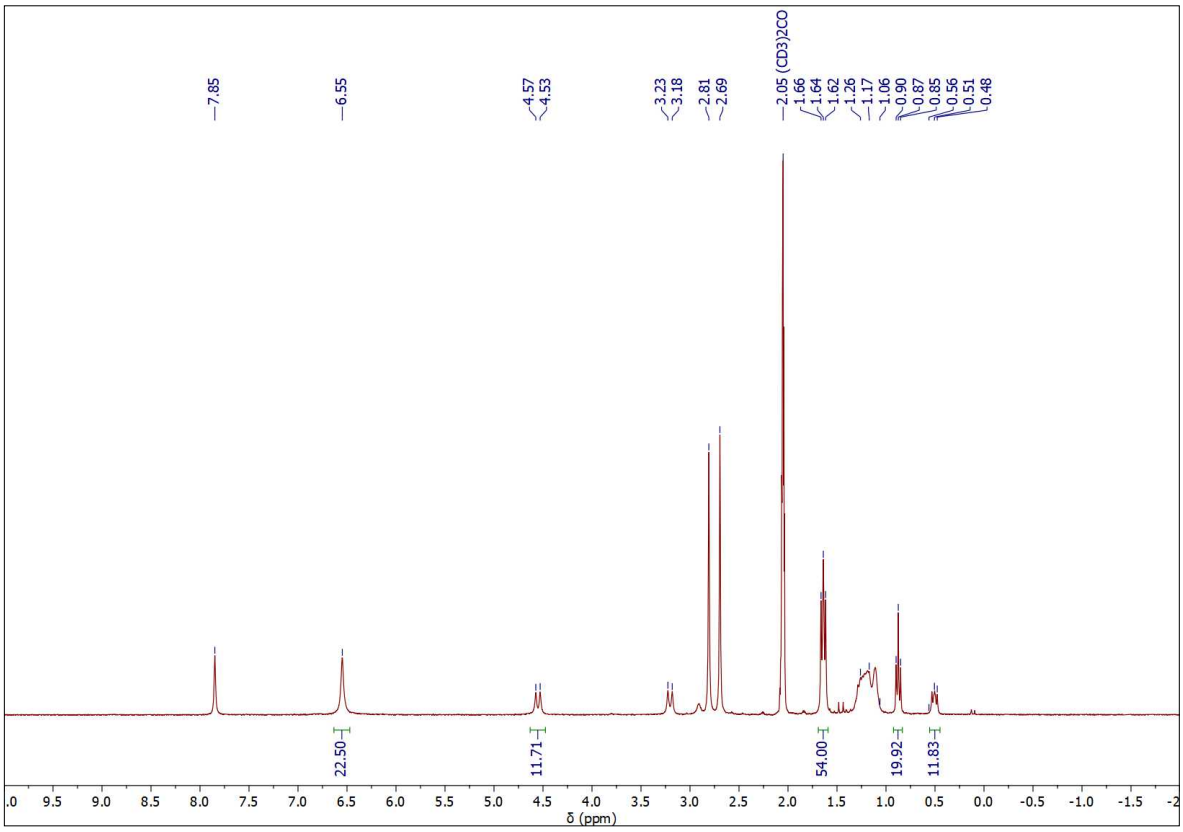

Figure S49. ^{1}H NMR spectra of **H** in the presence of 1 equivalent of **3** in $(CD_3)_2CO$ (with integrals to confirm stoichiometry).

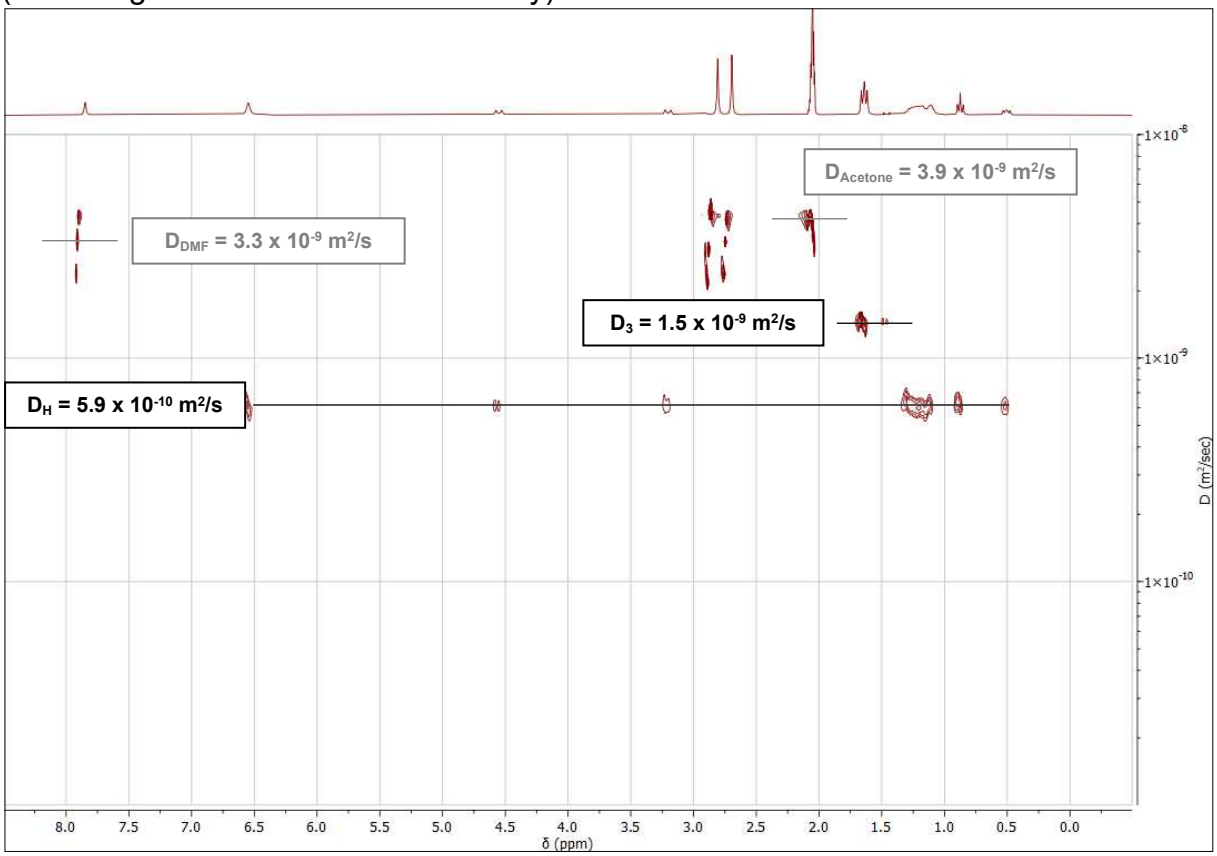

Figure S50. ^{1}H DOSY NMR spectrum of a 1/1 mixture of **3** and **H** in $(CD_3)_2CO$. (Δ=80 ms, δ=1000 μs).

6.5 Encapsulation studies with $(PPh_3)_2AuPF_6$ (4):

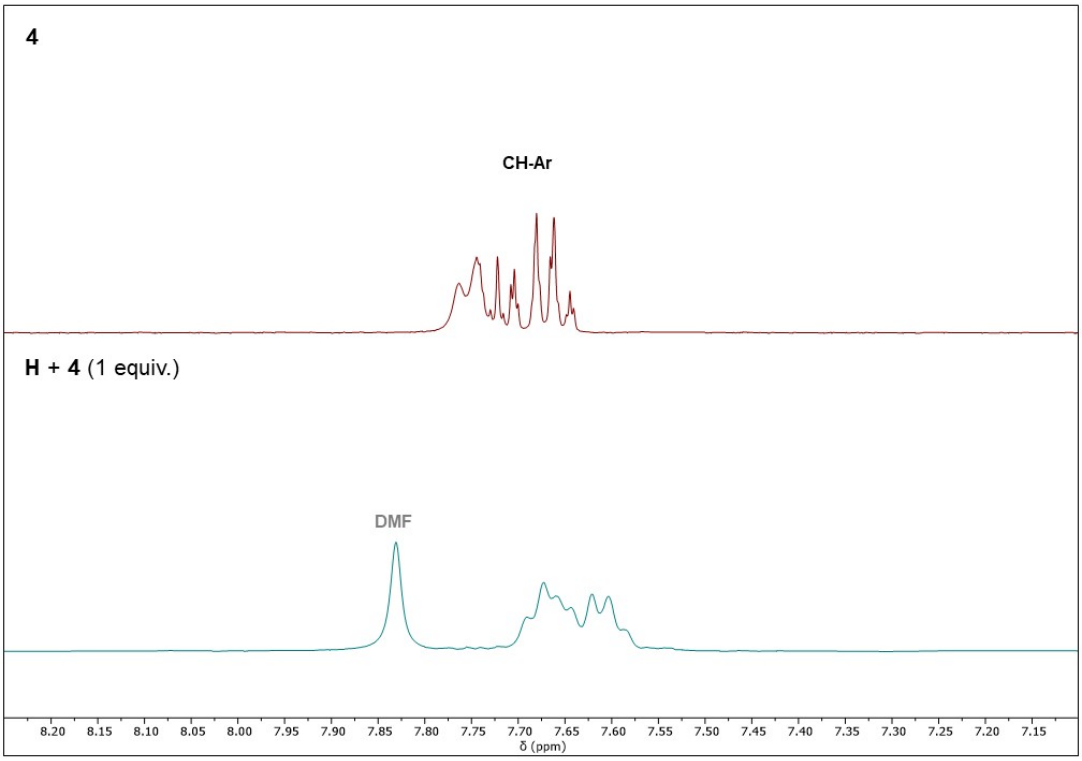

Figure S51. ^{1}H NMR spectra of **4** and **H** in the presence of 1 equivalent of **4** in $(CD_3)_2CO$.

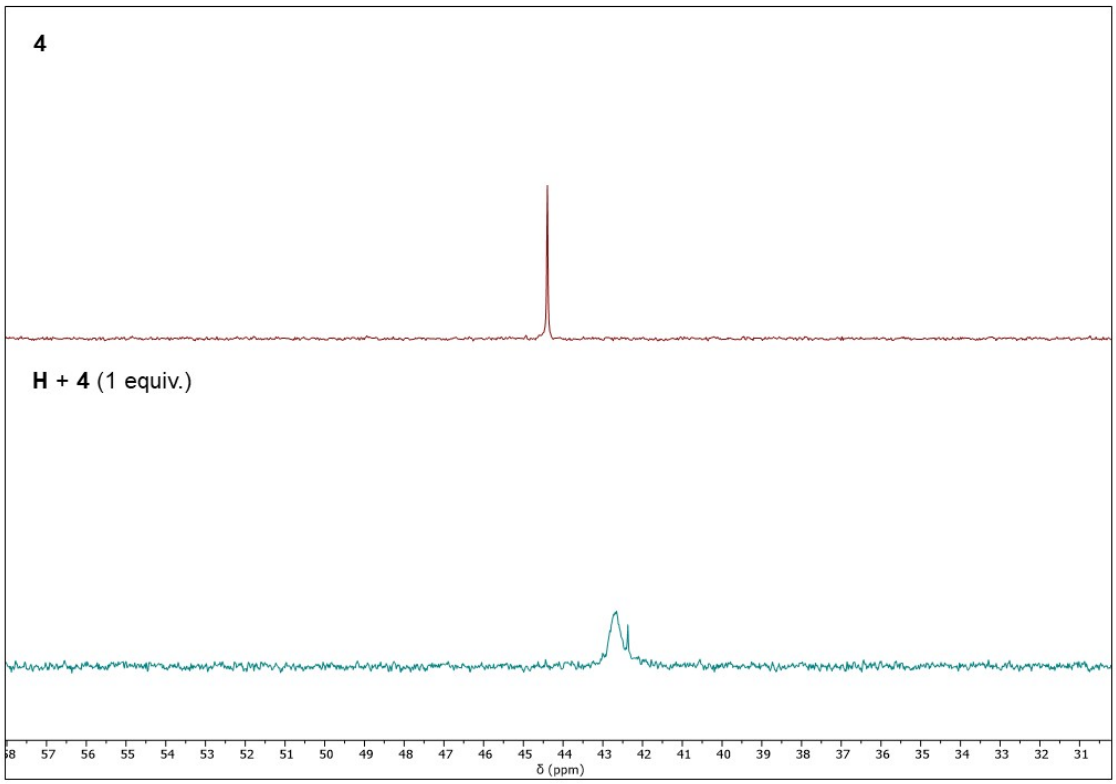

Figure S52. $^{31}P\{H\}$ NMR spectra of **4** and **H** in the presence of 1 equivalent of **4** in $(CD_3)_2CO$.

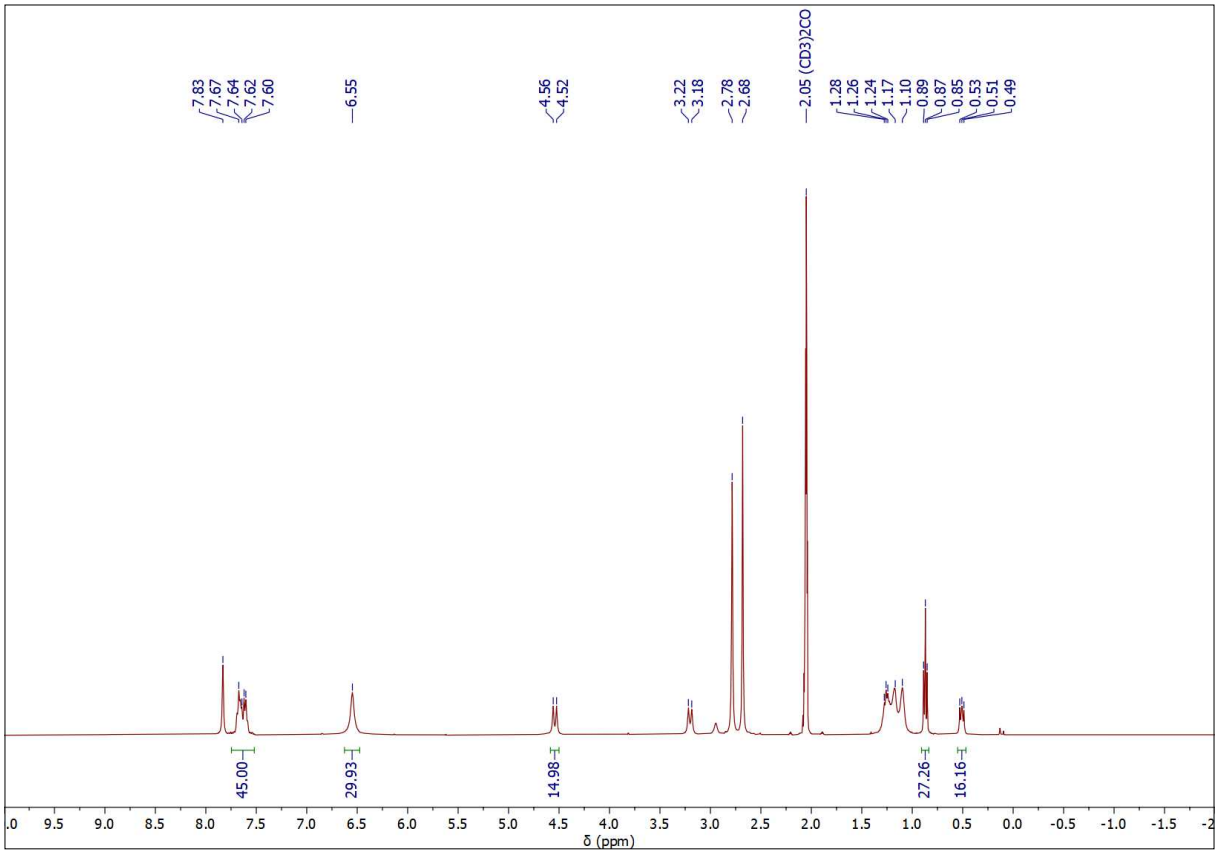

Figure S53. ^{1}H NMR spectra of **H** in the presence 1 equivalent of **4** in $(CD_3)_2CO$ (with integrals to confirm stoichiometry).

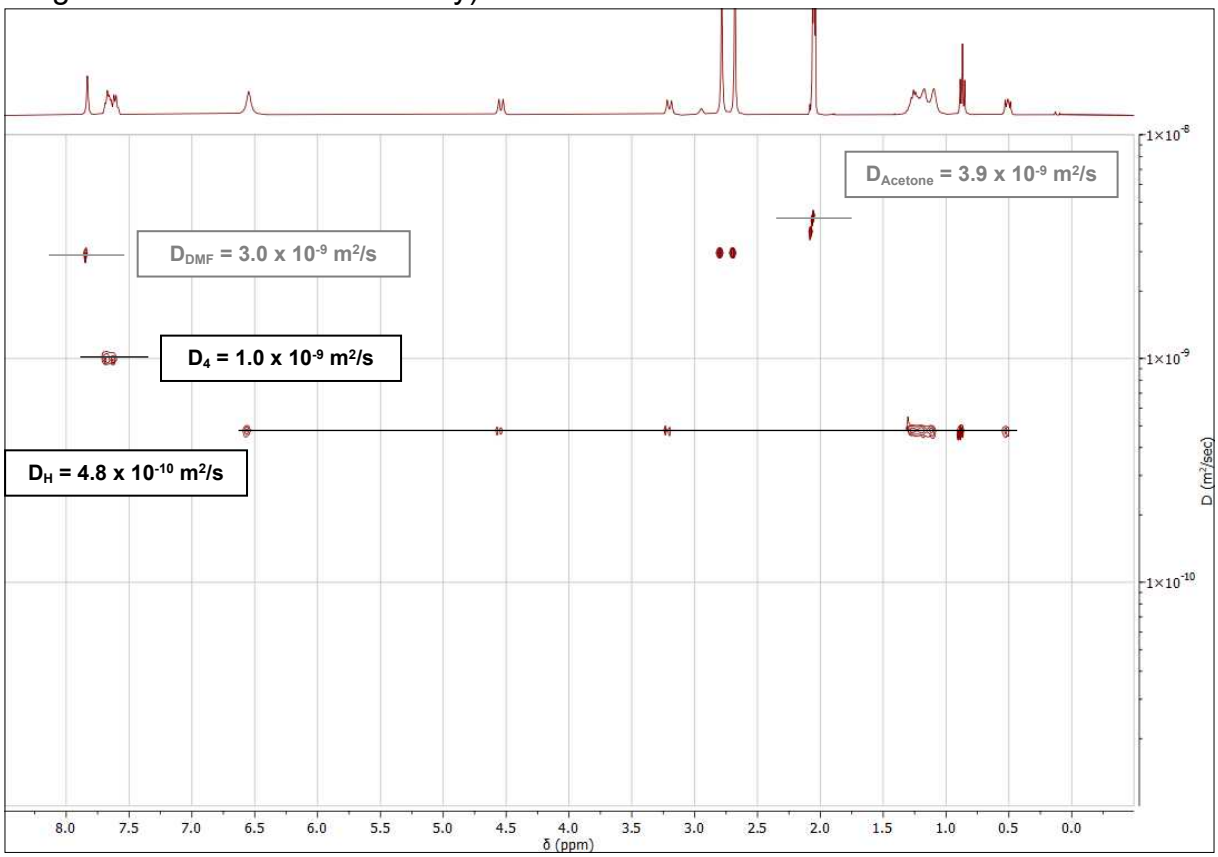

Figure S54. ^{1}H DOSY NMR spectrum of a 1/1 mixture of **4** and **H** in $(CD_3)_2CO$. (Δ=100 ms, δ=1000 μs).

7. HRMS spectra:

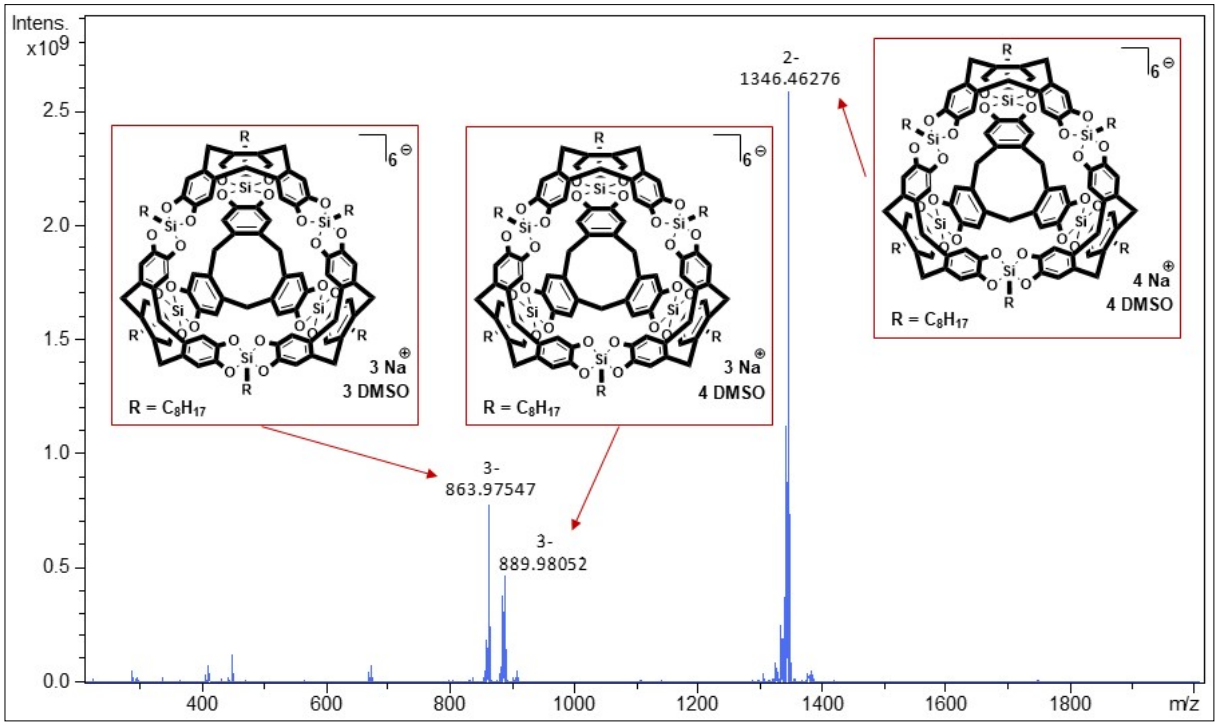

Figure S55. ESI-FTICR spectrum of **H**.

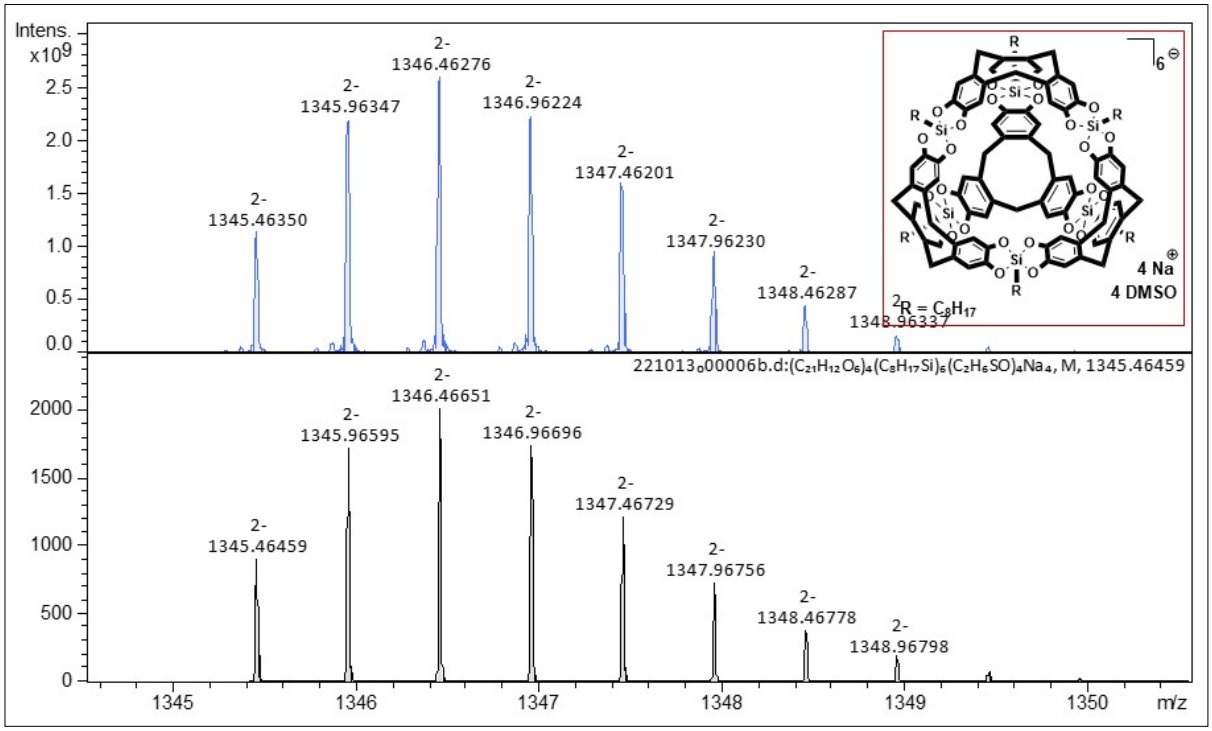

Figure S56. ESI-FTICR spectrum of **H**.

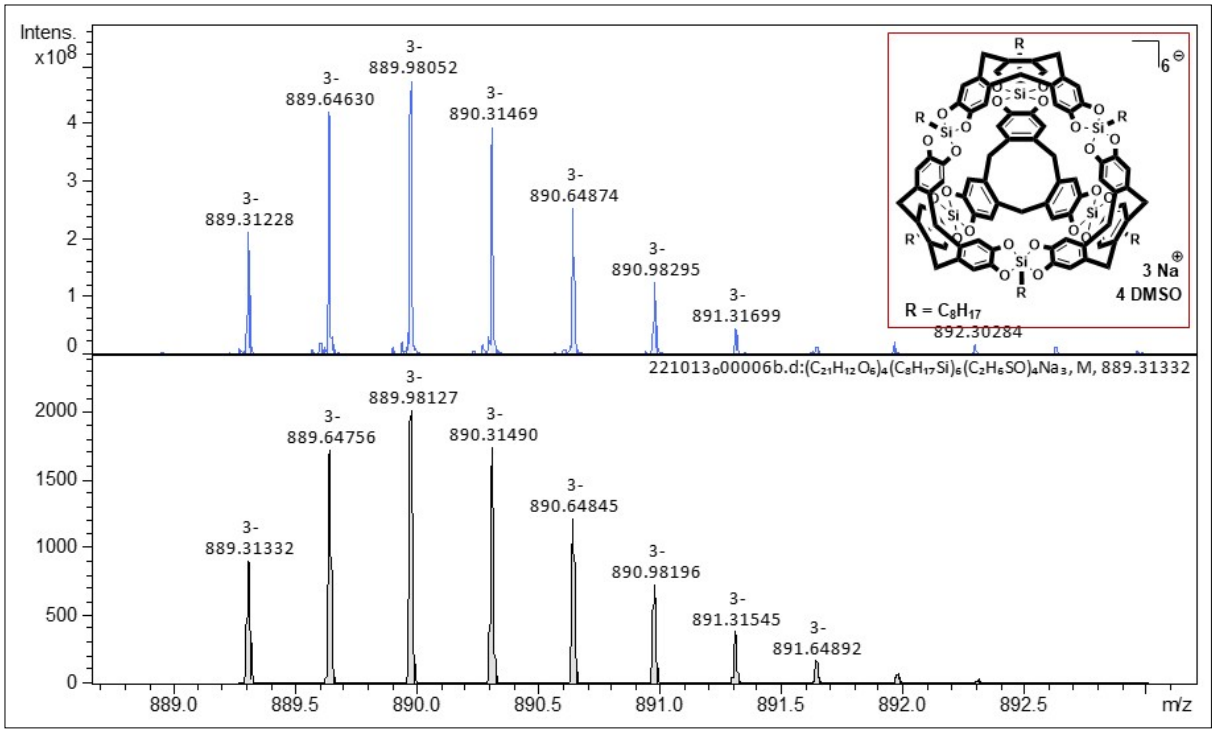

Figure S57. ESI-FTICR spectrum of **H**.

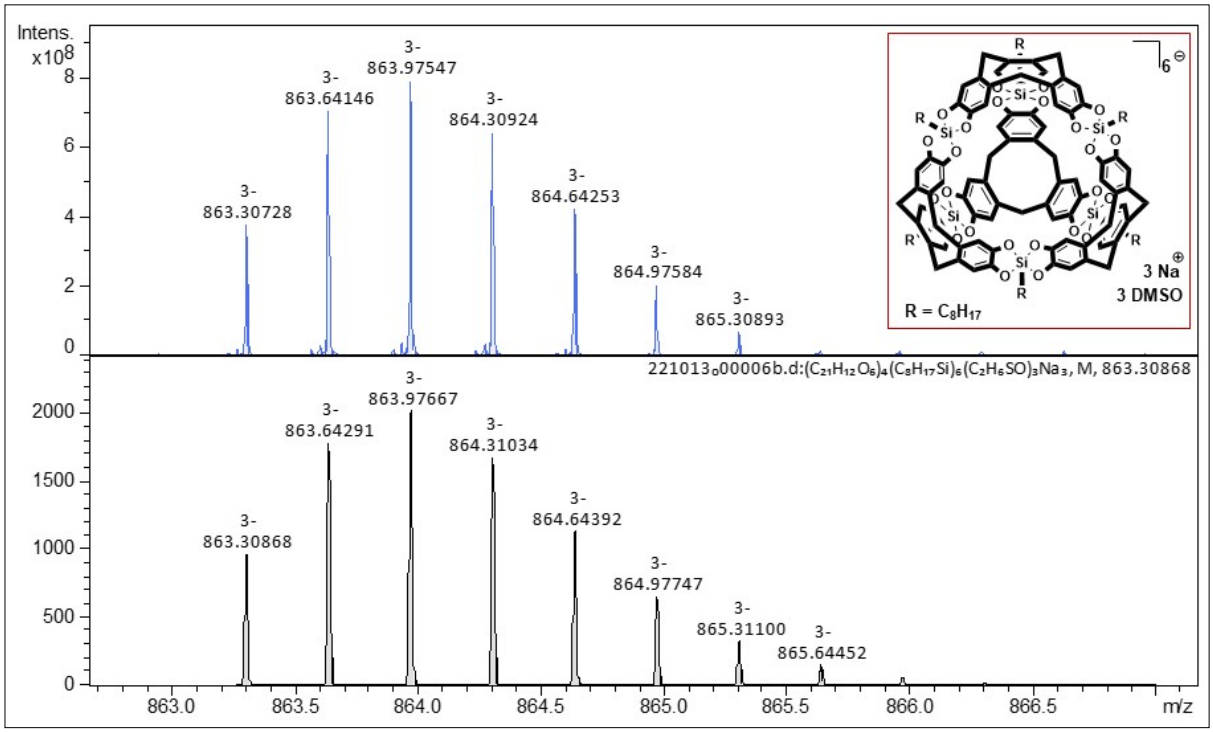

Figure S58. ESI-FTICR spectrum of **H**.

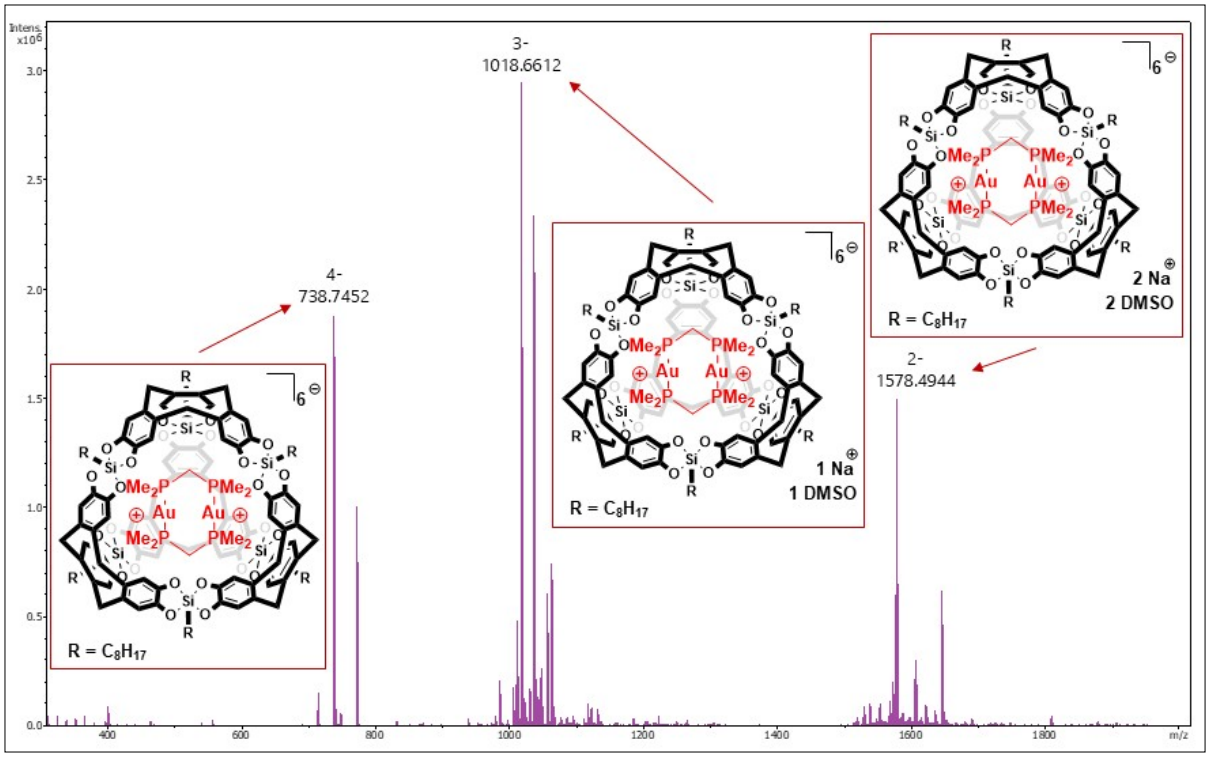

Figure S59. TIMS-ToF spectrum of a 10/1 mixture of **2** and **H**.

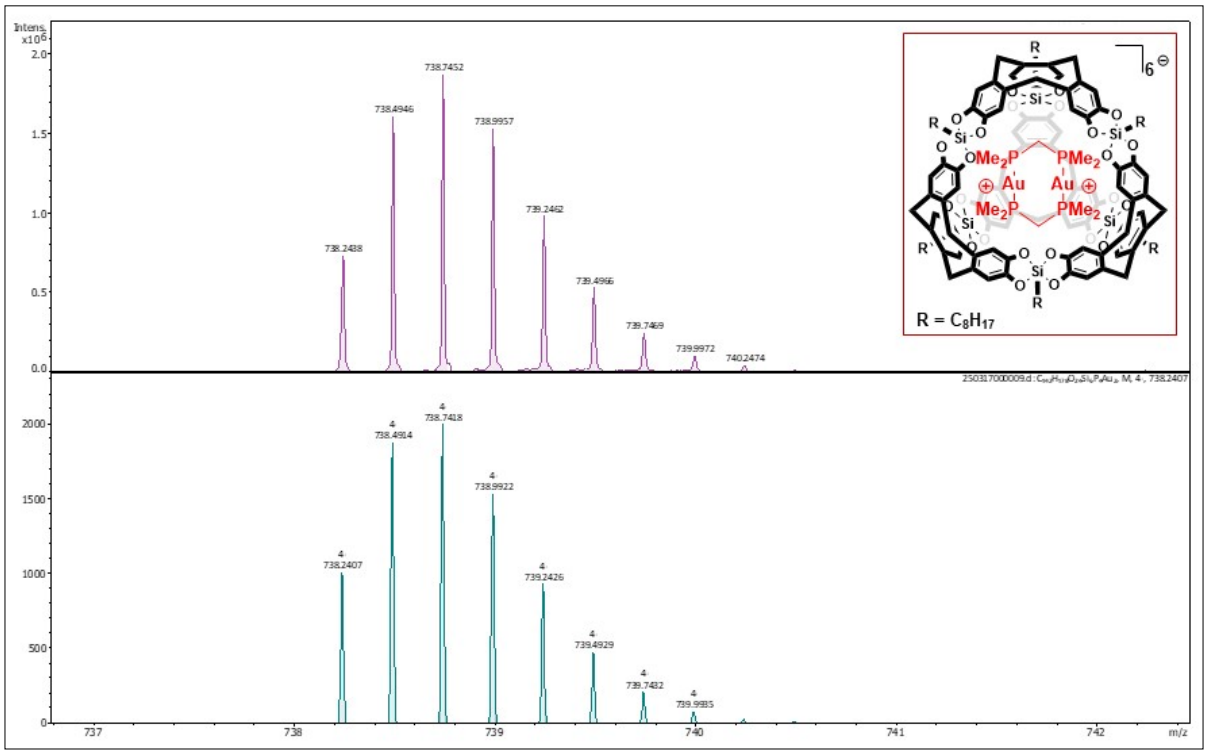

Figure S60. TIMS-ToF spectrum of a 10/1 mixture of **2** and **H**.

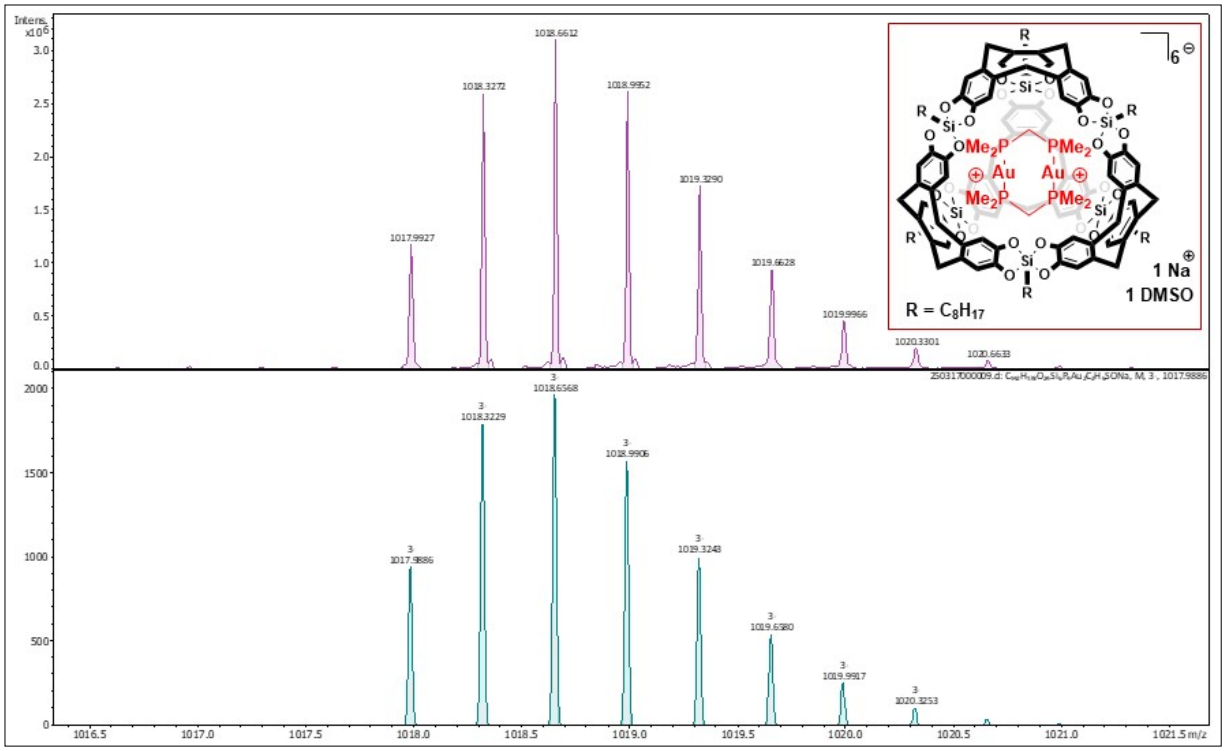

Figure S61. TIMS-ToF spectrum of a 10/1 mixture of **2** and **H**.

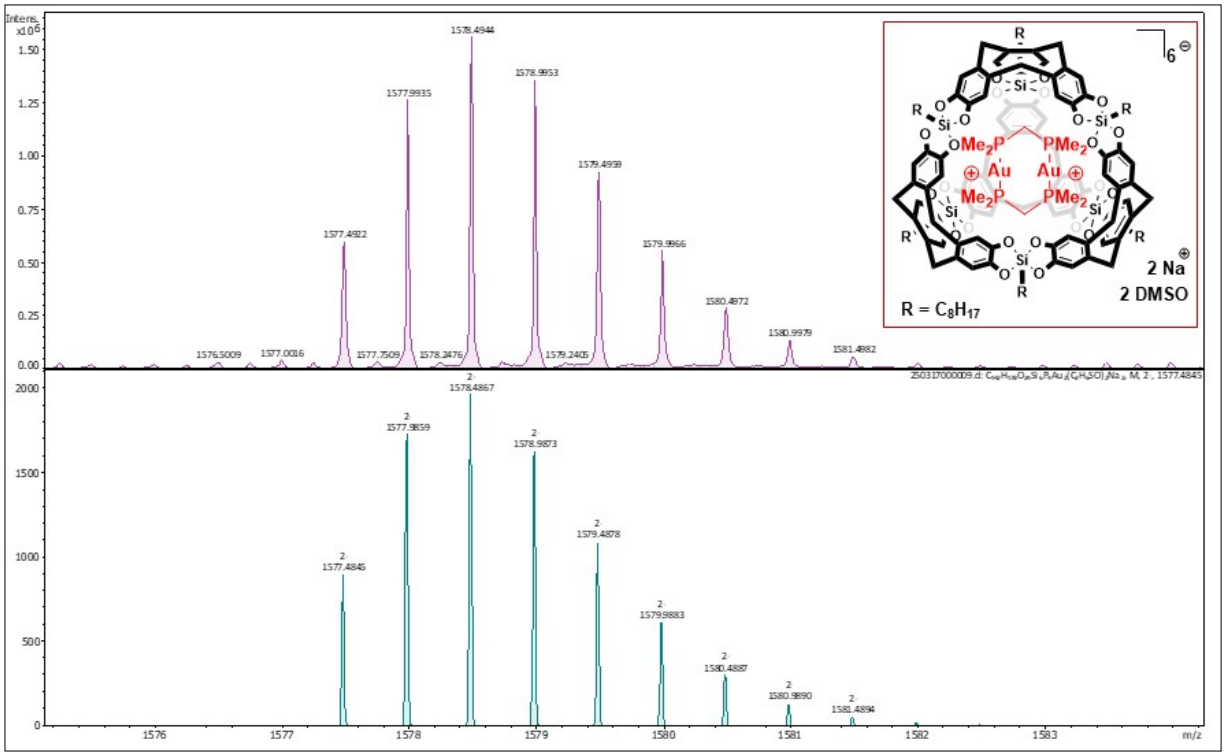

Figure S62. TIMS-ToF spectrum of a 10/1 mixture of **2** and **H**.

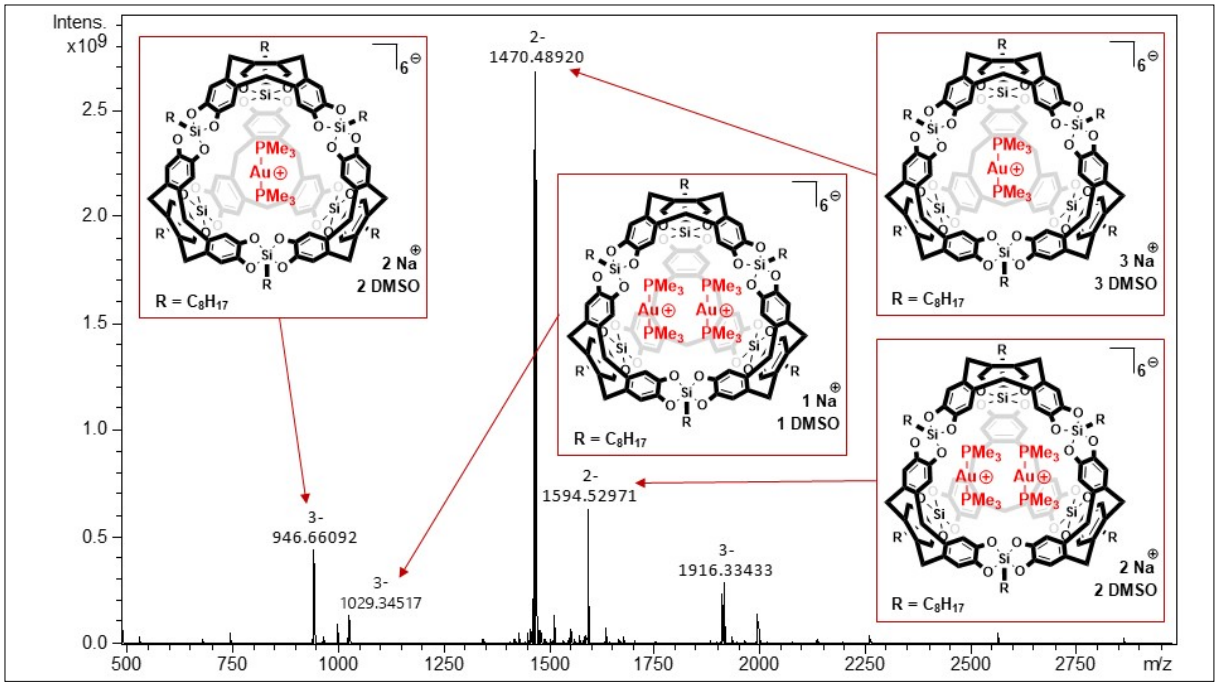

Figure S63. ESI-FTICR spectrum of a 10/1 mixture of **G** and **H**.

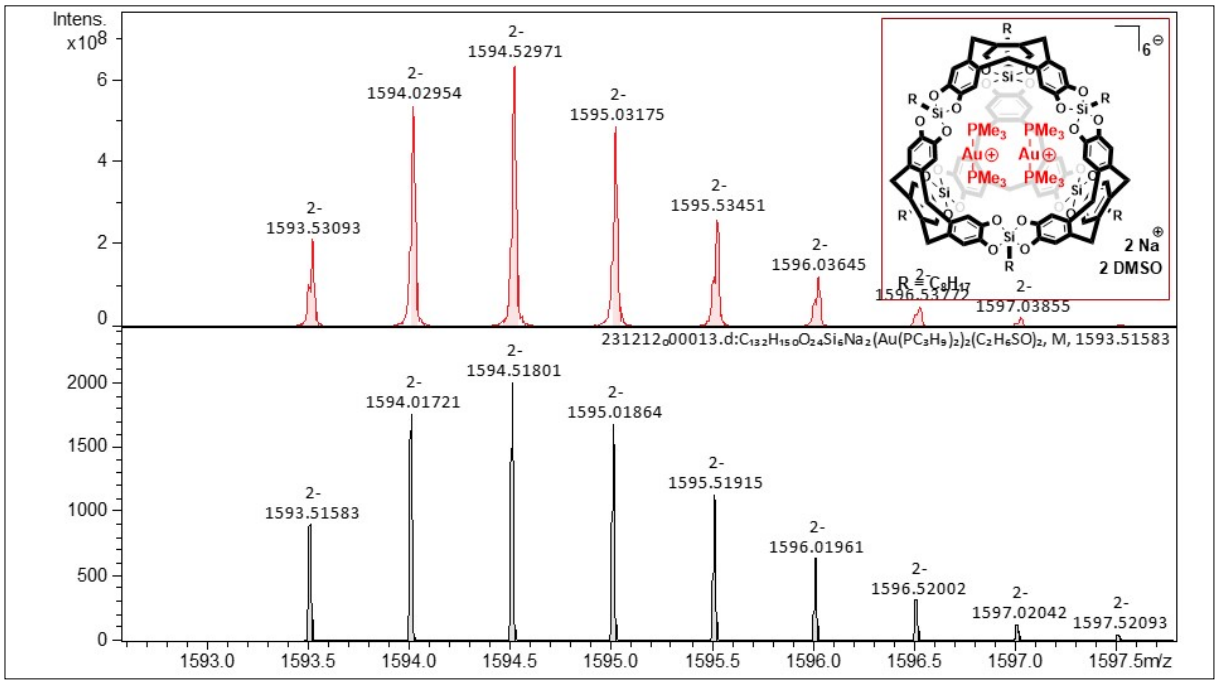

Figure S64. ESI-FTICR spectrum of a 10/1 mixture of **G** and **H**.

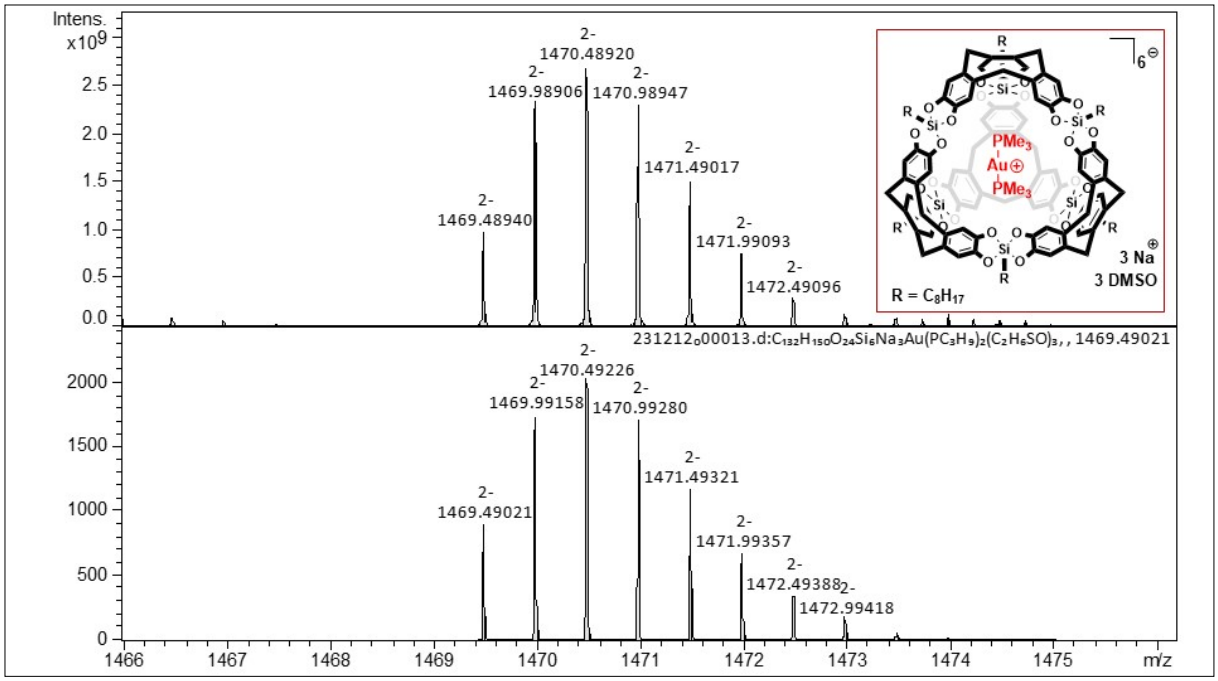

Figure S65. ESI-FTICR spectrum of a 10/1 mixture of **G** and **H**.

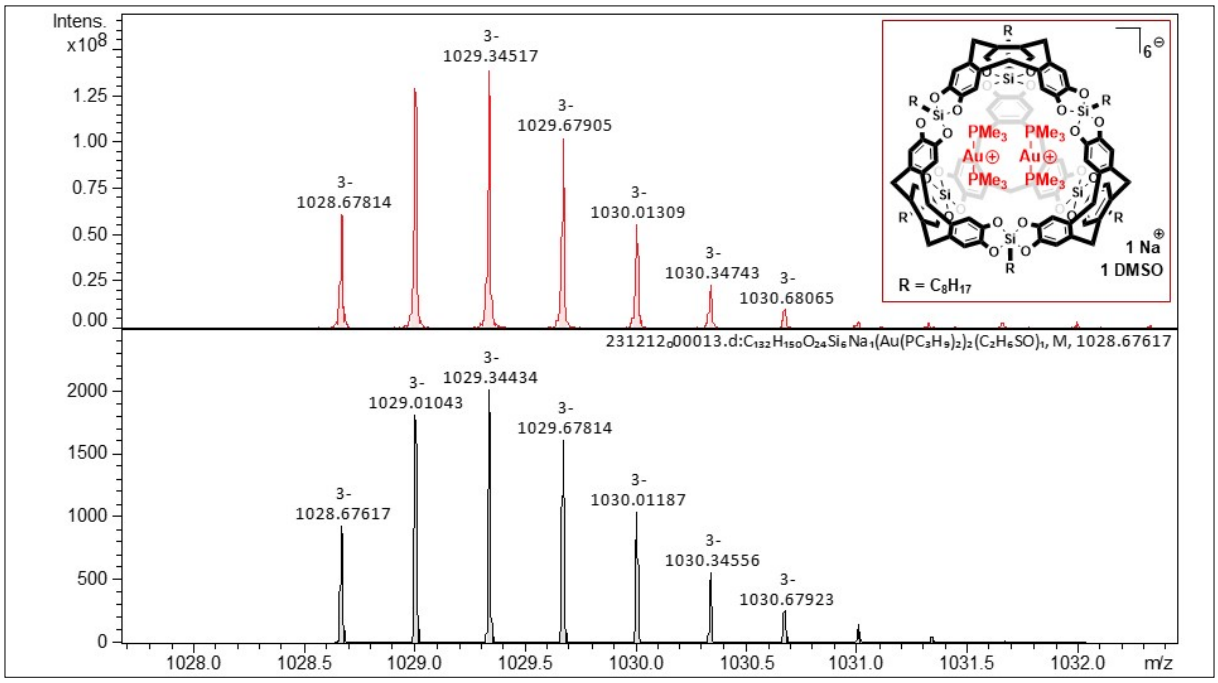

Figure S66. ESI-FTICR spectrum of a 10/1 mixture of **G** and **H**.

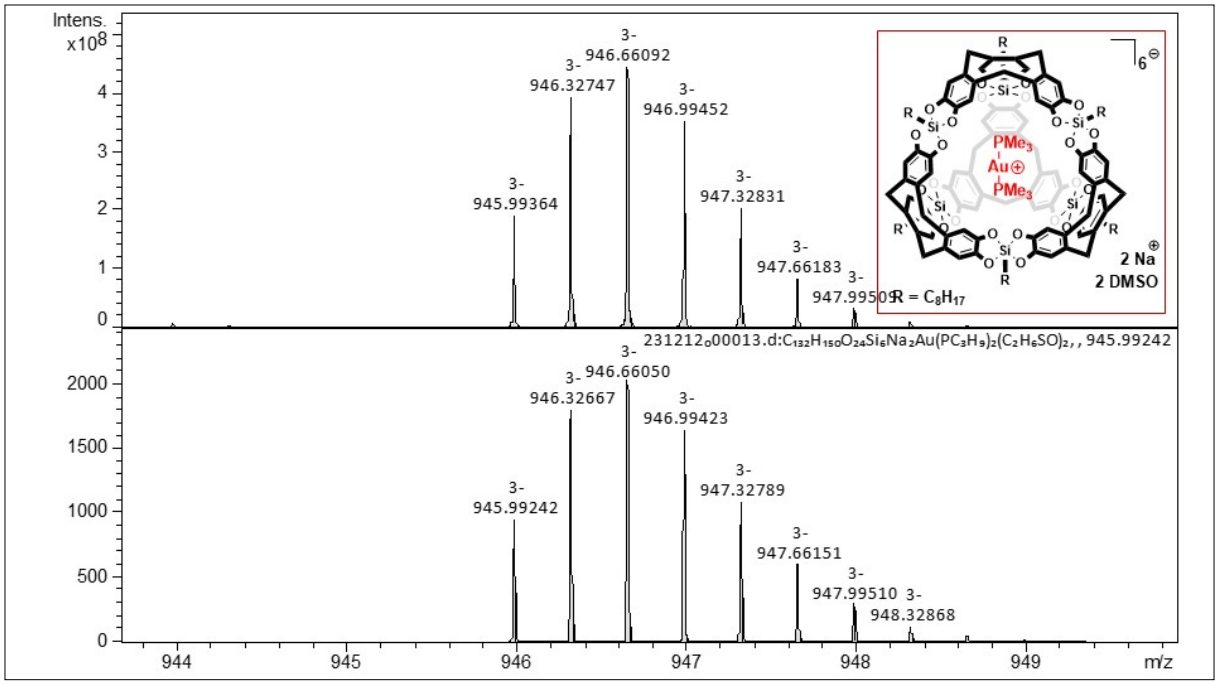

Figure S67. ESI-FTICR spectrum of a 10/1 mixture of **G** and **H**.

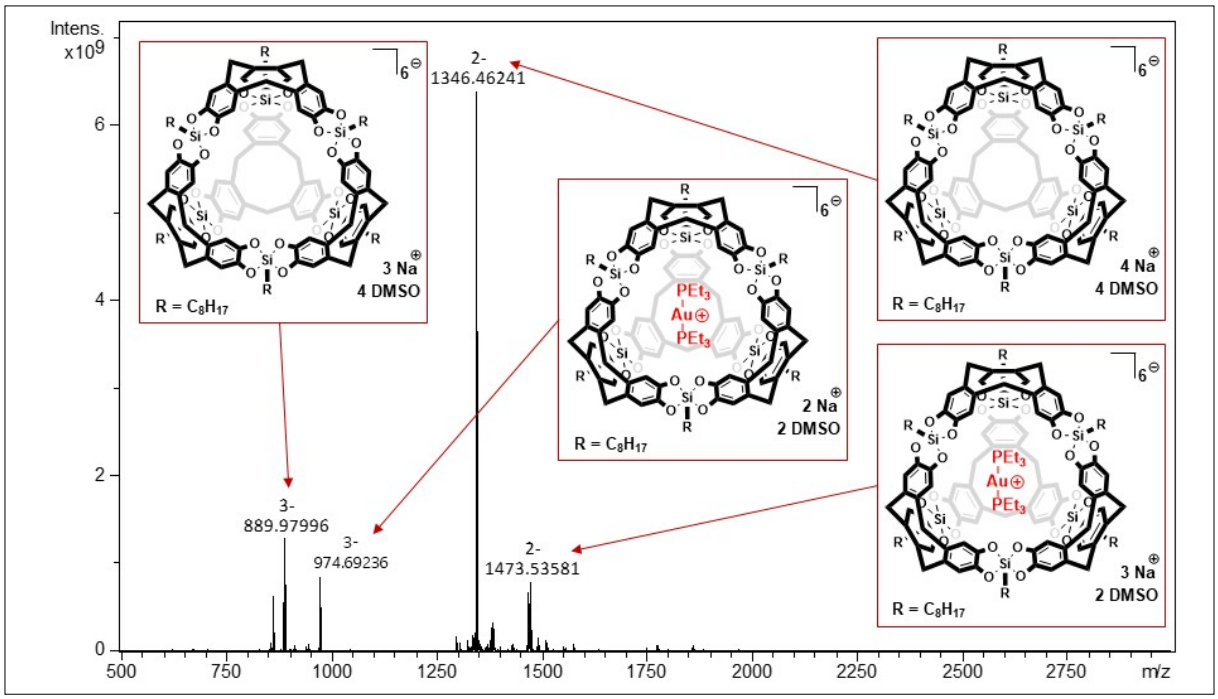

Figure S68. ESI-FTICR spectrum of a 10/1 mixture of **1** and **H**.

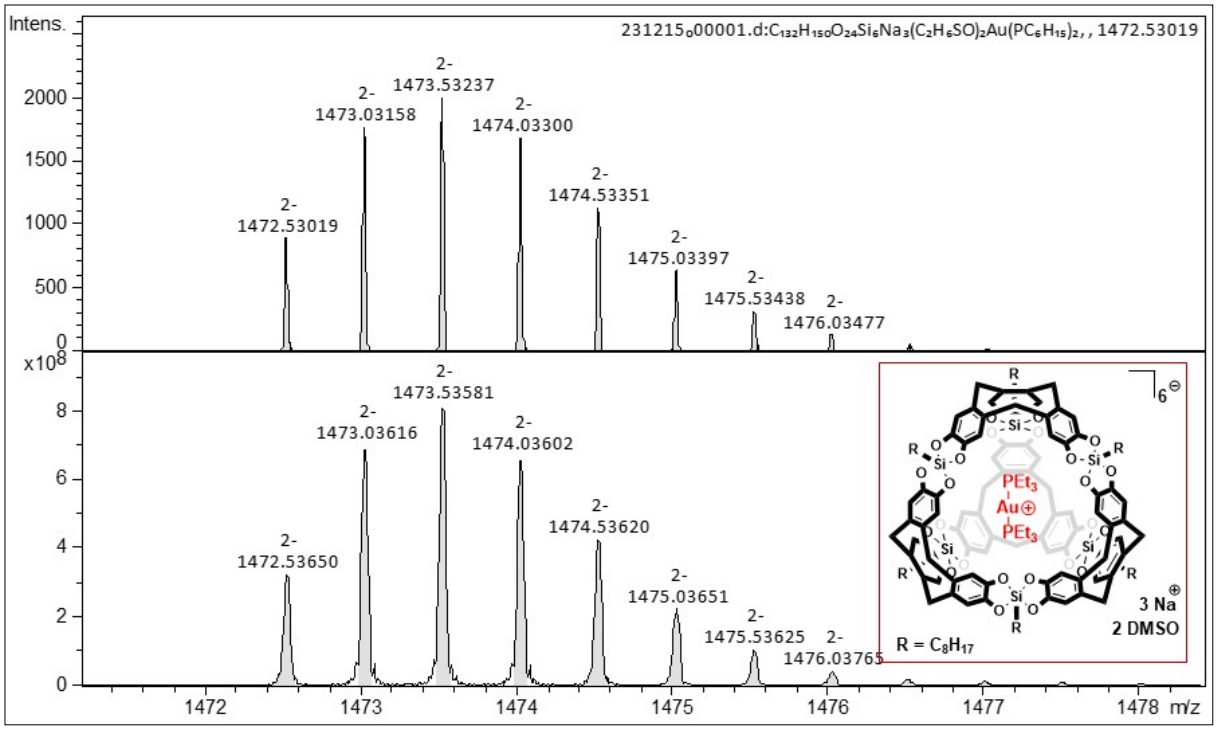

Figure S69. ESI-FTICR spectrum of a 10/1 mixture of **1** and **H**.

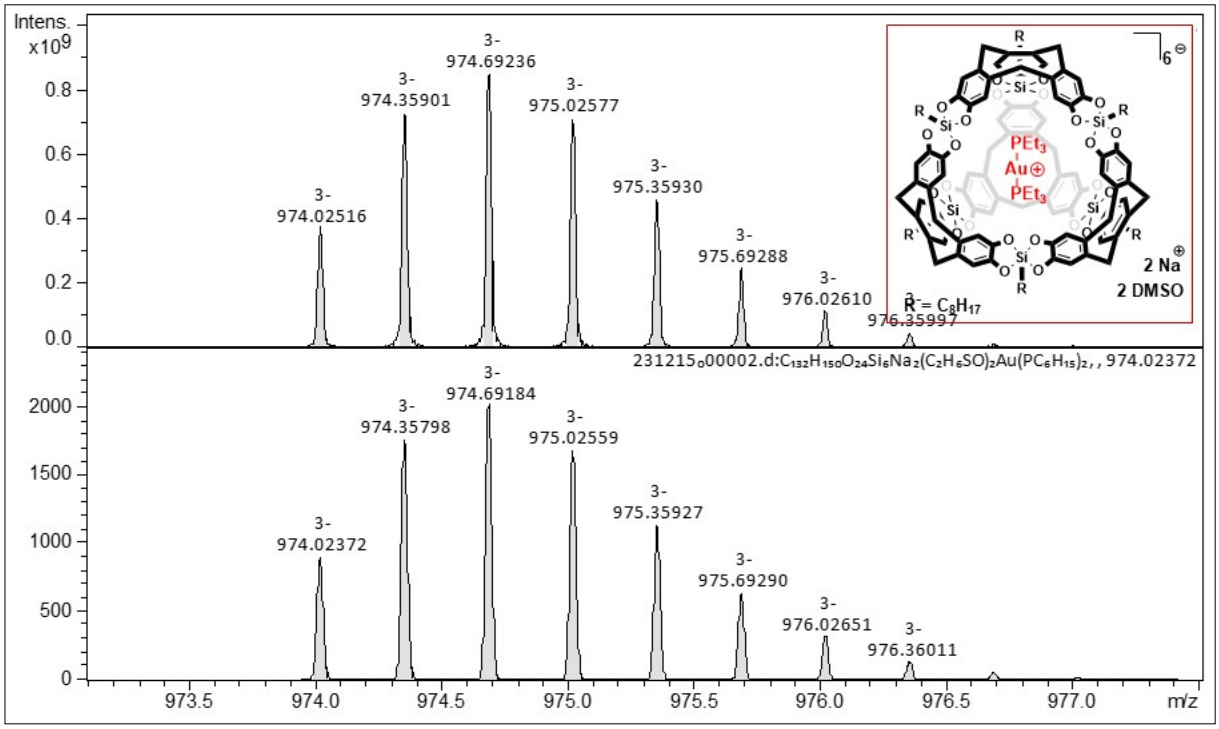

Figure S70. ESI-FTICR spectrum of a 10/1 mixture of **1** and **H**.

8. Cavity and guest size calculations:

8.1 Calculating the cavity size of the cage:

For the $[C_4(SiR)_6]^{6-}$ (R = Ph) cage, the original CIF file (CCDC identifier: 1892128)[4] was downloaded from the Cambridge Structural Database (CSD). The structure of $[C_4(SiR)_6]^{6-}$ (R = $^nC_8H_{17}$) cage (**H**) was derived from the original CIF file of **GG@H** (2427802), that can be also accessed from CSD. These structures were preprocessed by removing atoms and molecular fragments that are not part of the cage-framework (e.g. solvent/guest molecules and outward-pointing phenyl/alkyl groups, that do not affect the calculated cavity size), using Diamond Crystal and Molecular Structure Visualization software. The processed structures were then saved in a PDB format. The cavity size was determined based on this pdb file using pyKVFinder software with the following detection parameters:

- step size: 0.25 Å;
- probe in: 1.40 Å;
- probe out: 10.00 Å;
- removal distance: 1.00 Å;
- volume cutoff: 5.00 Å.

For further methodological details and accuracy, please refer to the cited reference.[6] The source and the processed structural files of the Raymond cages B1, B2, B3, B4 and B10 can be also find therein.

Cage	Cavity size (Å^3)	Reference
1892128	558	This work
H	563	This work
B1	283	6
B2	284	6
B3	269	6
B4	438	6
B10	251	6

Table S1. Calculated cavity sizes for each cage analyzed in this work.

8.2 Calculating the size of the gold complexes:

The structure of the gold complexes **G**, **1**-**4** was optimized using HyperChem molecular modeling software. The structure of **GG** was extracted from the original CIF file of **GG@H** (2427802). Then the volumes were calculated using the Vega ZZ molecular modeling toolkit.[7]

The processed structural data files for Cages 1892128, **H**, B1, B2, B3, B4, B10 and gold complexes (**G**, **GG** and **1**-**4**) along with the calculated volumes and cavity sizes are available on Zenodo *via* the following URL: [https://zenodo.org/uploads/14795286?token=eyJhbGciOiJIUzUxMiJ9.eyJpZCI6ImQwNzEzYmMzLTYyZGYtNGE5ZS1iNmE5LWFjMTA0NjBkZDhjYyIsImRhdGEiOnt9LCJyYW5kb20iOiIzNDMzMDk3YzBjM2M1ZjRlYmNlMzY0NTg5ZDlhN2VlYiJ9.LaRgIgwTTYkhreY2TYmoUKECTCgAMT9s9ovgELOOPhfWh9SUUca3ioRtMjKYoIDMLR8TtMi6az4hQhSXa5Rg7w].

9. Crystallographic data:

Crystallographic data were collected at low temperature (193(2) K) on a Bruker APEX II Quazar diffractometer equipped with a 30 W air-cooled microfocus source using MoKα radiation (λ = 0.71073 Å). Phi and Omega scans were performed for data collection. An empirical absorption correction was applied[8] and the structures were solved by intrinsic phasing method (ShelXT).[9] All non-hydrogen atoms were refined anisotropically by means of least-squares procedures on F² with ShelXL.[10] All the hydrogen atoms were refined isotropically at calculated positions using a riding model, except for the H atoms on terminal carbon atoms in incomplete disordered chains (C95, C95' and C102 for **H**, C52, C52', C60, and C60' for **2@H** and C115, C215, C123, C107, and C207 for **GG@H**). Some electron density was difficult to model, therefore the SQUEEZE tool[11] of PLATON was used to remove the corresponding electron density from the intensity data. This electron density can be attributed to solvent molecules (dimethyl sulfoxide for **H**, acetonitrile for **2@H**, and methanol for **GG@H**), missing atoms of dimethyl sulfoxide bound to sodium atoms for **H**, and missing atoms of alkyl chains.

Deposition Numbers 2427801 (**H**), 2427802 (**GG@H**) and 2427803 (**2@H**) contain the supplementary crystallographic data for this paper. These data are provided free of charge by the joint Cambridge Crystallographic Data Centre (http://www.ccdc.cam.ac.uk/structures).

TableS2. Crystal Data, Data Collection, and Structure Refinement for **GG@H**, **H** and **2@H**.

	GG@H	**H**	**2@H**
formula	$C_{154.76}H_{219}Au_2Na_4O_{38}P_{3.96}Si_6$	$C_{144}H_{188.41}Na_6O_{41}S_{12}Si_6$	$C_{114}H_{105}O_{24}Si_6$, $3(C_{10}H_{28}Au_2P_4)$, $2(C_2H_3N)$
M_r	3464.50	3266.55	4108.06
crystal system	triclinic	triclinic	monoclinic
space group	$P\bar{1}$	$P\bar{1}$	$C2/c$
a (Å)	17.1106(9)	20.808(2)	37.0345(14)
b (Å)	22.0464(12)	22.891(3)	25.8098(10)
c (Å)	26.2211(14)	23.911(3)	23.2625(8)
α (°)	89.918(2)	94.956(3)	90
β (°)	89.321(2)	106.576(3)	94.1740(10)
γ (°)	70.050(2)	108.561(3)	90
V (Å^3)	9297.1(9)	10149(2)	22176.6(14)
Z	2	2	4
ρ_{calc} (g cm^{-3})	1.238	1.069	1.230
μ (mm^{-1})	1.723	0.237	4.12
F(000)	3593.9	3445	8108
crystal size (mm^3)	0.20 x 0.18 x 0.10	0.20 x 0.16 x 0.06	0.16 x 0.16 x 0.10
T/K	193(2)	193(2)	193(2)
measd reflns	368128	341213	279228
Unique reflns (Rint)	39509 (0.0444)	34662 (0.1530)	20341 (0.0497)
Data/restraints/parameters	39509/1366/ 2425	34662/1914/2542	20341/572/1137
GOF on F²	1.094	1.535	1.156
R_1[a] [I>2σ(I)]	0.0423	0.1917	0.0680
wR_2[b] [all data]	0.1286	0.5053	0.1590

[a] $R_1 = \Sigma\,||F_o| - |F_c||\,/\,\Sigma\,|F_o|$. [b] $wR_2 = [\Sigma[\,w(F_o^2 - F_c^2)^2] / \Sigma\,[w(F_o^2)^2]]^{1/2}$.

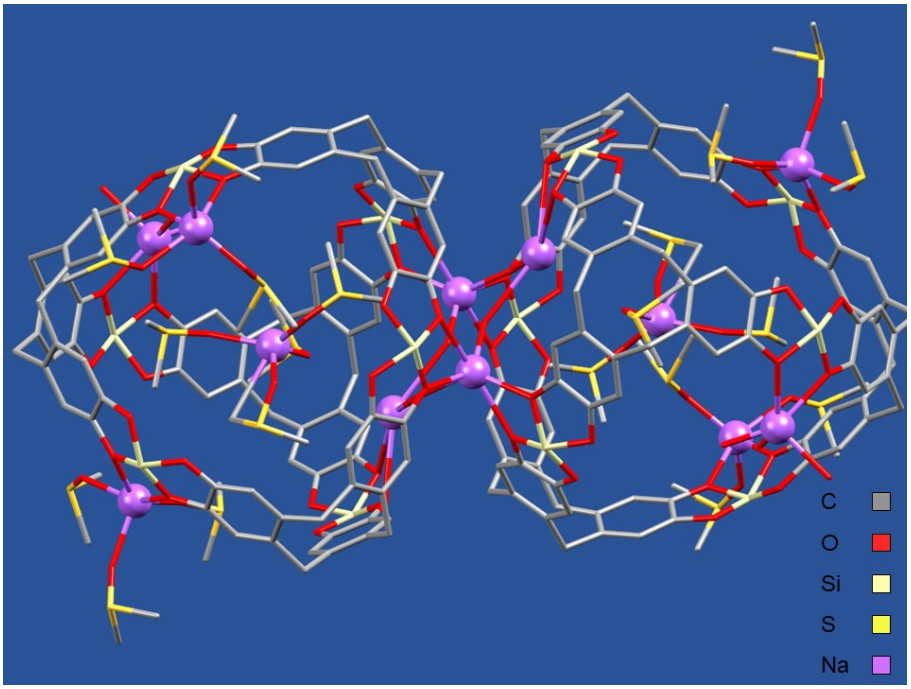

Figure S71. XRD structure of **H**. For the sake of clarity, hydrogen atoms and the *n*-octyl chains at Si are omitted.

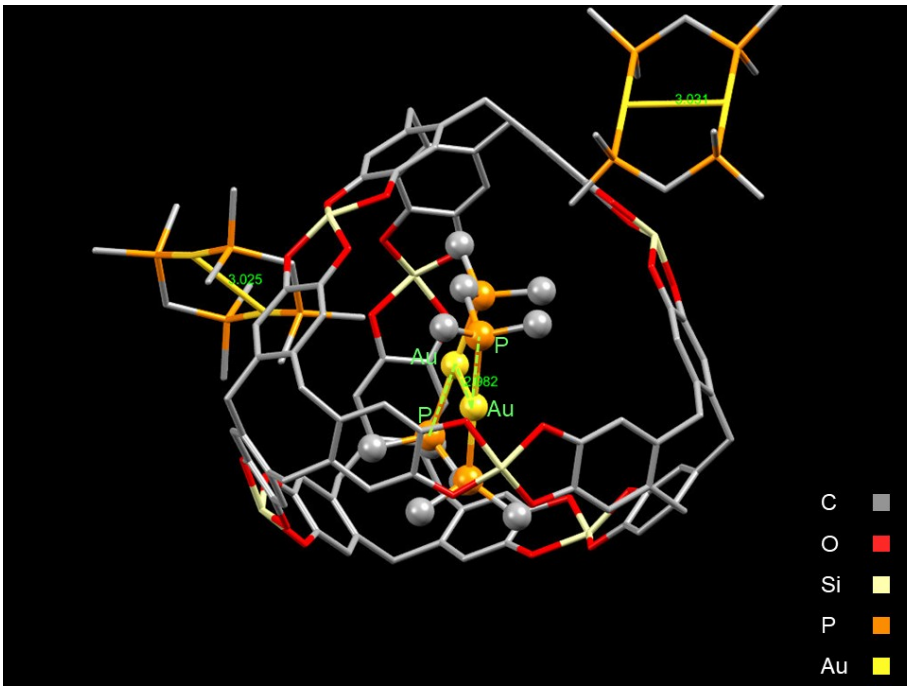

Figure S72. XRD structure of **2@H**. For the sake of clarity, hydrogen atoms and the *n*-octyl chains at Si are omitted. The endohedral guest (**2@H**) is represented with a ball and stick model, while the exohedral guests (**2ex/H**) are represented with a stick model. Au⋯Au distances are depicted in green. The distortion of the PAuAuP dihedral angle can be also seen on the image: 165.41(9)° *vs* the ideal 180°.

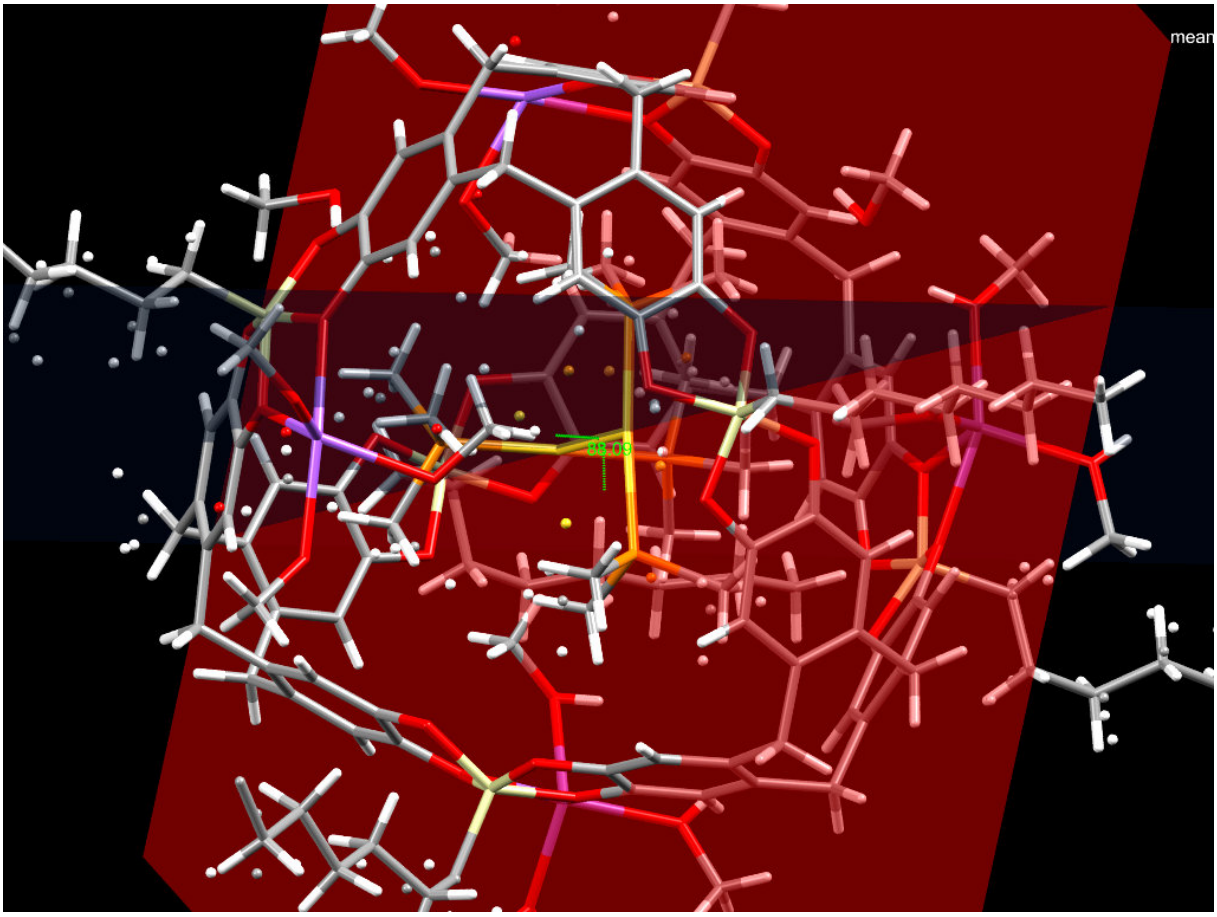

Figure S73. XRD structure of **GG@H**. The distortion of the PAuAuP dihedral angle is depicted on the image: 88.09°.

10. References:

[1] (a) Ogoshi, T.; Kitajima, K.; Umeda, K.; Hiramitsu, S.; Kanai, S.; Fujinami, S.; Yamagishi, T.; Nakamoto Y. Lewis acid-catalyzed synthesis of dodecamethoxycalix[4]arene from 1,3,5-trimethoxybenzene and its conformational behavior and host–guest property *Tetrahedron* **2009**, *65*, 10644; (b) Roche, C.; Sun, H.-J.; Prendergast, M. E.; Leowanawat, P.; Partridge, B. E.; Heiney, P. A.; Araoka, F.; Graf, R.; Spiess, H. W.; Zeng, X.; Ungar, G.; Percec, V. Homochiral Columns Constructed by Chiral Self-Sorting During Supramolecular Helical Organization of Hat-Shaped Molecules *J. Am. Chem. Soc*. **2014**, *136*, 7169.

[2] (a) Miyamoto, Y.; Aggarwal, S.; Celaje, J. J. A.; Ihara, S.; Ang, J.; Eremin, D. B.; Land, K. M.; Wrischnik, L. A.; Zhang, L.; Fokin, V. V.; Eckmann, L. Gold(I) Phosphine Derivatives with Improved Selectivity as Topically Active Drug Leads to Overcome 5-Nitroheterocyclic Drug Resistance in Trichomonas vaginalis *J. Med. Chem.* **2021**, *64*, 6608; (b) Diversi, P.; Cuzzola, A.; Ghiotto, F. Chemistry of Polynuclear Cationic Gold(I) Thiolates of Formula $[Au_2(S\mathit{t}Bu)(L_2)][BF_4]$ *Eur. J. Inorg. Chem*. **2009**, *4*, 545; (c) Sinha, P.; Wilson, A. K.; Omary, M. A. Beyond a T-Shape *J. Am. Chem. Soc*. **2005**, *127*, 12488.

[3] McTiernan, C. D.; Morin, M.; McCallum, T.; Scaiano, J. C.; Barriault, L. Polynuclear gold(I) complexes in photoredox catalysis: understanding their reactivity through characterization and kinetic analysis *Cat. Sci. Technol*. **2016**, *6*, 201.

[4] Kawakami, Y.; Ogishima, T.; Kawara, T.; Yamauchi, S.; Okamoto, K.; Nikaido, S.; Souma, D.; Jin, R.-H.; Kabe, Y. Silane catecholates: versatile tools for self-assembled dynamic covalent bond chemistry *Chem. Commun*. **2019**, *55*, 6066.

[5] Reddy, T. S.; Privér, S. H.; Mirzadeh, N.; Bhargava, S. K. Synthesis of gold(I) phosphine complexes containing the $2\text{-}BrC_6F_4PPh_2$ ligand: Evaluation of anticancer activity in 2D and 3D spheroidal models of HeLa cancer cells *Eur. J. Med. Chem*. **2018**, *145*, 291.

[6] Guerra, J. V. S.; Alves, L. F. G.; Bourissou, D.; Lopes-de-Oliveira, P. S.; Szalóki, G. Cavity Characterization in Supramolecular Cages *J. Chem. Inf. Model*. **2023**, *63*, 3772.

[7] Pedretti A., Mazzolari A., Gervasoni S., Fumagalli L., Vistoli G. The VEGA suite of programs: a versatile platform for cheminformatics and drug design projects. *Bioinformatics* **2021**, *37*, 1174.

[8] Bruker, SADABS, Bruker AXS Inc., Madison, Wisconsin, USA, **2008**.

[9] ShelXT, Sheldrick, G. M. University of Göttingen, *Acta Crystallogr. Sect. A* **2015**, *71*, 3.

[10] ShelXL, Sheldrick, G. M. University of Göttingen, *Acta Crystallogr. Sect. C* **2015**, *71*, 3.

[11] PLATON SQUEEZE, Spek, A. L. University of Utrecht, *Acta Crystallogr. Sect. C* **2015**, *71*, 9.